PROYECTO FIN DE CARRERA

TECNOLOGÍA PARA LA CONSTRUCCIÓN DE CUBIERTAS DOBLEMENTE CURVADAS A PARTIR DE ELEMENTOS PLANOS

TECHNOLOGY TO BUILD DOUBLE CURVED SHELLS FROM PLANE ELEMENTS

Institute for Structural Engineering
Vienna University of Technology

ejecutado con el fin de obtener el título superior de **Ingeniero Industrial**
bajo la dirección de

Dr. Jorge López Puente

Departamento de Mecánica de Medios Continuos y Teoría de Estructuras
Universidad Carlos III de Madrid
Escuela Politécnica Superior

realizado por

Rocío Martín-Oar Luca de Tena

Abril 2009

EXTRACTO

Arquitectos e ingenieros buscan constantemente nuevas soluciones para la creación de espacios envolventes eficientes. La industrialización y el desarrollo del mundo moderno han estimulado inevitablemente la demanda de cubiertas eficientes y capaces de encerrar grandes áreas libres de columnas. Las estructuras espaciales, sin duda, satisfacen dicha demanda y, si son bien diseñadas, requieren un uso mínimo de materiales estructurales.

Este proyecto presenta un estudio sobre una nueva tecnología para construir cubiertas de doble curvatura a partir de elementos planos. Este trabajo se ha llevado a cabo en el ***Instituto de Ingeniería Estructural*** de la ***Universidad Tecnológica de Viena***, bajo la dirección de O.Univ.Prof. Dipl.-Ing. Dr.-Ing. Johann Kollegger, y la supervisión de Dipl.Ing. Sonja Dallinger.

Este nuevo método de construcción consiste en la transformación de un plato plano, formado por elementos, en una cubierta semiesférica mediante el uso combinado de elementos prefabricados, cables tensionados y un globo neumático. Además, este método no sólo es adecuado para cubiertas de hormigón, sino también para cubiertas de hielo. Diferentes experimentos se han realizado en el Instituto desde el 2005.

Las cubiertas delgadas de hormigón son duraderas y demandan un mantenimiento mínimo. Este nuevo sistema mantiene todas las ventajas de las cubiertas de hormigón, pero elimina la necesidad de encofrados temporales y los altos costes asociados a estos. Por lo tanto, este nuevo sistema ofrece una alternativa atractiva a otros sistemas estructurales utilizados en cubiertas de grandes espacios.

En las dos primeras secciones se presentan las estructuras semiesféricas.

En la primera sección se ofrece una visión general sobre las estructuras semiesféricas: aplicaciones, características generales, clasificación; y una exposición de la teoría general para el análisis de membranas delgadas.

La segunda sección se centra en el diseño y análisis de una cúpula. En primer lugar se presenta una visión general de las cúpulas a lo largo de la historia. Su comportamiento estructural, así como las distintas técnicas para la construcción de cubiertas semiesféricas delgadas.

Posteriormente en la tercera sección, el nuevo método de construcción basado en el uso combinado de elementos prefabricados, cables tensionados y un globo neumático, se explica en profundidad. Tres experimentos diferentes: una cubierta semiesférica de hormigón en Viena y dos cubiertas semiesféricas de hielo en el Tirol, se analizan y exponen en detalle. La planificación, selección de materiales y elementos utilizados

durante el proceso de construcción, se prueban en el laboratorio a fin de garantizar sus propiedades mecánicas y resistentes.

En la cuarta sección, se lleva a cabo un análisis analítico y de elementos finitos en la estructura estudiada. Se realiza una modelación numérica de la cubierta semiesférica utilizando el programa de elementos finitos ABAQUS. Los resultados de los modelos numéricos son comparados con los analíticos para asegurar el adecuado comportamiento de la estructura.

Por último en la quinta sección, el globo neumático y los cables tensionados utilizados en el proceso de construcción de la estructura, también se estudian en profundidad.

Conclusiones y propuestas de mejora de esta tecnología se obtienen a partir de este estudio.

Estructuras semiesféricas

Las estructuras semiesféricas deben proporcionar fuerza, rigidez y estabilidad. Deben ser capaces de soportar las cargas aplicadas y el peso propio sin deformación excesiva o desplazamientos. Similar a un arco, las cúpulas desarrollan fuerzas internas en dirección meridional (meridional forces) que transfieren las cargas a una estructura de apoyo en su base, Figura 1. Estas fuerzas de compresión aumentan de magnitud desde la corona superior en cualquier cúpula cargada simétricamente por peso propio.

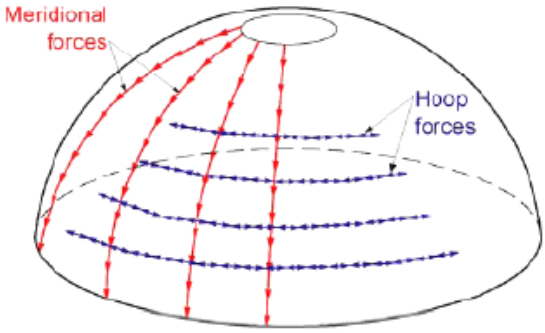

Figura 1. Fuerzas desarrolladas en una cúpula.

Sin embargo, en la cúpula se producen fuerzas adicionales, llamadas fuerzas circunferenciales (hoop forces), perpendiculares a las fuerzas meridionales. Como resultado de ello, a pesar de que un arco es inestable sin su base, una cúpula con un óculo es perfectamente estable.

Nueva tecnología de construcción

Hoy en día, mediante distintos métodos de construcción, cúpulas con excelentes calidades se pueden obtener. Sin embargo, estos procesos de construcción son por lo general complejos, largos y costosos. La construcción de cubiertas con doble curvatura mediante encofrados es larga y costosa, debido al cada vez mayor coste de la mano de obra. Otros métodos como el uso de una membrana neumática que se cubre posteriormente con una capa de hormigón fresco, también llevan demasiado tiempo y elevados costes asociados. Para reducir el tiempo de construcción en el lugar de la instalación de la estructura se emplean elementos prefabricados.

En el *Instituto de Ingeniería Estructural* en la *Universidad Tecnológica de Viena* un nuevo método de construcción de cúpulas está en desarrollo. Con este nuevo método, se obtienen cubiertas de doble curvatura a partir una placa formada por elementos prefabricados planos.

Una semiesfera es una superficie no desarrollable, no se puede transformar en una superficie plana sin comprometer la estructura. Para poder obtener una forma semiesférica, la superficie ha de ser dividida en elementos, en este caso de estudio se divide en 96 elementos. La placa plana, a partir de la cual se obtiene la semiesfera, está formada por 16 segmentos longitudinales espaciados simétricamente. Cada segmento longitudinal está formado por 6 elementos, Figura 2.

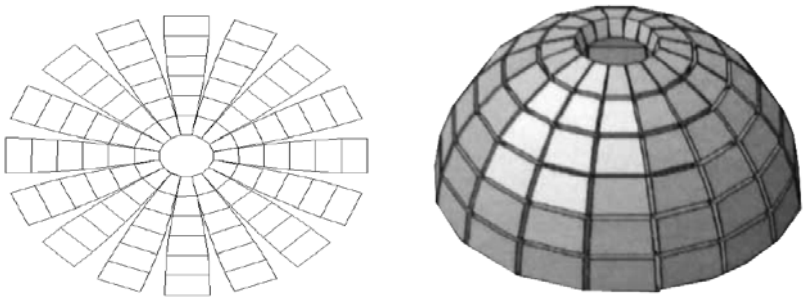

Figura 2. Semiesfera, estructura no desarrollable.

Distintos modelos de madera fueron creados, Figura 3, para demostrar este nuevo método de construcción, con el fin de encontrar la mejor manera para lograr la transformación de un plato plano en una forma semiesférica con éxito.

Figura 3. Modelo de madera.

En este nuevo método de construcción el uso de elementos prefabricados, cables tensionados y una estructura neumática se combina:

- Colocación del globo neumático correctamente plegado.
- Colocación de los elementos empezando por el anillo interior de menor diámetro.
- Colocación elementos tensores para cables meridionales en el anillo central.
- Colocación de los cables tensores en dirección circunferencial y meridional a medida que se van colocando los elementos.
    - Colocación elementos tensores para cables en dirección circunferencial en cada uno de los 6 anillos.
    - Colocación elementos tensores para cables meridionales en el anillo de mayor diámetro.
- Inflar globo neumático.
- Tensar cables hasta obtener forma semiesférica final.

La construcción de cubiertas semiesféricas mediante elementos prefabricados es un procedimiento ya conocido, pero en el pasado se utilizaban elementos doblemente curvados para su confección. Por lo tanto, el transporte y montaje con elementos no planos eran de gran dificultad. Con este nuevo método, el posicionamiento de los elementos es llevado a cabo con la ayuda de la estructura neumática, en vez de con el uso de encofrados.

Elementos prefabricados

En las estructuras con elementos de hormigón, se posicionan conductos guía en el interior de los elementos durante su proceso de fabricación, por donde posteriormente pasarán los cables en tensión. Estos elementos previamente diseñados se transportan apilados al lugar de la instalación de la cúpula.

En las estructuras con elementos de hielo, se prepara un marco circular en donde se verterá el agua necesaria para forma un plato de espesor uniforme de hielo. Posteriormente se eliminarán los segmentos de hielo no deseados, se realizarán cortes para favorecer el posterior proceso de erección de la estructura y se harán orificios longitudinales para introducir los cables.

Estructura neumática

Una estructura neumática, en este caso una membrana de plástico semiesférica, de 2.5mm de espesor, se posiciona previamente debajo de los elementos prefabricados en el caso de la estructura de hormigón, o debajo del plato de hielo en el caso de la estructura de hielo. Cuando todos los elementos se encuentran en su posición se inicia el proceso de inflado del globo neumático. El inflado del globo neumático permite la erección de la estructura semiesférica y así se va produciendo la correcta colocación de los elementos planos.

Cables tensionados

Los cables tensionados mantienen los elementos en su posición correcta en el proceso de construcción de la estructura y la post-tensión aplicada en ellos garantiza el adecuado comportamiento estructural de la cubierta obtenida.

En las estructuras de hormigón los cables se introducen en el interior de los conductos guía de los elementos, a medida que se colocan los elementos prefabricados sobre el globo desinflado, empezando por el anillo de menor diámetro, con ayuda de una grúa.

Se utilizan dos cables meridionales en cada uno de los 16 segmentos pasando por los 6 elementos. En dirección circunferencial un cable se sitúa en cada uno de los 6 anillos, Figura 4.

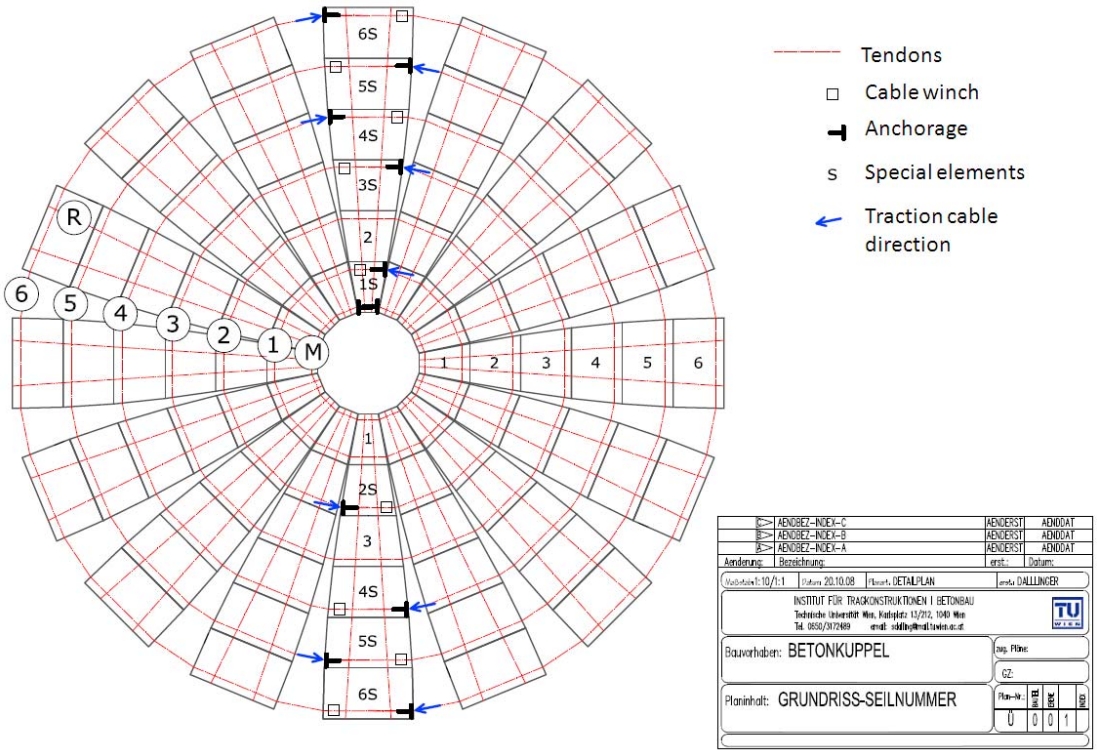

Figura 4. Planos de los elementos prefabricados de hormigón.

A medida que la estructura se eleva con el inflado del globo, los cables se ajustan y tensan debidamente hasta finalmente obtenerse la estructura semiesférica deseada.

Construcción de cúpulas de hormigón y hielo en Viena

Las estructuras construidas para los ensayos poseen el mismo diseño y forma que los modelos de madera anteriormente construidos en el laboratorio. El diámetro de la placa plana, a partir de la cual se obtiene la forma semiesférica formada por 96 elementos,

alcanzaba 13m. Por lo tanto, la cúpula obtenida posee un diámetro de 8,3 m y una altura de 4,1 m.

Se exponen los planos detallados de cada uno de los seis tipos de elementos. Cabe destacar la necesidad de sostener los cables tanto en dirección circunferencial como en dirección meridional. En dirección circunferencial se emplean dos tornos de cable motorizados, en cada uno de los seis anillos, durante el proceso de erección de la estructura. En dirección meridional de ajustan los cables mediante el uso de elementos de sujeción de cables de acero.

Los elementos para la sujeción de cables de acero son sometidos en el laboratorio a diferentes ensayos con el fin de verificar su comportamiento estructural y asegurar sus propiedades y suficiente capacidad en la estructura, Figura 5. Distintas configuraciones con estos elementos en serie son estudiadas para seleccionar la más adecuada en esta aplicación.

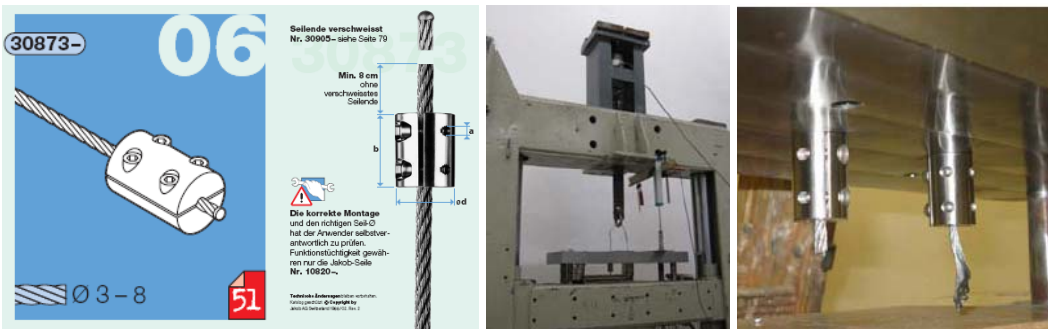

Figura 5. Elementos para la sujeción de cables.

Se llevó a cabo la construcción de una cúpula de hormigón en Viena, Figura 6, y de una cúpula de hielo en el Tirol, Figura 7, en Austria, con las dimensiones anteriormente citadas. Estos dos procesos se monitorizaron con el fin de encontrar posibles fallos para la mejora de este nuevo método de construcción.

Figura 6. Proceso de construcción de la cúpula de hormigón en Viena.

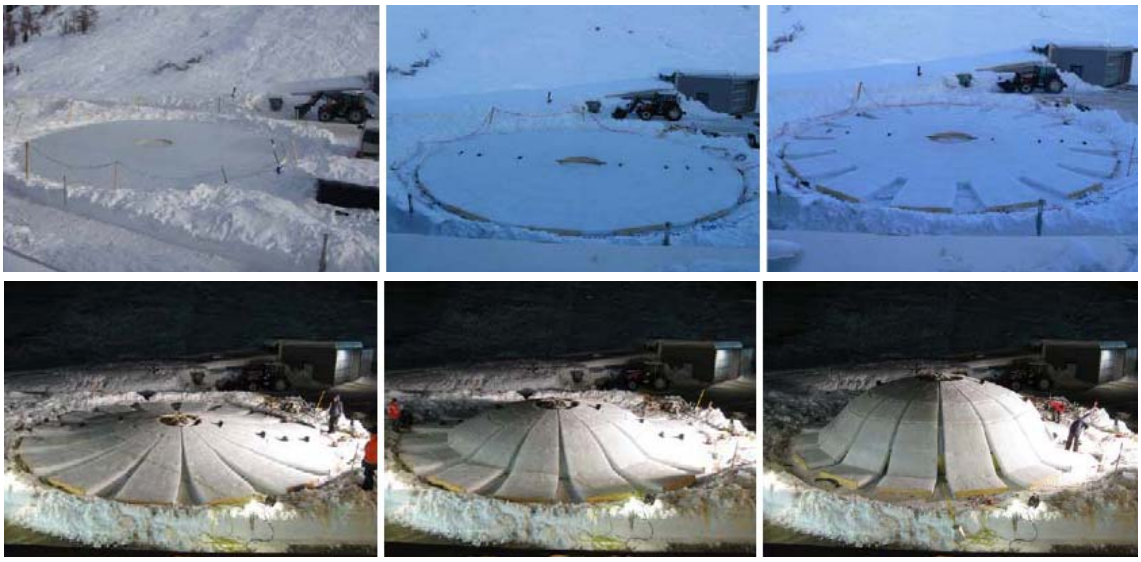

Figura 7. Proceso de construcción de la cúpula de hielo en El Tirol.

Análisis analítico y numérico de la estructura

El comportamiento estructural de la estructura semiesférica de hormigón y de hielo son estudiados mediante el uso de dos métodos independientes: análisis de elementos finitos y fórmulas analíticas. Para los cálculos analíticos de las tensiones en la estructura, véase el anexo I y anexo II.

Para el análisis de elementos finitos de la estructura se emplea ABAQUS 6.6-2. Herramienta suficientemente potente para los cálculos estáticos realizados en nuestro estudio.

Tres casos de carga diferentes son considerados: peso propio, carga de nieve, y efecto del viento. En el estudio de las cargas de nieve y el efecto del viento en la estructura, son empleados los *Eurocódigos estructurales* relativos a acciones en estructuras.

El análisis en esta sección se lleva a cabo en un modelo semiesférico y no en la estructura final formada por 96 elementos planos. Esta aproximación nos permite obtener resultados con métodos de cálculo más simples. También se estudia el comportamiento de la estructura con una puerta, Figura 8.

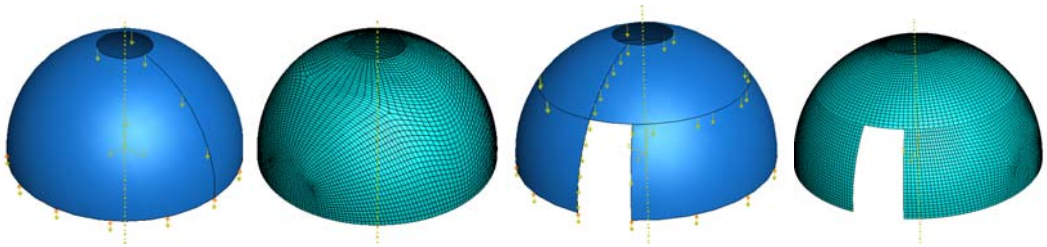

Figura 8. Modelización de la cúpula con y sin puerta en ABAQUS.

Análisis de las tensiones en los cables y la estructura neumática

Cada elemento en la estructura posee un peso propio, y este peso se puede dividir en dos fuerzas. La primera componente paralela a la superficie del elemento será soportada por los cables; y la segunda, normal a la superficie del elemento, por la estructura neumática.

El proceso de erección de la estructura se divide en seis etapas, Figura 9. Cada una de las etapas corresponde a la erección de cada anillo, empezando por el anillo interior de menor diámetro.

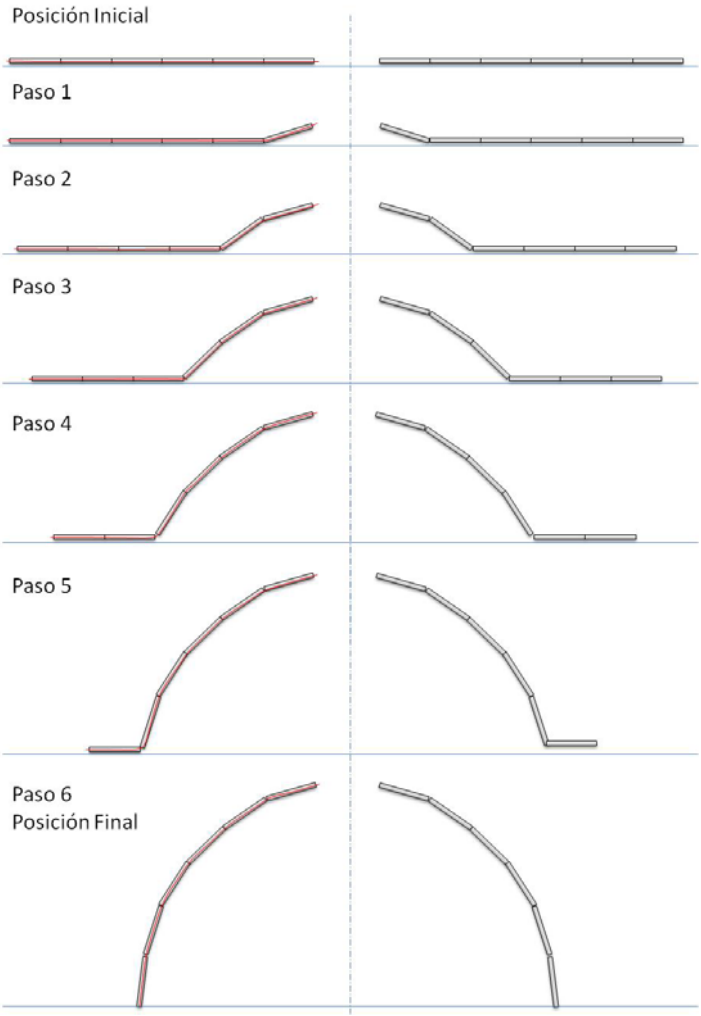

Figura 9. Posición de los elementos en las distintas etapas durante el proceso de erección de la estructura.

Las tensiones que deben soportar los cables son calculadas, en cada uno de los pasos, para la cúpula de hormigón y la de hielo. También se calcula la fuerza máxima, en el anillo central de menor diámetro. Para los cálculos de las tensiones en los cables, véase el anexo III y anexo IV.

La presión necesaria en la estructura neumática dependerá del peso de la estructura que tiene que soportar, y el área de la base de la estructura neumática. La presión se calcula para el uso de hormigón y hielo.

Conclusiones

Este proyecto presenta un estudio sobre una nueva tecnología para construir cubiertas de doble curvatura a partir de elementos planos, llevado a cabo en el *Instituto de Ingeniería Estructural* de la *Universidad Tecnológica de Viena*.

Estas estructuras curvadas delgadas son consideradas, tanto por diseñadores como por el público, uno de los más sorprendentes sistemas estructurales, no sólo por su estética superior, sino también por su capacidad para integrarse a la perfección en cualquier medio natural. Esta tecnología puede utilizarse en edificios con diferentes aplicaciones, como escuelas, gimnasios, centros comunitarios, o instalaciones industriales.

Las estructuras de hielo destacan debido a su naturaleza y belleza efímera. Estas estructuras pueden ser utilizadas, en lugares donde el clima lo permita, como arquitectura de carácter temporal, como cubiertas para instalaciones deportivas y eventos musicales, o presentaciones y promociones de venta de productos. Por otra parte, la naturaleza transparente del hielo, permite infinidad de posibilidades para la creación de estructuras atractivas. Por ejemplo, la iluminación interior de las estructuras de hielo durante la noche, crea un ambiente cautivador en los alrededores.

Al igual que el arco, las estructuras doblemente curvadas son naturalmente estructuras fuertes, permitiendo amplias áreas libres de soportes internos, lo que nos permite una cubierta abierta y libre de obstáculos en el interior. Las cubiertas delgadas de hormigón destacan por su resistencia y un mantenimiento mínimo.

Una de las principales ventajas de esta nueva tecnología es el aspecto económico. El uso del hormigón como material de construcción reduce los costes tanto de las materias primas como los costes de construcción, siendo el hormigón relativamente barato y fácilmente moldeable en elementos. Además, las estructuras resultantes son extremadamente fuertes y seguras.

Este nuevo método de construcción consiste en la transformación de un plato plano formado por los elementos en una estructura semiesférica mediante el uso combinado de elementos prefabricados, cables tensionados y estructuras neumáticas.

Las piezas de una cubierta de hormigón son prefabricadas en una fábrica y estos elementos son fácilmente transportados al emplazamiento de la estructura para su montaje. En el caso de la cubierta de hielo los elementos se cortan a partir de una placa de hielo inicial.

Los cables en dirección radial y meridional en la cúpula mantienen los elementos unidos y ayudan a mantener la estructura. Los globos neumáticos permiten la elevación de la estructura de una manera rápida y económica. El primer globo neumático fabricado en el laboratorio, tuvo problemas en el cumplimiento de sus funciones en el proceso de erección de la estructura. Un nuevo globo neumático fue fabricado buscando la mejor forma de obtener un elemento fuerte capaz de soportar los elementos prefabricados.

Esta tecnología elimina la necesidad de encofrados temporales y los altos costes de mano de obra asociados a ellos.

Los elementos utilizados para la sujeción de los cables se sometieron a ensayos en el laboratorio con el fin de garantizar sus propiedades y su adecuada capacidad estructural. Se observó que los elementos seleccionados para la sujeción de cables funcionaban mejor manteniendo dos cables en lugar de uno solo. Esto nos lleva a concluir que en futuros diseños se seleccionarán elementos de unión de dos cables, por lo que las modificaciones oportunas en el diseño de elementos tendrían que hacerse en consecuencia.

El programa ABAQUS, de análisis de elementos finitos, es una poderosa herramienta que nos permite estudiar profundamente la estructura con diferentes configuraciones de carga de forma precisa y rápida.

Los resultados de los modelos numéricos se compararon con los analíticos para garantizar el adecuado comportamiento de la estructura.

Esta nueva tecnología de construcción, en desarrollo hoy en día, tiene grandes posibilidades en el mercado. Nuevos experimentos se llevarán a cabo para garantizar sus capacidades estructurales y mejorar el método de construcción para encontrar el equilibrio entre costes y beneficios.

ACKNOWLEDGEMENTS

This final thesis constitutes the colophon to my master degree in Industrial Engineering, majoring in mechanics and structures. Now I would like to thank to all persons involved during this learning period.

First I would like to express my profound gratitude to my parents. Especially to my father, industrial engineer as well, who has continuously supported and gave me encouragement during my whole studies period as well as he always had full confidence in my work.

I am very grateful to the *Institute for Structural Engineering* of the *Vienna University of Technology*, for providing me the opportunity to work with them in this wonderful project. This allowed me to be part in a real investigation project and acquire new abilities and skills in the matter.

I would like to give my heartfelt thanks to O.Univ.Prof. Dipl.-Ing. Dr.-Ing. Johann Kollegger Head of the *Institute for Structural Engineering* for his help and unfailing support; and to my supervisor Dipl.-Ing. Sonja Dallinger, for her enthusiastic approach, continuous inspiration and enlightening guidance.

My sincere thanks also to my friends that had supported me unconditionally in the hard moments, and my colleagues and professors in the *Carlos III University of Madrid* who contributed to my work in some manner.

ABSTRACT

Architects and engineers constantly seek new solutions to the problem of efficient space enclosure. The industrialization and development of the modern world has inevitably spurred demand for efficient and adaptable roofs for enclosing large columnfree areas. Spatial structures without doubt, meet such demand and, if properly designed, require a minimum use of structural materials.

This thesis presents a study into a new technology to build double curved shells from plane elements. This work has been carried out the last years by the *Institute for Structural Engineering* of the *Vienna University of Technology*, under the management of O.Univ.Prof. Dipl.-Ing. Dr.-Ing. Johann Kollegger.

This new construction method consists on transforming a plate formed by plane elements into a shell with the combined usage of precast elements, post tensioning and pneumatic formworks. Moreover, this method is not only suitable for concrete shells but also for ice shells. Different experiments had been performed in the Institute since 2005.

Thin concrete shells are durable and demand minimal maintenance. This new system retains all the benefits of thin concrete shells, but eliminates the need for temporary formwork and the high costs associated. Therefore, the new system offers an attractive alternative to other structural systems for large-span roofs.

In the first two sections a general overview about the shell structures, design and analysis of domes is presented; as well as known techniques in the building of thin shells.

Then the new construction method based on the combined usage of precast elements, post tensioning and pneumatic formworks, is explained in detail. Three different experiments, one concrete shell in Vienna and two ice shells in Obergurgl, are monitored and deeply exposed. The planning, selection of materials and elements used during the building process are tested in the laboratory in order to ensure their demanded properties.

An analytical and finite element analysis is carried out on the structures. A numerical modeling of the hemispherical shells using the finite elements program ABAQUS was undertaken. The numerical modeling results are compared to the analytical ones to ensure the adequate behavior of the structure.

Finally the pneumatic formwork and tendons used in the building process of the shell are also studied deeply. Conclusions and improvement proposals for this technology are obtained from this study.

INDEX

1. SHELL STRUCTURES OVERVIEW 17
1.1. Introduction to shell structures 18
1.2. Applications of shell structures 18
1.3. General structural features of shells 19
1.3.1. Continuity and curvature 19
1.3.2. The empirical approach 20
1.3.3. Closed and open shells 20
1.3.4. A simple geometric approach: convexity. 21
1.3.5. A disadvantage of rigidity 21
1.3.6. Catastrophic failures 21
1.4. Classification of shells surfaces 22
1.4.1. Thickness ratio 22
1.4.2. Shell curvature 22
1.4.3. Geometrical developability 23
1.4.4. Shell surface generation 24
1.4.5. Shell surfaces summary 25
1.4.6. Basic shell types 26
1.5. General theory of thin shells 29
1.5.1. Arch versus dome 29
1.5.2. Beam versus barrel 30
1.5.3. Analysis of thin shells 32

2. DESIGN AND ANALYSIS OF A DOME 36
2.1. Historical overview 37
2.2. Structural behavior 48
2.3. Domes and thin shells construction techniques 54
2.3.1. Flattened conduit 54
2.3.2. Hub and strut dome 55
2.3.3. Tube and hub 55
2.3.4. Beam and hub 56
2.3.5. Panelized domes 56
2.3.6. Stressed skin 57
2.3.7. Space frame 58
2.3.8. Brick and former 58
2.3.9. Foam and render 59
2.3.10. Monolithic dome 59
2.4. Thin concrete shells 62
2.4.1. Decline of concrete shells 62
2.4.2 Thin concrete shells and space grid structures 64
2.4.3. Alternative ways of forming thin concrete shells 65

3. NEW CONSTRUCTION METHOD AT VIENNA UNIVERSITY OF TECHNOLOGY 69
3.1. Introduction 70
3.1.1. New assembly method for precast elements 71
3.1.2. Shell formed by plane elements 72
3.1.3. New construction method 75
3.1.4. Wooden models 77
3.1.5. Innovations and advantages 80
3.2. Concrete shell construction 81
3.2.1. Previous planning 81
3.2.2. Anchorage elements 90
3.2.3. Construction process 99
3.3. Ice shell construction 102
3.3.1. Ice as construction material 102
3.3.2. Ice shell in the laboratory 103
3.3.3. Small ice shell 104
3.3.4. Big ice shell in Obergurgl 106

4. ANALYTICAL AND NUMERICAL ANALYSIS OF A SHELL 108
4.1. Shell parameters 109
4.1.1. Geometrical parameters of the shell 109
4.1.2. Material properties of the shell 110
4.1.3. Loads and boundary conditions 110
4.2. Analytical analysis formulation 111
4.2.1. Case 1: Dead load 114
4.2.2. Case 2: Snow effect. 115
4.2.3. Case 3: Wind effect. 118
4.3. FEM analysis with ABAQUS 128
4.3.1. ABAQUS overview 128
4.3.2. Steps in running ABAQUS 128
4.3.3. Data preparation. Units. 129
4.4. Concrete shell analysis 130
4.4.1. Case 1. Dead load. 130
4.4.2. Case 2. Snow effect. 136
4.4.3. Case 3. Wind effect. 138
4.5. Ice shell analysis 143
4.5.1. Case 1. Dead load. 143
4.5.2. Case 2. Snow effect. 148
4.5.3. Case 3. Wind effect. 150
4.6. Shell with a door analysis 153
4.6.1. Concrete shell 154
4.6.2. Ice Shell 158
4.6.3. Comparison analysis 160

5. TENDONS AND PNEUMATIC FORMWORK ANALYSIS 162
5.1. Tendons analysis 163
5.1.1. Shell planar elements 163
5.1.2. Geometrical calculations 164
5.1.3. Forces calculation 166
5.2. Pneumatic Formwork 172

6. CONCLUSIONS 174

References 177

List of Figures 180

List of Tables 185

ANNEXES 186
ANNEX I. DEAD LOAD IN THE SHELL 187
ANNEX II. WIND LOAD IN THE SHELL 188
ANNEX III. TENDONS ANALYSIS - CONCRETE SHELL 190
ANNEX IV. TENDONS ANALYSIS - ICE SHELL 192

1. SHELL STRUCTURES OVERVIEW

1.1. Introduction to shell structures

The word *shell* is an old one and is commonly used to describe a hard covering, spatially curved structure which supports external applied loads. Shells are found in a variety of natural structures such as eggs, plants, leaves, skeletal bones, and geological forms. The dictionary says that the word shell is derived from the Latin *scalus*, as in fish scale. But to us now there is a clear difference between the tough but flexible scaly covering of a fish, and the tough but rigid shell of a turtle [1]. Shell structures have also been built by man since the most ancient times. Many shell domes built of masonry and stone in ancient times, are still in existence in some parts of the world [2].

There are many interesting aspects of the use of shells in engineering, but one alone stands out as being of paramount importance: the *structural* aspect. The *theory of structures* tends to deal with a class of idealized mathematical models, stripped of many of the features that make them recognizable as useful object in engineering. Thus a beam is often idealized as a line endowed with certain mechanical properties, irrespective of whether it is a large bridge, an aircraft wing, or a flat spring inside a machine. In a similar way, the theory of shell structures deals, for example, with the "cylindrical shell" as an idealized entity: it is a cylindrical surface endowed with certain mechanical properties. The treatment is the same whether the actual structure under study is a gas-transmission pipeline, a grain storage silo, or a steam boiler.

In this introductory chapter, first some references will be made to a number of important and well-known fields of applications of shell structures. Then, engineering classifications of surfaces, as the main geometrical feature of shells, will be presented. Moreover, the general theory of thin shells basics is stated.

1.2. Applications of shell structures

Shell structures can be efficiently and economically used in various fields of engineering and architecture. The introduction of the *thin shell* as a structural form was an important contribution to the development of several branches of engineering. The following is a brief list, which is by no means complete [1].

Architecture and building. The development of masonry domes and vaults in the middle ages made the construction of more spacious buildings possible. In more recent times the availability of reinforced concrete has stimulated interest in the use of shells for roofing purposes. A great variety of shell roofs have been designed and constructed in many parts of the world.

Power and chemical engineering. The development of steam power during the Industrial Revolution depended to some extent on the construction of suitable boilers. These thin shells were constructed from plates suitable formed and joined by riveting. More recently the used of welding in pressure vessel construction has led to more efficient designs. Pressure vessels and associated pipework are key components in

thermal and nuclear power plants, and in all branches of the chemical and petroleum industries.

Structural engineering. An important problem in the early development of steel for structural purposes was to design compression members against buckling. A striking advance was the use of tubular members in the construction of the Forth railway bridge in 1889: steel plates were riveted together to form reinforced tubes as large as 12 feet in diameter, and having a radius/thickness ratio of between 60 and 180.

Vehicle body structures. The construction of vehicle bodies in the early days of road transport involved a system of structural ribs and non-structural panelling or sheeting. The modern form of vehicle construction, in which the skin plays an important structural part, followed the introduction of sheet-metal components, preformed into thin doubly curved shells by large power presses, and firmly connected to each other by welds along the boundaries. The use of the curved skin of vehicles as a load bearing member has similarly revolutionized the construction of railway carriages and aircraft. In the construction of all kind of spacecraft the idea of a thin but strong skin has been used from the beginning.

Composite construction. The introduction of fiberglass and similar lightweight composite materials has impacted the construction of vehicles ranging from boats, racing cars, fighter and stealth aircraft, and so on. The exterior skin can be used as a strong structural shell.

Miscellaneous Examples. Other examples of the impact of shell structures include water cooling towers for power stations, grain silos, armour, arch dams, tunnels, submarines, and so forth.

1.3. General structural features of shells

1.3.1. Continuity and curvature

The essential ingredients of a shell structure in all of the foregoing examples are *continuity* and *curvature* [1].

A pressure vessel must be obviously constructed to hold a fluid at pressure, although the physical components may be joined to each other by riveting, bolting or welding. On the other hand, an ancient masonry dome or vault is not obviously continuous in the sense that it may be composed of separate stone subunits or voussoirs not necessarily cemented to each other. But in general domes are in a state of compression throughout, and the subunits are thus held in compressive contact with each other. The important point here is that shells are *structurally continuous* in the sense that they can transmit forces in a number of different directions in the surface of the shell, as required. These structures have quite a different mode of action from *skeletal structures*, of which

simple examples are trusses, frameworks, and trees. These structures are only capable of transmitting forces along their discrete structural members.

The fundamental effect of *curvature* and its effect on the strength and stiffness of a shell is discussed in section 1.4.2.

1.3.2. The empirical approach

Many of the structures listed in 1.2 were constructed long before there was anything like a textbook on the subject of shell structures. The early engineers had a strongly empirical outlook. They could see the advantages of shell construction from simple small-scale models, and clearly understood the practical benefits of doing "overload tests" on prototypes or scale models. But in other areas of engineering, where precision is needed in the interest of economical design and where the geometry is more straightforward, the *theory of shell structures* is an important design tool [1]. The theory of shells will be explained later on in section 1.5.

1.3.3. Closed and open shells

Before describing the main body of the theory it is useful to discuss quantitatively an important practical point. Anyone can realise that a *closed* box is rigid, whereas an *open* box is easily deformable. The same sort of thing applies to an aluminium can, which may be squashed far more easily after an end has been removed [1].

There seems to be a *principle* here that *closed surfaces are rigid*. This is used in many areas of engineering construction. For example, the deck of a ship is not only a horizontal surface to walk on: it also closes the hull, making a box-like structure.

In practice, of course, it is not usually possible to make completely closed structural boxes. In a ship, for example, there will be various cut-outs in the deck for things such as hatches and stairways. It is sometimes possible to close such openings with doors and covers that provide structural continuity. Submarines and aircraft are obvious examples. But this is often not possible and compromise solutions must be adopted. The usual plan is to reinforce the edge of the hole in such a way as to compensate, to a certain extent, for the presence of the hole. The amount of reinforcement that is required depends on the size of the hole, and to what extent the presence of the hole makes the structure an open one. Large openings are essential in some forms of construction, such as cooling towers. A more extreme example is provided by shell roofs in general. Here the shell is usually very open, being merely a "cap" of a shell, and the provision of adequate edge ribs, together with suitable supports, is of crucial importance.

A main objective in the design of shell roofs is to eliminate those aspects of behaviour that spring from the open nature of the shell.

Moreover, it is difficult to quantify intermediate cases. The majority of actual shell structures fall into a grey area, neither open or close areas. While the effect of a small

cut-out on the overall rigidity of a shell structure may be trivial, the effect of a large cut-out can be serious. The crux of this problem is to quantify the ideas of "small" and "large" in this context. Unfortunately there is no simple way to do this, because the problem involves the interaction between "global" and "local" effects. It is largely for this reason that the subject of shell structures generally is a difficult one.

1.3.4. A simple geometric approach: convexity.

The notion that a closed surface is rigid is well known in the field of pure Euclidean geometry. There is a theorem of Cauchy which states that a convex polyhedron is rigid. The concept of *rigidity* is hedged around with suitable restrictions. It is significant that the qualifier *convex* appears in the theorem. Although it is possible to demonstrate by means of simple examples that some *non-convex* polyhedra (that is, polyhedra with regions of non-convexity) are rigid, it is also possible to demonstrate special cases of non-convex polyhedra which are not rigid, and are capable of undergoing infinitesimal distortions at least. This is a difficult area of pure mathematics [1].

For the present purposes we note that convexity guarantees rigidity whereas non-convexity may produce deformability.

1.3.5. A disadvantage of rigidity

While *rigidity* and *strength* are in many cases desirable attributes of shell structures, there are some important difficulties that can occur precisely on account of unavoidable rigidity. An example of this occurs in a chemical plant where two large pressure vessels, firmly mounted on separate foundations, are connected by a length of straight pipe. Thermal expansion of the vessels can only be accommodated without distortion if the pipe contracts in length. If it also expands thermally very large forces can be set up as a result of the rigidity of the vessels. In cases like this it is often convenient to accommodate expansion by a device such as a bellows unit. Alternatively, when the interconnecting pipework has bends, it is sometimes possible to make use of the fact that the bends can be relatively flexible. In the case of bellows and bends the flexibility is to a large extent related to the geometry of the respective surfaces. It is significant that both are *non-convex*. Nevertheless this of itself does not constitute a proper explanation of their flexibility [1].

1.3.6. Catastrophic failures

The property of closed shell structures being rigid and strong is of great practical values. But it should not be in ignorance of a well known design principle: *efficient structures may fail catastrophically*. Here the term "efficient" describes the consequences of using the closed shell principle. By designing a shell structure as a closed box rather than an open one we may be able to use thinner sheet material and hence produce a more efficient design.

On the other hand, thin shells under compressive membrane forces are prone to *buckling* of a particularly unstable kind. The rapid change in geometry after buckling and consequent decrease of load capacity leads to catastrophic collapse. This is illustrated by the well known experience of "crumpling" of thin wall cylinders like soda cans, under axial compression. The crumpling of a thin convex shell is accompanied by a loss of convexity, which partly explains why the post-buckling rigidity is so low [1].

1.4. Classification of shells surfaces

1.4.1. Thickness ratio

As in the case of plates, one can classify shell mathematical models in terms of the ratio of the thickness to a characteristic dimension [1]:

- Very thick: 3D effects
- Thick: stretching, bending and higher order transverse shear
- Moderately thick: streching, bending and first order transverse shear
- Thin shells: stretching and bending energy considered but transverse shear neglected.
- Very thin shells: dominated by stretching effects. Also called membranes.

The main difference from flat plates is that the determination of characteristic dimensions is more complex.

In this study the thin shell model will be followed.

1.4.2. Shell curvature

Using the definition of *Gaussian curvature* the shells are classified depending on the curvature [2].

The *geometry of a shell* is defined by the prescription of its middle surface and its thickness at all points. The plane curves formed by three intersecting planes containing normal to the surface are called *normal sections* of the surface at a point. In all these plane curves, formed by intersection, there will be one curve having a maximum value of curvature (K_1) and another having a minimum value of curvature (K_2). The two plane curves, formed by the normal plane sections are called the *principal sections*, and their curvatures K_1 and K_2 are called *principal curvatures*. These two intersecting principal sections are always *orthogonal* to each other.

The product of the two principal curvatures, $K=K_1 \cdot K_2$ is an algebraic quantity which is called the *Gaussian curvature*. Knowing the parametric equations of a surface, we can obtain the expressions for the principal curvatures, K_1 and K_2.

Depending on the Gaussian curvature value, we have three surfaces possibilities, see Figure 1:

— If $K>0$, the surface is said to have a *positive Gaussian curvature* or *synclastic* surface: as for example spherical domes and elliptic paraboloids.
— If $K<0$, the surface has a *negative Gaussian curvature* or *anticlastic* surface: as for example hyperbolic paraboloids.
— If $K_2=0$, $K_1\neq0$, the surface is said to have a single or *zero Gaussian curvature*: as for example cylinders and cones.

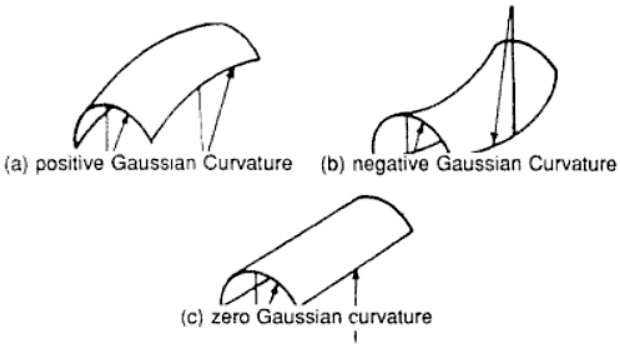

Figure 1. Surfaces with positive, negative and zero Gaussian curvature. (Source: [2]).

1.4.3. Geometrical developability

According to the geometrical developability shell surfaces are either *developable* or *nondevelopable*. Developable surfaces are the ones which can be "developed" into a plane form without cutting and/or stretching their middle surface. A nondevelopable surface, on the other hand, is a surface which has to be cut and/or stretched in order to be developed into a planar form [2].

Surfaces with double curvature are usually nondevelopable, whereas surfaces with single curvature are always developable. Surfaces with positive and negative Gaussian curvature are nondevelopable, while those with zero Gaussian curvature are developable, Figure 2.

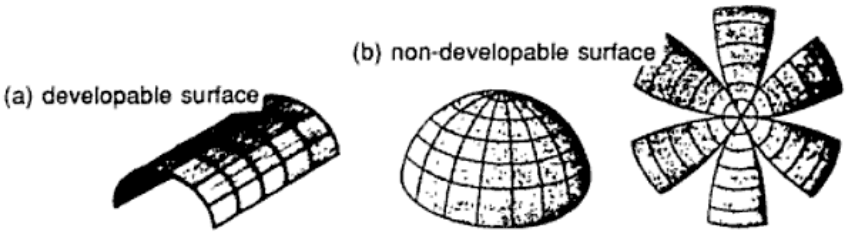

Figure 2. Developable and nondevelopable surfaces. (Source: [2]).

The classification of shell surfaces into developable and non-developable has some structural significance. From physical point of view, shells with nondevelopable surface

require more external energy, than do developable shells, to be "stretched out", i.e., to collapse into a plane form. Hence, one may conclude that nondevelopable shells are, in general, stronger and more stable than the corresponding developable shells having the same overall dimensions.

1.4.4. Shell surface generation

A third type of classification of surfaces, which is very useful in shell analysis and design, is the categorization of various surfaces into *surfaces of revolution*, *translational surfaces*, and *ruled surfaces* [2].

Surfaces of revolution

Surfaces of revolution are generated by the revolution of a plane curve, called the *meridional curve*, about an axis, called the *axis of revolution*. The axis of revolution, does not always have to intersect the meridional curve. In the special case of conical surfaces, the meridional curve consists of a linear segment. Examples of surfaces of revolution are shown in Figure 3.

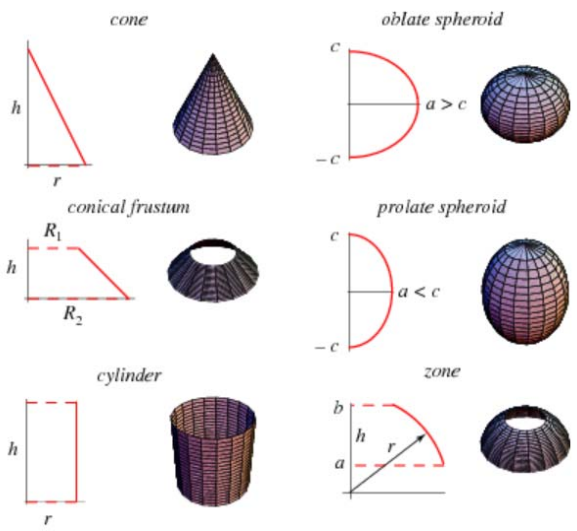

Figure 3. Surfaces of revolution examples. (Source: mathworld.wolfram.com)

Translational surfaces

Surface that is formed by the translation (linear movement) of a plane curve along a straight line or a plane curve, Figure 4.

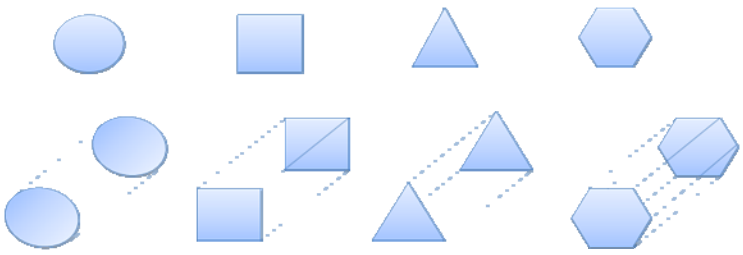

Figure 4. Translational surfaces.

Ruled surfaces
A ruled surface is a surface that can be swept out by moving a line in space. It therefore has a parameterization form. The straight lines themselves are called rulings. The rulings of a ruled surface are asymptotic curves.

Examples of ruled surfaces include the elliptic hyperboloid of one sheet (a doubly ruled surface). The only ruled minimal surfaces are the plane and helicoids, Figure 5.

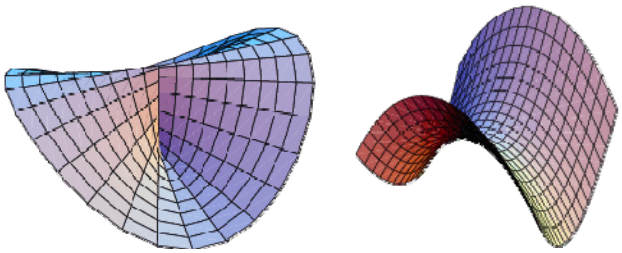

Figure 5. Ruled surfaces. (Source: mathworld.wolfram.com)

1.4.5. Shell surfaces summary

We can summarize and broadly classify the shell surfaces which are commonly used in engineering practice. It may be noted that the same type of shell may very well appear in more than one category [2].

— Singly curved, or shells of zero Gaussian curvature. In some cases, developable.
  Shells of revolution: circular cylinders, cones
  Shells of translation and ruled surfaces: circular or non-circular cylinders, cones
— Doubly curved shells having positive Gaussian curvature (synclastic shells); non-developable shells.
  Shells of revolution: spherical domes, ellipsoids of revolution, paraboloids of revolution.
  Shells of translation and ruled surfaces: elliptic paraboloids, paraboloids of revolution.
— Doubly curved shells with negative Gaussian curvature (anticlastic shells); non-developable shells.
  Shells of revolution: hyperboloids of revolution of one sheet.
  Shells of translation and ruled surfaces: hyperboloic paraboloids, conoids, hyperboloids of revolution of one sheet.
— Combinated shells, partly synclastic and partly anticlastic shells; shells composed of simpler shell forms.
— Shells with discontinuous curvature: folded plates.

1.4.6. Basic shell types

There are thousands of types of combined shells but only the basic types of shells are described here, with the elements of the structure, and the structural action [3].

Barrel Shells

The elements of a barrel shell are: the cylinder, the frame or ties at the ends, including the columns, and the side elements, which may be a cylindrical element, a folded plate element, columns, or all combined. For the shell shown in the sketch, Figure 6, the end frame is solid and the side element is a vertical beam.

A barrel shell carries load longitudinally as a beam and transversally as an arch. The arch, however, is supported by internal shears, and so may be calculated.

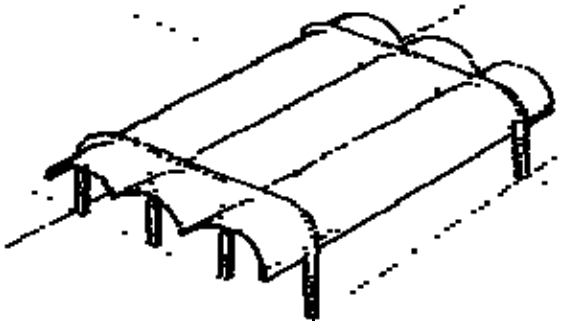

Figure 6. Barrel shells. (Source: [3])

Folded Plates

The elements of a folded plate structure are similar to those of a barrel shell except that all elements are planar, and the moments in the slab elements are affected by the differential movement of the joints.

For the structure shown, Figure 7, the end supports and the side supports are both complete walls

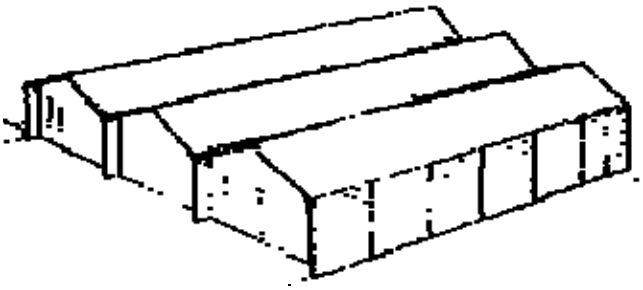

Figure 7. Folded plates. (Source: [3])

Short Shells

The elements of a short shell are the barrel, which is relatively short compared to radius, the element at the base of the cylinder to pick up the arch loads, and the arches or rigid frame to pick up the entire ensemble. In this case it is a ridgid frame arch. The size of the arch could have been reduced by horizontal ties at the springings. There may be multiple spans, Figure 8.

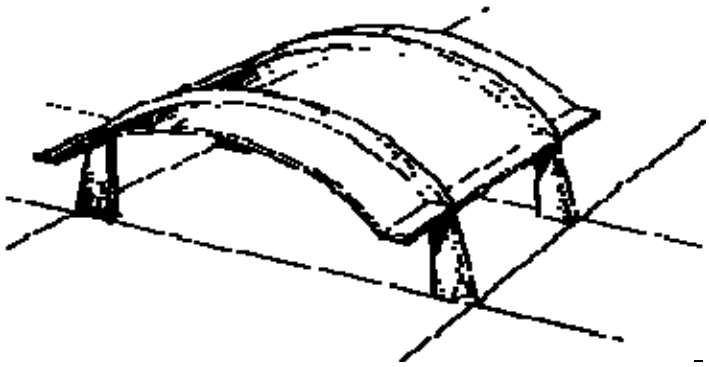

Figure 8. Short shells. (Source: [3])

The short shell carries loads in two ways: as an arch carrying load to the lower elements, and as a curved beam to the arches. The thickness of the shell can be quite thin due to these properties.

Hyperbolic Paraboloid

This is only one of thousands of possibile shapes for hypars, Figure 9. The surfaces are made by sliding a line over two other lines that are at varying angles. Consequently this surface can be constructed with straight boards. They have a slight twist depending on their width.

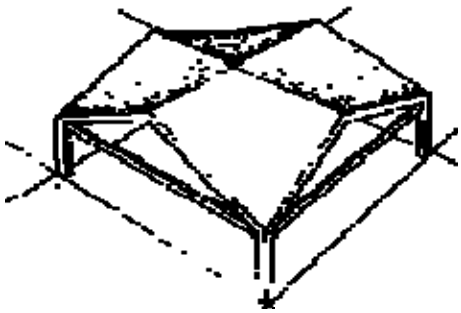

Figure 9. Hyperbolic paraboloid. (Source: [3])

The hyperbolic carries load in two directions. In this case, the diagonal element that sags is in tension, and the other element is an arch and is in compression. These forces must be picked up by the side ribs and delivered to the supports.

Domes

Domes are membrane structures, Figure 10; the internal stresses are tension and compression and are statically determinate if the proper edge conditions are fulfilled. In a dome of uniform thickness, under its own weight, the ring stresses are compression until the angle to the vertical is about 57 degrees.

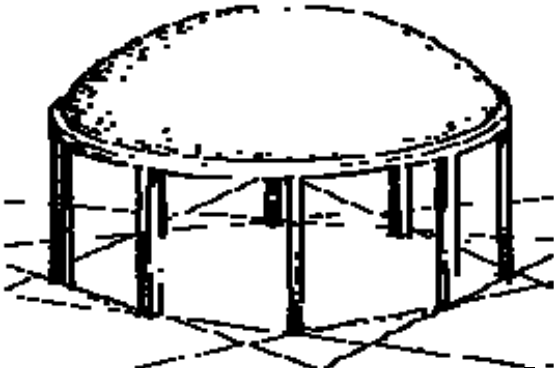

Figure 10. Dome. (Source: [3])

Translation Shells

A translation shell is a dome set on four arches, Figure 11. The shape is different from a spherical dome and is generated by a vertical circle moving on another circle. All vertical slices have the same radius. It is easier to form than a spherical dome.

Figure 11. Translation shells. (Source: [3])

The stresses in a translation shell are much like a dome at the top, but at the level of the arches, tension forces are offset by compression in the arch. However there are high tension forces in the corner.

1.5. General theory of thin shells

The purpose of this section is to introduce the design of thin shells by describing the physical behavior of certain well-defined systems and by deriving the general equations for the elastic analysis.

The design of thin concrete shells is a difficult issue mainly due to two reasons: rigorous analysis is so complex that the designer must resort to simplifications, this leads to extra caution; and the load-carrying capacity of thin curved structures often far exceed the prediction, hence thin shells are often stronger than the expert designer expectations.

The two most well-defined systems of thin shells commonly used in reinforced concrete construction are the dome and the segment of a cylinder. In each case some insight into the structural action can be obtained by comparing and contrasting systems for thin shells with similar planar ones [4].

1.5.1. Arch versus dome

Both structures are going to be considered. First we consider the loads acting on the arch. The uniform load on a parabolic arch produces practically no bending if the boundary conditions do not permit horizontal displacement. However, once the load is changed to a partial load, substantial bending develops in the arch. In the case of the dome the uniform load is carried by forces in the plane of the shell that are similar to the forces which carry the uniform load in the arch. However, in the dome additional forces (called *hoop forces*) are set up at right angles to these arching or *meridional forces*, Figure 12.

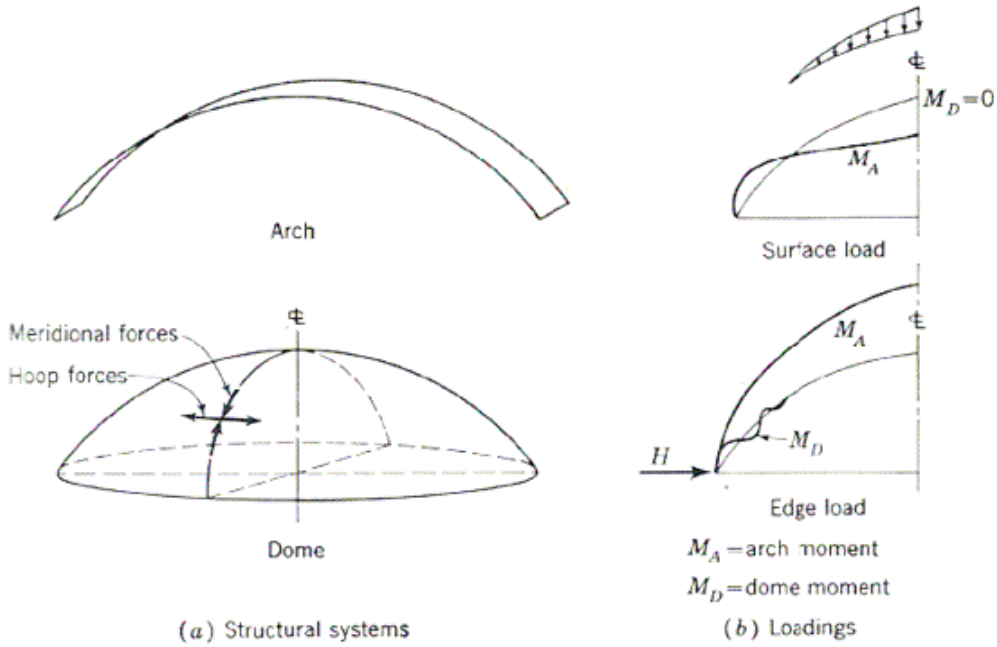

Figure 12. Arch and dome structures. (Source: [4])

The existence of two sets of forces in two separate directions within the shell makes this structural system similar to *plate structures*. The hoop forces, however, do not enter into the equations of vertical equilibrium. Therefore the entire vertical load must be transmitted by the meridional forces.

Now the case of the dome with a *partial load* is going to be considered. As long as this load has a smooth variation, that is to say as long as there is no strong discontinuity at the point where the load goes to zero, it will be observed that the shell is able to carry this load almost entirely by the same arching forces as before. This action is quite unlike the action of the arch, and the reason for the difference is the existence of the hoop forces. Physically one may say that as an arch segment of the dome attempts to bend under the partial load in the same way that the arch bends, the hoop forces restrain it just as if stiff rings were wrapped around the structure. Thus whereas the arch is best suited to only one type of loading, the dome is well suited to almost any type of loading within certain restrictions.

The effect of *boundary conditions*, or edge restraints, on both the arch and the dome structures must be taken into account. If the arch is given a horizontal push at one side, this force must be held in equilibrium by an equal and opposite force acting at the other support. The only way that the force can be transmitted through the system is up through the arch, over the crown, and down the other side. The effect clearly is to produce high bending moments throughout the entire arch system, with a maximum moment at the crown. We see, therefore, that the arch is not only restricted in its most efficient form by the nature of the loading but it is also very sensitive to foundation displacements or edge forces.

The same corresponding *horizontal force* can be also given to the dome. Such a force may be considered as a uniform horizontal thrust applied all around the circular edge of the dome. In cross section it would appear that this horizontal force would create bending moments throughout the dome similar to those created in the arch. This is, however, not the case. As the horizontal force tends to bend the shell, and thus to be carried up a meridian, the *hoop forces* again come into play and cause a rapid damping of the bending so that at a relatively short distance from the edge the bending effect is no longer observable. Thus edge forces in equilibrium applied to an arch propagate throughout the entire structural system and create large bending moments in a very narrow region near the edge and have generally no effect throughout a large portion of the structure.

1.5.2. Beam versus barrel

Just as arches are limited by functional requirements and do not find as wide application as beams, domes are also limited and do not find as wide application as barrels. In Figure 13 we can see beam and barrel systems, both of which are used in the framing of rectangular plan areas.

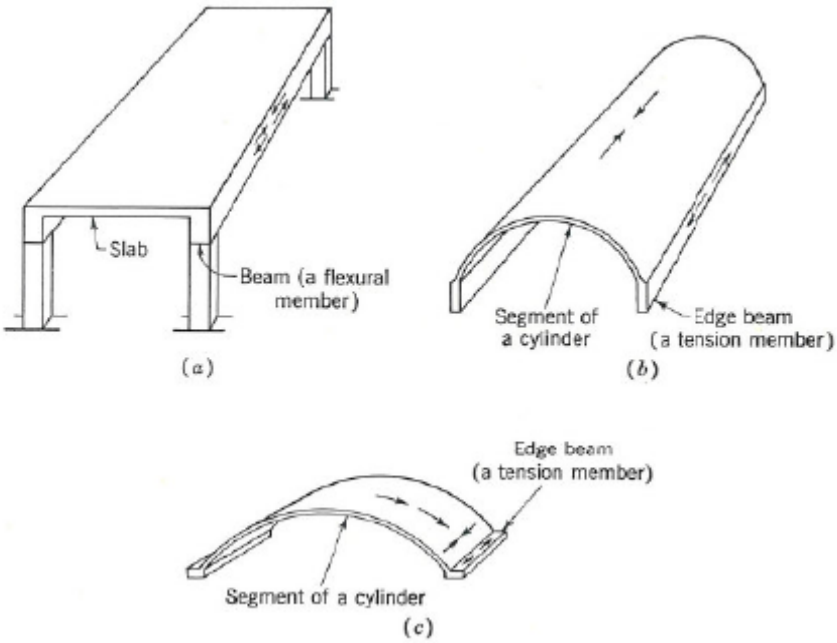

Figure 13. Beam and barrel systems. (Source: [4])

To make a close comparison, the shown framing plan in Figure 13a is going to be considered, in which the loads are essentially carried transversely by the slab and longitudinally by the beams. We may improve this system by building the slab and the beam monolithically, thus obtaining some T-beam action and thereby increasing considerably the stiffness of the beams. Since the beam is relatively shallow compared to its span, it is known that the simple flexural theory is valid and that the magnitudes of the stresses are directly proportional to the depth and vary as a straight line from top to bottom. Even in the slab the loads are essentially carried by bending moments, the sizes of which are functions of the transverse span.

If now the slab is given a curvature and the longitudinal beams are reduced in cross section, as shown in Figure 13b, a typical simply supported barrel shell spanning the same distance as the beams in Figure 13a is obtained. The structural action, however, is significantly different.

Considering the transverse slab, which is now curved, it is logical to think that this would act as an arch, but it does not because the slender edge beam is unable to sustain horizontal forces. Therefore, although the curved slab will try to act as an arch, the thrust contained at the springing lines will be very small. The principal structural action of this system is found to be longitudinal. In the previous case the beam had to carry the entire load with perhaps some additional flange help from the slab, but in this case the entire system acts as a beam with curved cross section to carry the load.

The principal action, therefore, of the barrel shell with small flexible edge beams is longitudinal bending, but the bending stresses are within the plane of the shell itself. Thus the entire shell-and-edge-beam system can be like a beam with the compression stresses near the crown and with the tension stresses concentrated in the edge beam on either side. In fact one approximation for a certain class of barrel shells which makes

use of the simple flexural theory is based entirely upon this physical picture of the system.

However, the simple flexural theory, which leads to a straight-line stress distribution, requires that all points within the cross section of a member deflect exactly the same amount, which is the case in a solid rectangular beam. In a T beam with wide flanges the extremities of the flanges may not deflect the same as the web. In a barrel shell the cross section may undergo substantial lateral distortion, and it is principally this distortion which causes the longitudinal stresses to depart from the straight-line distribution of the beam theory.

It is roughly true that the longer the span in comparison with the transverse-chord width, the more the entire cross section behaves as a beam. The shorter span compared with the chord width, the more the structure behaves as an arch with a supporting sloped deep beam near the edge, see Figure 13c.

All of the analysis which follows are based on elastic behavior and are thus suitable for working-load analyses. A number of procedures have been proposed for analyzing various types of thin shells for ultimate loads. Experimental evidence is, however, not very abundant. It is a defect of current design methods that ultimate-load analyses are not available for thin shells.

In dome-type shells the small ratio of thickness to radius of curvature often results in a buckling-load capacity which is considerably below the ultimate-load capacity based on steel yield strength and on concrete cylinder strength. It is also important to treat stability or plasticity (ultimate-load behavior) of thin shells.

A general elastic theory of thin shells is developed. First formulated by A.E.H. Love in 1888 [41], and then well presented by Wang [42] and others. The alternative approach of developing the equations separately for each system was well presented by Timoshenko [43].

1.5.3. Analysis of thin shells

A *thin shell* is a curved slab whose thickness h is small in compared with its other dimensions and compared with its principal radio of curvature r_x and r_y. The surface that bisects the shell thickness is called the *middle surface*, and by specifying the form of this surface and the thickness h at every point, we completely define the geometry of the shell.

This method of *thin shells analysis* consists first of establishing equilibrium of a differential element cut from the shell, Figure 14, and second of achieving strain compatibility so that each element remains continuous with each adjacent element after deformation.

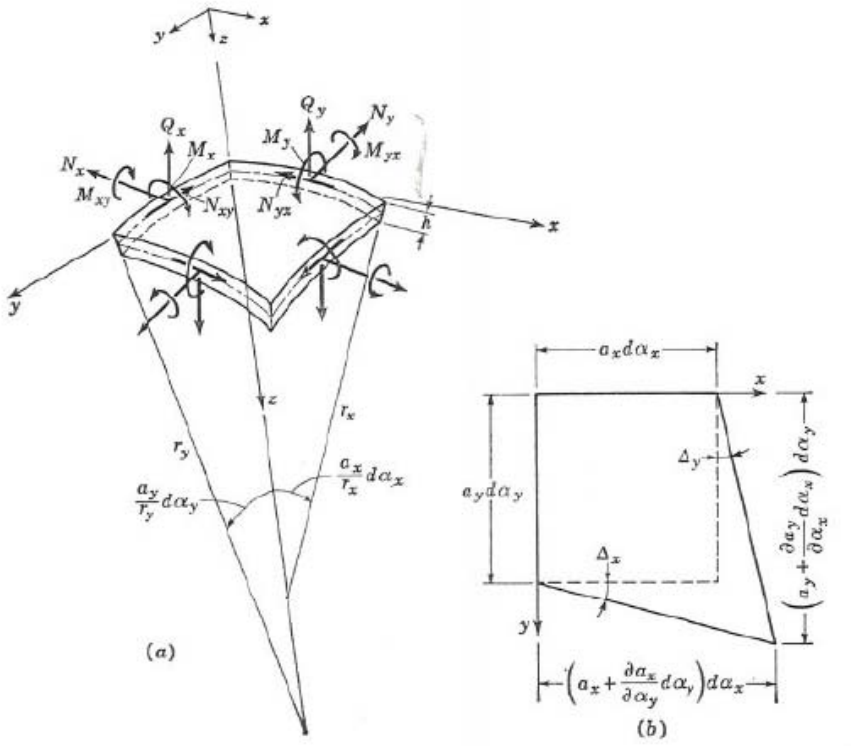

Figure 14. Equilibrium of a differential element cut from the shell. (Source: [4])

Stress resultants and *stress couples*, defined as the total forces and moments acting per unit length of middle surface, Figure 14, are the integrals of stress over the shell thickness, Figure 15.

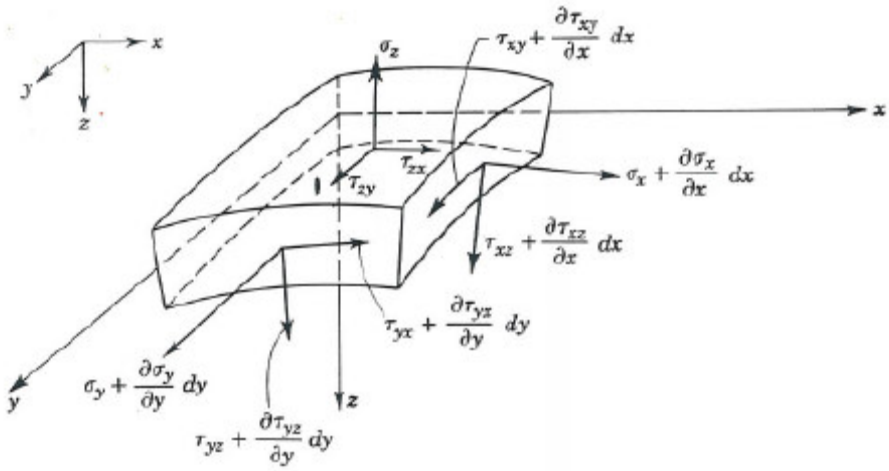

Figure 15. Stress resultants and stress couples. (Source: [4])

$$N_x = \int_{-h/2}^{+h/2} \sigma_x \left(1 - \frac{z}{r_y}\right) dz \qquad N_y = \int_{-h/2}^{+h/2} \sigma_y \left(1 - \frac{z}{r_x}\right) dz$$

$$N_{xy} = \int_{-h/2}^{+h/2} \tau_{xy} \left(1 - \frac{z}{r_y}\right) dz \qquad N_{yx} = \int_{-h/2}^{+h/2} \tau_{yx} \left(1 - \frac{z}{r_x}\right) dz$$

$$Q_x = \int_{-h/2}^{+h/2} \tau_{xz} \left(1 - \frac{z}{r_y}\right) dz \qquad Q_y = \int_{-h/2}^{+h/2} \tau_{yz} \left(1 - \frac{z}{r_x}\right) dz$$

$$M_x = \int_{-h/2}^{+h/2} \sigma_x z \left(1 - \frac{z}{r_y}\right) dz \qquad M_y = \int_{-h/2}^{+h/2} \sigma_y z \left(1 - \frac{z}{r_x}\right) dz$$

$$M_{xy} = -\int_{-h/2}^{+h/2} \tau_{xy} z \left(1 - \frac{z}{r_y}\right) dz \qquad M_{yx} = -\int_{-h/2}^{+h/2} \tau_{yx} z \left(1 - \frac{z}{r_x}\right) dz \qquad (1)$$

If the terms z/r_y and z/r_x are neglected when they appear with unity, then Equation 1 with $\tau_{xy} = \tau_{yx}$,

$$N_{xy} = N_{yx}$$
$$M_{xy} = -M_{yx} \qquad (2)$$

The stresses σ_z, τ_{zx}, and τ_{zy} are also neglected because of the small shell thickness, Figure 15; thus the twisting moments about the z axis are normally taken as zero.

Small-deflection theory, which is normally the basis for analysis of thin shells, implies that the deflections under load are small enough so that changes in geometry of the shell will not alter the static equilibrium of the system. This assumption is used in frame analysis to justify superposition.

Linear elastic behavior, also generally used in analysis of thin shells, provides a direct relationship between stress and strain by which the equilibrium of the stress resultants and stress couples is related to the strain compatibility equations.

In addition, the following assumptions are made:

- Points on lines normal to the middle surface before deformation remain on lines normal to the middle surface after deformation.
- Deformations of the shell due to radial shears (Q_x and Q_y) are neglected.

Both of these assumptions have been used in elementary beam theory as plane sections remain plane after bending, and deformations due to shear are neglected.

Based on the above definitions and assumptions, the *general shell theory* can be formulated in five steps by:

1. Determining the *equilibrium* of forces on the differential element (five equations with eight unknowns).

2. Establishing *strain-displacement relationships* (six equations with three unknowns).
3. Establishing *stress-strain relationships* by assuming material properties (three equations with six unknowns) and then deriving *force-displacement equations* (six equations with three unknowns).
4. Transforming the force-strain relationships into force-displacement equations (still six equations with three unknowns).
5. Obtaining a complete formulation by combining the force-displacement equations with the equilibrium equations (11 equations with 11 unknowns).

2. DESIGN AND ANALYSIS OF A DOME

2.1. Historical overview

The first and ancient presence of thin double curved shells structures can be found in nature: hard covering of eggs, plants, fruits, crustacea, tortoises, skeletal bones, or geological forms, are some examples. These shells are spatially curved structures which support external applied loads and protect from environmental changes [2].

Shell structures have been built by man since the most ancient times. Dome, in architecture, is a curved roof or vault, usually hemispherical in section and circular or oblong in plan, without angles or corners, which allows huge spaces in buildings, as well as the possibility of a powerful lighting. Despite they can be thin; domes are a stronger architectural element, thanks to compressive forces they create.

Until the 19th century, domes were constructed of masonry, of wood, or of combinations of the two, frequently reinforced with iron chains around the base to contain the outward thrust of the structure. Since then, as industrial technology developed, domes have been constructed of cast iron, reinforced concrete, steel, aluminum, laminated wood, or plastic [9] [5].

Origins

The dome seems to have developed as roofing for circular mud-brick huts in ancient Mesopotamia about 6,000 years ago. In the 14th century BC the Mycenaean Greeks built tombs roofed with steep corbelled domes in the shape of pointed beehives (tholos tombs). Otherwise, the dome was not important in ancient Greek architecture.

After about 1600 BC the Mycenaeans, ancient inhabitants of the south-eastern Greek mainland, buried their dead in tholos tombs, stone chambers with beehive-shaped domes. This tholos tomb, (c. 1300-c. 1250 bc), mistakenly named as the *Treasury of Atreus*, Figure 16, by its discoverer, consists of stone blocks arranged in superimposed concentric circles. The vault reaches a height of about 12 m, Figure 17, [9].

Figure 16. Treasury of Atreus, Mycenae. (Source: [9])

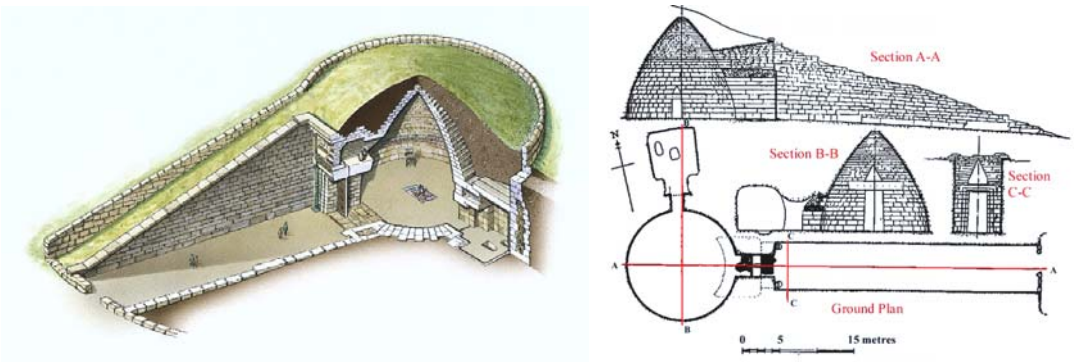

Figure 17. Sectioned view of Treasury of Atreus at Mycenae, Greece. (Source: dkimages.com)

The *Stupa in Sanchi* (India, 3rd century BC) is also remarkable, Figure 18. The most elaborate and well known of the more than 50 magnificent Buddhist monuments that crown the hilltop of Sanchi, India, is Stupa Number One or the Great Stupa. It is part of an entire complex of structures, mostly stupas, built between the 3rd Century BCE and the 12th Century AD. The stupa is not a building in any traditional sense. Once a burial or reliquary mound, the stupa has become a purely symbolic object. The Great Stupa is 120 feet across (36.6 meters) and, excluding the railing and umbrella, is 16,46m high [8].

Figure 18. Stupa in Sanchi. (Source: fog.ccsf.org)

The Romans developed the masonry dome in its purest form, culminating in the *Pantheon of Hadrianus*, Figure 19. The Pantheon in Rome is one of the most famous buildings in the world. It was commissioned by Hadrian in 118 and completed in 128 AD. Set on a massive circular drum 6 m thick that conceals eight interlocked masonry piers, the coffered dome rises 43 m to form a perfect hemisphere on the interior, with a large oculus (roundel) in the centre. The oculus (a round opening) at the top is 8.5 m in diameter and provides the only source of light for the interior [9].

Figure 19. Pantheon of Hadrianus, Rome. (Source: [9])

The massive size of the Pantheon is accompanied by a tremendous weight. Roman architects used ingenious design to create a stable structure without the use of internal supports. The tremendous weight of the stone on top of the entryways, windows, and passages would cause them to collapse. The architects solved this problem with the use of arches, Figure 20. Arches take the tremendous force of the stone above it and redirect this force through its sides to the Pantheon's support walls and piers. These support walls and pillars provide a horizontal normal force to counteract the force of the stone above the arches. The structure's weight is channeled through the piers to its foundation [7].

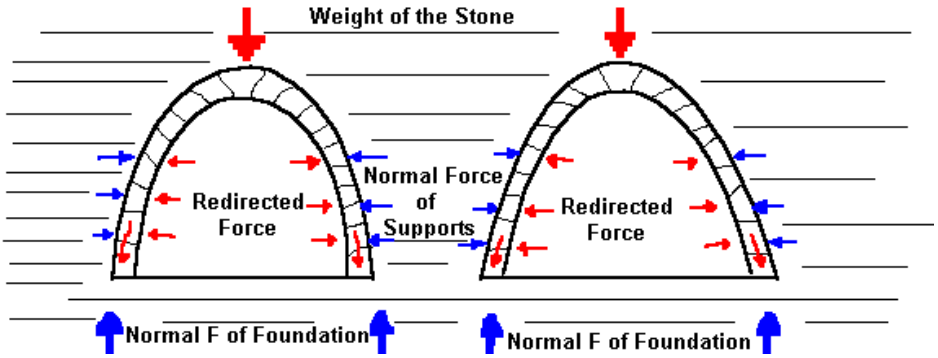

Figure 20. Distributing the Pantheon's Weight. (Source: [7])

Parallel, in Persia appeared the first domes in which pendentives were used from the beginning. This new element provided a strong support to domes, allowing them to become higher and the walls to become progressively thinner. First examples are found in the Sassanid *palaces of Firuzabad and Fars*, erected around 240 and 430, respectively. The technique spread to other areas of Central Asia, being most important the *mausoleums of Bokhara* (943) *and Tim* (978), but it did not evolve dramatically, Figure 21 [5].

Figure 21. The mausoleums of Bokhara. (Source: losviajeros.com)

The use of domes was continued in the Early Christian period for relatively small circular structures such as mausoleums and baptisteries. A typical example is the *Church of Santa Costanza* (c. 350), Rome, originally the tomb of Constantia, daughter of the emperor Constantine the Great, Figure 22. Byzantine architects were far more inventive in their use of domes. In the Byzantine capital of Constantinople, a succession of large domed churches reached its apogee in *Hagia Sophia*, the church built (532-537) for the Emperor Justinian I. Its shallow dome, 31 m (100 ft) wide and ringed with windows at its base, is supported on four pendentives (spherical triangles) backed by immense exterior piers and by a series of semi-domes [9].

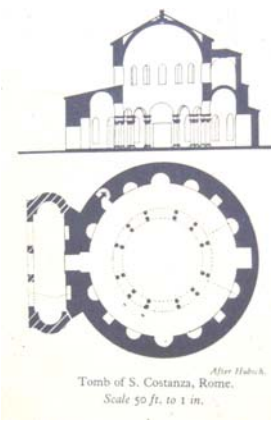

Figure 22. Church of Santa Costanza. (Source: intranet.arc.miami.edu and contracosta.edu)

After Constantinople fell to the Seljuk Turks in 1453, *Hagia Sophia* was converted into a mosque and became the model for a number of vast domed mosques built throughout the Ottoman Empire in subsequent centuries, Figure 23. Even before that, however, there was a long tradition of Islamic domed buildings (palaces, mosques, tombs, and baths); the Dome of the Rock (691) in Jerusalem is one of the earliest examples. Set on a pillared arcade, its double dome is of timber construction. Perhaps the most famous Islamic structure is the Taj Mahal in Agra, India, built (1631-1648) by the Mughal ruler Shah Jahan as a mausoleum for his favourite wife. Its slightly bulbous white marble dome rises on a tall drum over a spacious equilateral building.

Figure 23. Hagia Sophia, Constantinople (532). (Source: barber.org.uk and contracosta.edu)

It was also Byzantine engineers who designed the *Mosque of the Rock* (691) in Jerusalem and the *Great Mosque of Damascus* (715). Soon the Islamic style adopted the so-called onion dome, which later passed to Russia in the XIII century [5].

Figure 24. Mosque of the Rock (691) in Jerusalem. (Source: [5])

Meanwhile, in Western Europe, domes disappeared from architecture after the fall of the Roman Empire. There were several good attempts, such as half domes (apses), rib vaults or troncoconic domes such as the one in the *Baptistry of Pisa*, finished in 1363 (the current one is more recent, though), but the technique of the semispheric dome had disappeared [5].

Renaissance, Baroque, and Neo-Classical Domes

The first great Italian Renaissance dome was the majestic octagonal dome built (1420-1436) by the architect Filippo Brunelleschi for *Florence Cathedral*, Figure 25. The immense structure, 39 m (130 ft) in diameter and 91 m (300 ft) tall, is topped with a lantern 16 m (52 ft) high, and consists of an outer roof shielding an inner masonry shell. The 8 primary ribs and 16 secondary ribs form a tightly interlocked masonry cage. He took inspiration from the circular dome in the Rome Pantheon, and designed his with double shell and octogonal shape. The dome lied on a drum, instead of directly on the roof, thus avoiding scaffolds from the ground level [9].

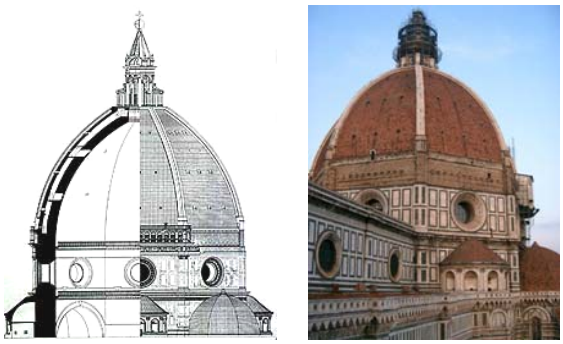

Figure 25. Santa Maria del Fiore, Florence. (Source: members.iinet.net.au)

In this manner he built the highest dome at the time, and a true architectonic model, since it was copied in *Saint Peter* of Rome by Giacomo della Porta (not Michelangelo) in 1593. The later domes of Saint Paul in London (1708) and the Capitol in Washington (1850) use the same technique [5].

In northern Europe, the most notable domes in Baroque style were built. The resplendent *Church of St Louis des Invalides* in Paris, built (1676-1706) by Jules Hardouin-Mansart has a dome (28 m/92 ft wide) set on two unusually tall drums pierced with large windows that flood the interior with light. Sir Christopher Wren's noble dome for *St Paul's Cathedral* (1675-1711), London, incorporates a shallow inner dome, a conical masonry shell supporting the high lantern, and an outer lead-sheathed dome of timber, Figure 26.

Figure 26. The main dome of St Paul's Cathedral, London. (Source: alps-uk.com)

The U.S. Capitol dome, built in 1793, gets its height from this engineering sleight of hand. The large outer dome is a thin shell, held up by a ring of curved iron ribs, Figure 27. Underneath it all is a smaller, self-supporting dome, visible only from the inside. The U.S. Capitol dome is also one of the earliest domes made of pre-fabricated cast-iron ribs. The switch from heavy masonry to lightweight metal ribs in the late 18th century greatly reduced the weight of domes being built around the world [6].

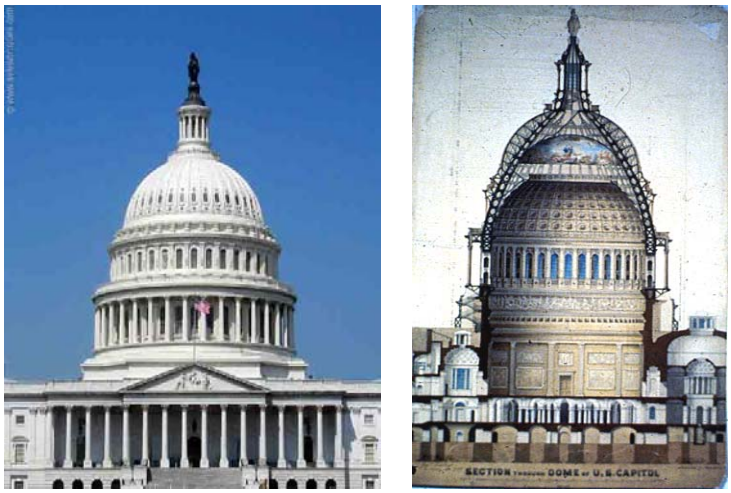

Figure 27. United States Capitol, Washington. (Source: [6])

Still paralelly, in Persia, the dome of the *Oljeitu Mausoleum* (Soltaniyeh, 1312) was built. This was, in fact, the first double-shell dome, and was additionaly reinforced with arches between both shells, which was an architectural revolution in the Muslim world, comparable to that of Brunelleschi. It started an architectural trend that designed domes as big as the *Mausoleum of Khoja Ahmed Yasavi* (Kazakhstan, 1405) and the *Taj Mahal (*India, 1653) [5].

The marble dome of the *Taj Mahal* has a height of about the same size as the base of the building, about 35 meters, and is accentuated as it sits on a cylindrical "drum" of about 7 metres high. This dome is a clear example of the so called onion-dome, Figure 28.

Figure 28. The Taj Majal dome. (Source: www.topnews.in)

One of the most characteristic elements of the Baroc architecture was the oval dome, invented by Giacomo da Vignola (chapel of Saint Andreas, Rome, 1553) and especially developed in the churches of Bernini and Borromini. This kind of dome gave a dramatic dynamism to Baroc churches. The biggest of this kind was built by Francesco Gallo in the *Basilica of Vicoforte* (Italia, 1773).

Through the XIX century some domes made out of glass and iron have been built. Walter Benjamin was the first who wrote about iron and glass construction in his work "Paris, capital of the 19th century". Then Günther Bantmann has designed the Galleria Vittorio Emanuele and since then several projects and constructions have been carried out by using this materials.

20th-Century Domes

The technological developments of the 20th century have radically changed the concept and construction of the dome. New techniques and construction procedures of domes have been developed, as well as new materials have been introduced.

Modern *thin concrete shells*, which began to appear in the 1920s, are made from thin steel reinforced concrete, and in many cases lack any ribs or additional reinforcing structures, relying wholly on the shell structure itself. Shells may be cast in place, or pre-cast off site and moved into place and assembled. The strongest form of shell is the *monolithic shell*, which is cast as a single unit. The most common monolithic form is the dome, but ellipsoids and cylinders are also possible using similar construction methods.

Monolithic domes are cast in one piece out of reinforced concrete, and date back to the 1960s. Advocates of these domes consider them to be cost-effective and durable structures, especially suitable for areas prone to natural disasters. They also point out the ease of maintenance of these buildings. Monolithic domes can be built as homes, office buildings, or for other purposes.

The *Seatle Kingdome* was the world's first (and only) concrete-domed multi-purpose stadium. It was completed in 1976 and demolished in 2000. The Kingdome was constructed of triangular segments of reinforced concrete that were cast in place. Thick ribs provided additional support.

The *geodesic dome*, patented by the American inventor R. Buckminster Fuller in 1947, is composed of a lattice of interlocking tetrahedrons and octahedrons made of lightweight materials, leaving the interior free of structural supports. A geodesic dome is an almost spherical structure based on a network of great circles (geodesics) lying approximately on the surface of a sphere. The geodesics intersect to form triangular elements that have local triangular rigidity and yet also distribute the stress across the entire structure. Geodesic domes are far stronger as complete units than the individual struts would suggest.

The first dome that could be called "geodesic" was designed just after the World War I by Walther Bauersfeld for a planetarium. The dome was patented and it was constructed on the roof of the Zeiss plant in Jena, Germany 1922. Some thirty years later R.Buckminster Fuller further investigated this concept and named the dome "geodesic" from field experiments. The geodesic dome appealed to Fuller because it was extremely strong for its weight, its "omnitriangulated" surface provided an inherently stable structure, and because a sphere encloses the greatest volume for the least surface area.

Its many uses are exemplified by the *Climatron*, the gigantic climate-controlled botanical garden completed in St Louis, Missouri, in 1960, Figure 29 [9].

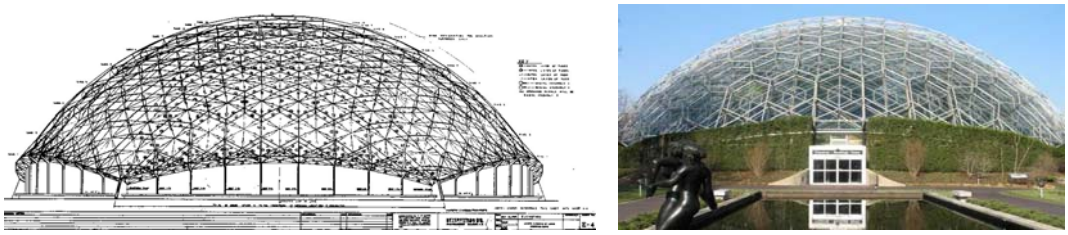

Figure 29. Climatron, botanical garden completed in St Louis, Missouri. (Source: jug.net and mobot.org)

Today, geodesic domes come in an almost endless variety of shapes and styles. The dome was successfully adopted for specialized industrial use, such as the 1958 Union Tank Car Company dome near Baton Rouge, Lousiana and specialty buildings like the Henry Kaiser dome, auditoriums, weather observatories, and storage facilities.

Another dome from Expo 67 in Montreal was built as part of the American Pavilion, Figure 30. The structure's covering later burned, but the structure itself still stands and, under the name Biosphère, currently houses an interpretive museum.

Figure 30. Geodesic Dome, Montreal. (Source: [9])

In the 1970s the *Cinesphere* dome was built at the Ontario Place amusement park in Toronto, Canada. In 1975, a dome was constructed at the South Pole, where its resistance to snow and wind loads is important.

Possibly one of the most famous domes in the world, the *Epcot Center* in Orlando, Florida, is also a geodesic dome, Figure 31. The EPCOT dome is a complete geodesic sphere which stands 54,8 m tall, is supported on 6 steel legs 4,5 m off the ground, and is constructed of a steel frame dressed with aluminum panels. The sphere diameter of 50 m encloses 523 thousand cubic meters of airspace.

Figure 31. Epcot Center in Orlando, Florida. (Source: destination360.com)

A new generation of domes equipped with retractable roofs, like the *Toronto SkyDome,* has become a popular choice for sports stadiums throughout the world.

Figure 32. Toronto SkyDome. (Source: dkimages.com and pbs.org)

Steel dome construction, which also leaves the interior free, dates back to the late 19th century but was spectacularly adapted to sports-arena use in the *Astrodome*, completed in Houston, Texas, in 1965, Figure 33. Its plastic roof is 195 m (642 ft) wide at the bottom tension ring of the structure [9].

Figure 33. Astrodome, Texas. (Source: johnnyroadtrip.com)

Reinforced concrete is also used in modern dome construction, as in the *Palazetto dello Sport* (Small Sports Stadium) created in Rome by the Italian architect-designer Pier Luigi Nervi for the 1960 Olympic Games; its pre-cast units are united by poured-in-place concrete ribs. Two domes that attracted a lot of publicity at the close of the

century were the work of British architects: Richard Rogers' *Millennium Dome* (1999) in London, Figure 34, and the remodeled roof of the *Reichstag* building in Berlin (1999), by Norman Foster.

Figure 34. Millenium Dome, O2 Complex, Greenwich. (Source: [9])

The O2 complex was originally built under the name "Millennium Dome", designed by Richard Rogers. The 12 pre-fabricated steel masts from which the dome's canopy is suspended, each 100 m (328 ft) high, were erected in October 1997, while work on the ground slab and service structures continued. The structural grid on which the dome's canopy would be suspended, consisting of 7 circumferential cable rings and 72 radial cables, was then put in place, with guy wires from the masts running from the innermost cable ring to anchor points outside the dome. From March 1998 the Teflon-coated roof panels began to be mounted, and the completion of this process in June 1998, exactly a year after construction began, marked the end of the main building phase. The dome's diameter is 320 m (1,050 ft), giving the floor of the structure an area of 80,425 sq m (865,370 sq ft, or almost 20 acres). Its circumference is 1,005 m (3,297 ft), and the height of the canopy at the centre is 50 m (164 ft). During the Millennium Experience exhibition the dome was able to accommodate about 37,000 people at any one time.

2.2. Structural behavior

Although the use of the dome begins with the Mycenae civilization, it presents a clear historical reference, the *Pantheon in Rome* (120-124 AD) consisting of a vertical cylinder with a hemisphere of 43.5 m of light, it would take nineteen centuries to be overcome [10].

Due to its compression operation the stone was the material most used in the construction of domes, with their form of voussoirs as meridians and parallels. In the fifteenth century Brunelleschi built the dome of *Santa Maria di Fiore*, with octagonal geometry and a double blade section, designed in successive overhangs to avoid the use of centrings, whose construction was not feasible.

The problem why the domes did not exceed the 43.5 m of high was the appearance of traction efforts which collapse the structure, hence the introduction of reinforced concrete suppose a revolution in the domes concept, allowing using both compression and traction resistance.

This led to an understanding of the domes as *surface of revolution*, which achieved to get higher slenderness.

Moreover, a dome presents certain geometric problems due to the need for accommodation of the circular floor on an octagonal or square support frame. Historically the following solutions have been used:

- In *Hagia Sophia* they started with a dome obtained by slicing the hemisphere by four vertical planes, is supported on four arches *fajones*, from there the main hemisphere and the four spherical triangles are separated by a row of windows.
- The use of a *drum* can be the easiest solution.
- The solution of Bramante for *St. Peter's*, based on using *chamfer pillars*, which are positioned in a octagon between the *drum* and the floor square frame. With this the support arches reduce the dome high and the *pechinas* are practically nonexistent.

Empirical Rules

The classical structural calculation of domes was based on a set of design and dimensioning empirical rules. Basically two types of rules can be followed: dimensioning with graphic construction design and through rational formulations.
Alberti, *Fray Lorenzo*, *Palladio* ..., studied in a quite successful way the domes behavior. *Alberti* got to know the rings and domes meridians behavior and he built domes with the successive cantilever construction method.

Frezier associate the thrusts of the domes with the thrusts of the barrel vault, saying that the thrust of the first is half of the thrust of the second. This assertion can be discussed analytically, and is quite accurate.

The Italian architect *Fontana* proposes a graphical construction for domes. This leads to successive motions from *Sangallo*, *Michelangelo* and *Della Porta*, being necessary to resort to the *pointed profile*. The Fountain solution is based on the pointed profile, with variable thickness and elevation over the drum. The thickness of the base is one fourteenth of the high, Figure 35.

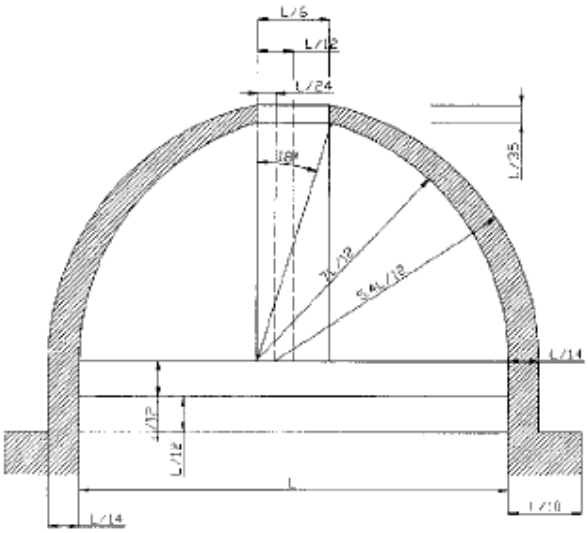

Figure 35. Fontana, graphical construction for domes. (Source: [10])

Structural behavior of domes

Dome structures must provide strength, stiffness and stability. They must be capable of supporting applied loads and self weight without excessive deflection or displacements. Similar to an arch, a dome develops internal *meridional forces* that transfer loads to a support structure at its base, Figure 36. These forces are compressive and increase in magnitude from crown to the base for any dome loaded axisymmetrically by self weight [11].

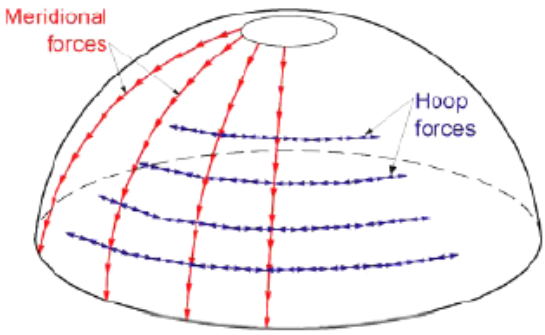

Figure 36. Domes develop internal meridional and hoop forces. (Source: [10])

Unlike an arch, a dome can resist out-of-plane bending of the meridian by developing internal *hoop forces* that act in the latitudinal direction as parallel rings. Hoop forces allow ring-by-ring construction of a dome without centering, an unfeasible task for an arch. As a result, though an arch is unstable without its keystone, a dome with an oculus is perfectly stable.

The resistant mechanism of the domes has a peculiarity that makes them far superior to the structural capacity of the arches. Each meridian is behaving like a funicular arch of the applied loads, so it resists the loads without developing flexion strains for any system of loads. The transversal curvature of the two opposite segments does not coincide with the catenary. The difference appears when 52º measured from the axis of rotation, Figure 37 [10].

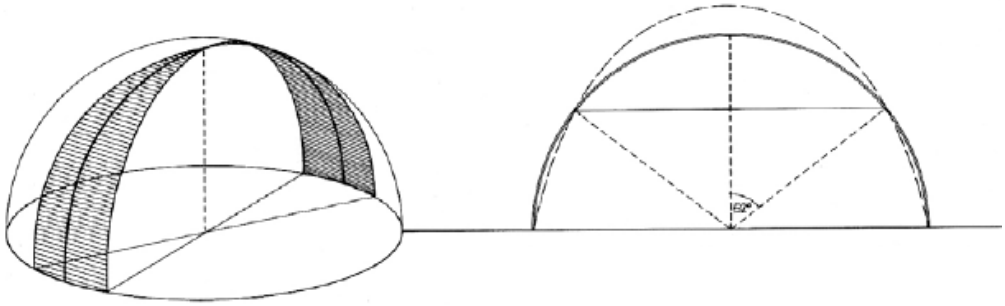

Figure 37. Division into segments of the dome. (Source: [10])

When a symmetric load acts, the upper zones of the segments descend and overlap with the edges when the curvature decreases. The lower zones deform outwards and open with the increasing in curvature, Figure 38.

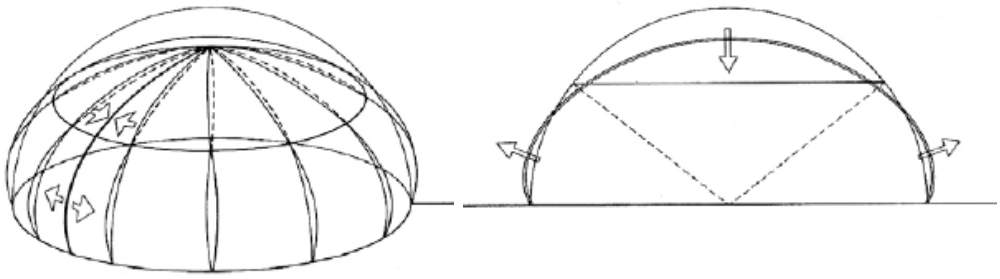

Figure 38. Segments deformation in the dome. (Source: [10])

The membrane ability of the dome to generate hoop efforts avoids the dome deformation. The annular continuity opposes to the deformation, the upper part act as a sequence of compressed rings and the lower part like tensile rings, Figure 39.

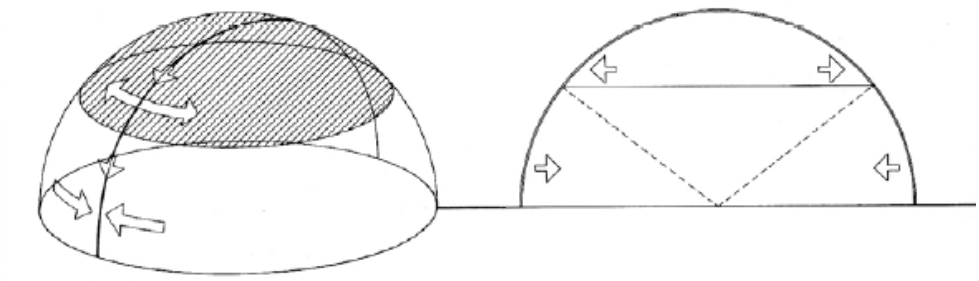

Figure 39. Effect of the hoop forces in the dome. (Source: [10])

The dome has some parallels which restrict its lateral movement developing tension in the ring and making possible a membrane behavior. In a reduced dome, with an angle less than 52º, the meridians are deformed inwards, toward the axis of the dome, and the parallels transversal to the meridians compress trying to stop it.
When the dome is very high, under the action of the loads, the highest points are moved inwards, but the lowest do outwards, so away from the axis: the parallels below the angle of 52º are subjected to traction efforts.
To all this can take place and knowing that the dome only hold its own membrane efforts, the edges have to be able to develop free *horizontal displacement* in their supports, Figure 40.

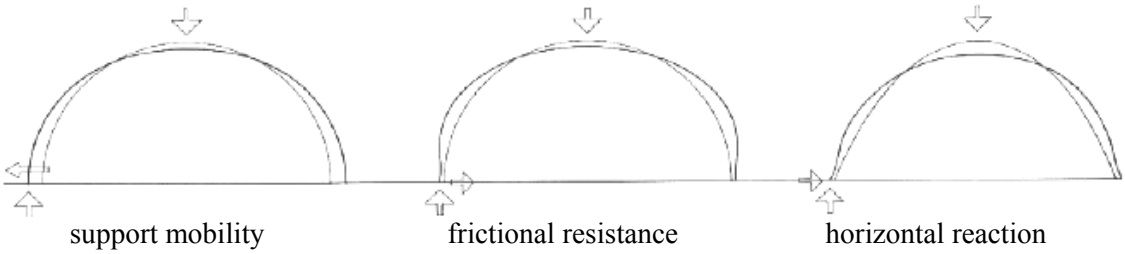

Figure 40. Boundary conditions effects. (Source: [10])

At the base of the dome, the *support structure* must resist the inclined loads from the dome with equal and opposite reactions, Figure 41. The support structure typically resists the *vertical component* of the inclined force with ease. However, the dome and support structure must also resist the *horizontal component*, the outward thrust, particularly near the base of the dome where the total thrust is greatest. External means of resistance may be employed, such as massive support structure walls or a metal tension ring around the dome´s base [11].

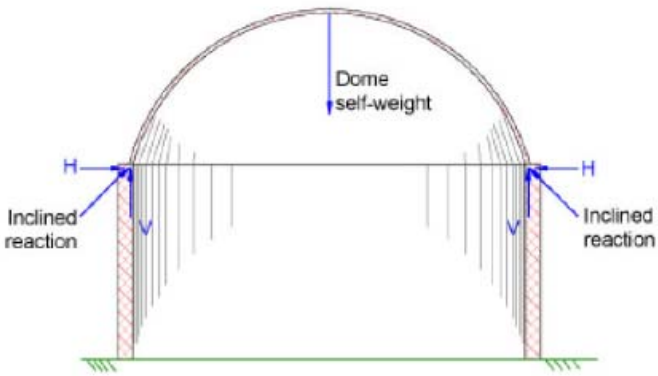

Figure 41. The support structure reactions to applied and gravity loads. (Source: [11])

Local or comprehensive *failure* of masonry´s domes may result from the inability of the material to resist tensile or bending forces that develop due to unanticipated loads on the dome. A typical failure or collapse mechanism consists of: first, the formation of radial cracks along its meridians that divide the dome into lunes, or pie-shaped arches. Second, two hinge circles form in the dome mid-section, with a third hinge circle formation at or near the base. The cap of the dome will fall straight down, while the base of the lunes, as defined by the radial cracks, will rotate outward, Figure 42 [11].

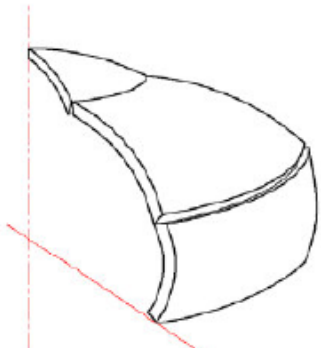

Figure 42. Typical collapse mechanism for a dome. (Source: [11])

The dome can be imagined as some segments or meridian arcs whose bending is avoided by the rings or horizontal parallels. In areas in which segments want to sink inwards, the parallels are working in compression to avoid it, and where segments want to open outside; the parallel has to avoid it working in traction [10].

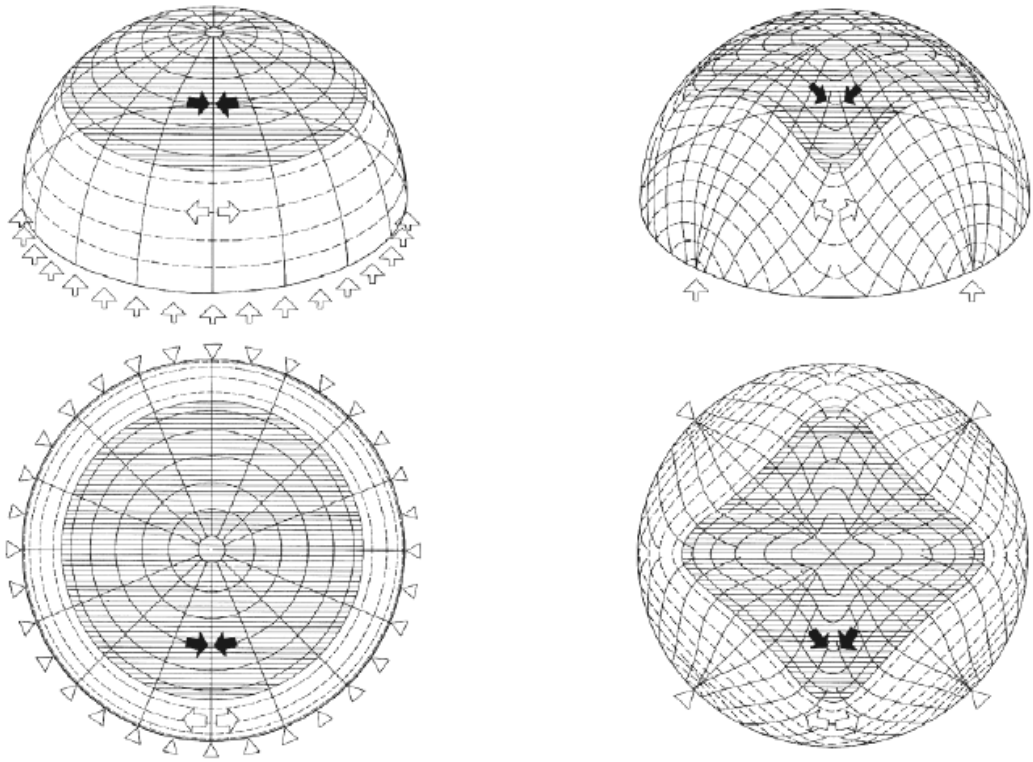

Figure 43. Load transmission in domes (symmetrical load). (Source: [10])

Efforts are transmitted according to the direction of the meridians and parallels. The meridional and hoop efforts direction are modified as if they were subjected to a magnetic field.

2.3. Domes and thin shells construction techniques

Dome Technology engages the latest engineering and architectural technologies to produce aesthetic, functional, and economical schools, gymnasiums, waterparks, community centers, and industrial facilities. At a fraction of the cost of a conventional structure, each building benefits from unobstructed views, seating efficiency, great acoustics, and space utilization [17].

There are several different construction techniques to build a dome; the following types will be bravely explained:

- Flattened conduit
- Hub and strut dome
- Tube and hub
- Beam and hub
- Panelized domes
- Stressed skin
- Space frame
- Brick and former
- Foam and render
- Monolithic dome
- Concrete and foam plastic domes

2.3.1. Flattened conduit

Steel-framework domes can be easily constructed of electrical conduit. One flattens the end of a strut and drills bolt holes at the needed length. A single bolt secures a vertex of struts. The nuts are usually set with removable locking compound, or if the dome is portable, have a castle nut with a cotter pin. This is the standard way to construct domes for climbing frames as jungle-gyms or tent structures, Figure 44 [14].

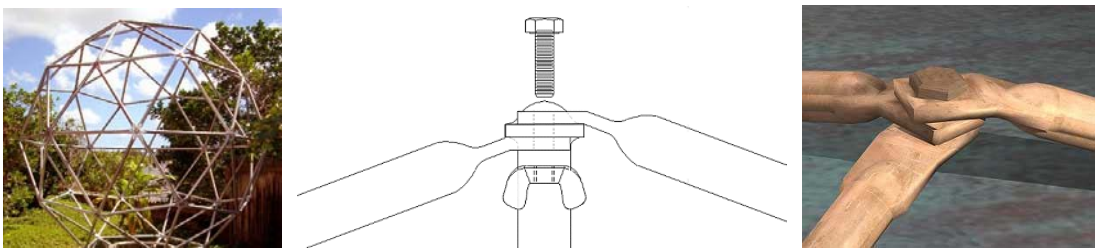

Figure 44. Use wing nuts for quick assembly/disassembly in flattened conduit. (Source: [14])

Advantages: Really easy to build, easily assembled/disassembled, no special tools required.

Disadvantages: Quite crude, can only be covered with material because joints don't finish level.

2.3.2. Hub and strut dome

Wooden domes have a hole drilled in the width of a strut. A stainless steel band locks the strut's hole to a steel pipe. With this method, the struts may be cut to the exact length needed. Triangles of exterior plywood are then nailed to the struts. The dome is wrapped from the bottom to the top with several stapled layers of tar paper, in order to shed water, and finished with shingles. This type of dome is often called a hub-and-strut dome because of the use of steel hubs to tie the struts together, Figure 45 [15].

Figure 45. Wooden Strut with Pipe Hub. (Source: [15])

2.3.3. Tube and hub

Another simple construction technique, slightly more work than the flattened conduit method but is a more professional and flexible system. Instead of joining the struts directly together a larger diameter pipe is used as a hub holes are drilled through the hub and the struts are bolted to it. This system is great for making canvas domes. Cut and stitch a canvas dome slightly smaller than the framework then pull the canvas tight through the centre of each hub, Figure 46 [14].

Figure 46. Tube and hub dome. (Source: [14])

Advantages: Makes a nice neat job with all struts finishing level while still being cheap and easy to build.

Disadvantages: Great for material covers but there is no easy way to fix a hard covering material.

2.3.4. Beam and hub

Wooden beams are attached to specially made hubs to form the dome framework; the angles are taken care of by the hubs so all you have to do is cut the beams to the correct length. More expensive to build than a tube type framework but makes a solid permanent dome, Figure 47.

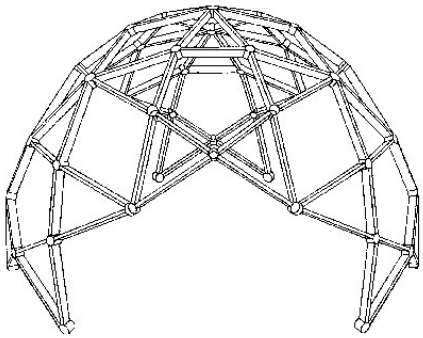

Figure 47. Geodesic dome. Fuller's dome, 1954. (Source: [14])

Advantages: Simple dome construction system that doesn't require specialist tools or knowledge to build.

Disadvantages: The hubs can be expensive and hard to find because they have to be specially made. When the beams have board nailed on both sides there is no way to ventilate the void between, in a heated dome this can lead to damp, dry rot and a number of other problems.

2.3.5. Panelized domes

Panelized domes are constructed of separately-framed timbers covered in plywood. The three members comprising the triangular frame are often cut at compound angles in order to provide for a flat fitting of the various triangles. Holes are drilled through the members at precise locations and steel bolts then connect the triangles to form the dome. These members are often 2x4's or 2x6's, which allow for more insulation to fit within the triangle. The panelized technique allows the builder to attach the plywood skin to the triangles while safely working on the ground or in a comfortable shop out of the weather, Figure 48. This method does not require expensive steel hubs [16].

Figure 48. Panel dome. (Source: [16])

Advantages: Simple and extremely fast way to build a permanent dome structure.

Disadvantages: Because the panels are factory made you don't get much design choice. Ventilation problems can occur when material is fixed to both sides.

2.3.6. Stressed skin

Metal or fibreglass panels are bolted/riveted together to form the dome, there are no beams, hubs or separate support structure the skin does everything, Figure 49.

Figure 49. Stressed skin dome. (Source: geo-dome.co.uk)

Advantages: Probably the most cost effective and efficient way to build a dome. Some simple fabrication is required but this can be easily sourced locally.

Disadvantages: Metal sweats when it gets cold so some form of insulation has to be glued to the inside of the panels to prevent condensation forming. Cutting holes for doors and windows can seriously weaken the dome structure.

2.3.7. Space frame

Building domes using space frame is actually quite simple, the struts are made from solid bar and they are connected together with solid balls that have fixing points machined into them. Very commonly seen at airports and exhibition halls. Too expensive for the DIY builder but still interesting, the Eden project was built using a space frame, Figure 50.

Figure 50. Industrial enclosures. (Source: www.triodetic.com/Photos.htm)

2.3.8. Brick and former

This building method dates back hundreds of years and was also used to build arches, bridges etc. A wooden former is made to the shape required then stone, brick, or concrete is laid on top of the former to produce the final dome shape. The former is used to hold the brick, stone or concrete in place until it sets and is able to support its own weight, Figure 51. Usually the former is removed but there is no reason why it couldn't be left in place.

Figure 51. Urstville boys' high school, 1973.

Advantages: Makes a very strong long lasting dome that can be built using reclaimed materials.

Disadvantages: A lot of expense is involved in making the former that MUST support the whole weight of the dome when the dome is finished the former becomes redundant. Building very large domes is not cost effective using this system.

2.3.9. Foam and render

This method uses polystyrene foam or urethane foam as a former. Cut and glue the foam together to form the dome shape. Next tie chicken wire over the foam to act as reinforcing mesh. Finally apply a thin layer of cement render over the whole structure to weatherproof and finish the dome.

Advantages: Easy to change or alter the foam former
Disadvantages: Only suitable for very small domes.

2.3.10. Monolithic dome

Simply defined, the Monolithic Dome is a super-insulated, steel-reinforced concrete structure that can be designed for virtually any use: office or business complex; school; church, synagogue or temple; gymnasium or sports arena; theater or amphitheater; airplane hangar; factory; bulk storage facility; house or apartment complex; military installation, etc [12].

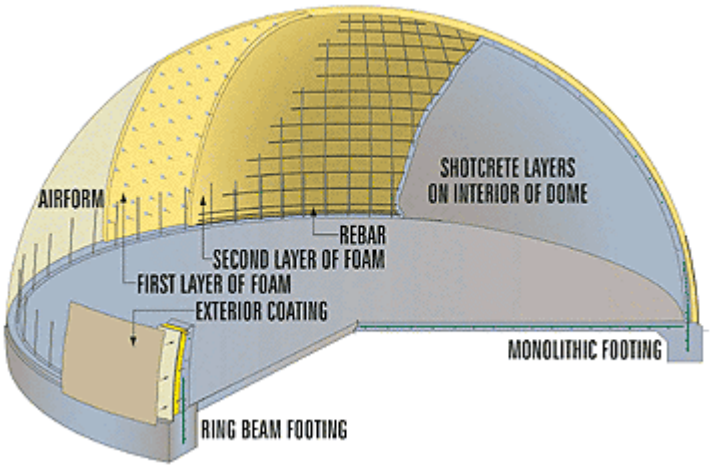

Figure 52. Monolitic dome layers. (Source: [14])

There are basically five stages involved in building a monolithic dome, Figure 52 [14]:

1. The Monolithic Dome starts as a concrete ring foundation, reinforced with steel rebar. Vertical steel bars embedded in the ring later attached to the steel reinforcing of the dome itself. Small domes may use an integrated floor/ring foundation. Otherwise, the floor is poured after completion of the dome, Figure 53.

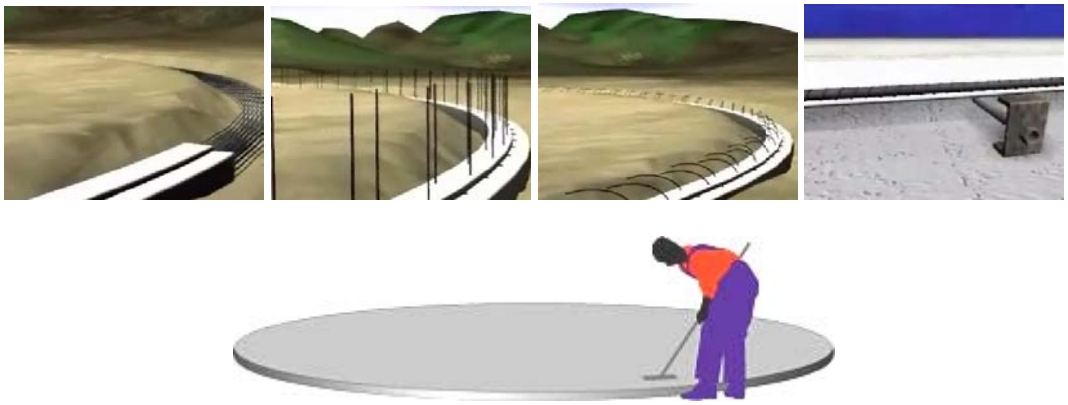

Figure 53. Building a Monolitic Dome. Step 1: Concrete ring foundation. (Source: [14], [17])

2. Inflation of an airform membrane, made of PVC coated nylon or polyester fabrics, placed on the ring base. When inflated, the Airform determines the shape and size of the finished building, and it remains on the structure as its roof membrane, Figure 54 [12].

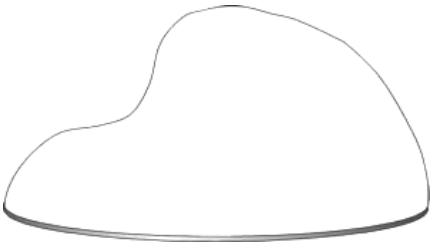

Figure 54. Building a Monolitic Dome. Step 2: Airform. (Source: [14], [17])

3. A polyurethane insulation is then sprayed onto the inside of the airform; reinforcing bar is pressed into the urethane ready for the final step. Polyurethane foam is a superior insulator. When sprayed in place, it expands to thirty times its original size, sets in seconds and fills every nook and cranny, completely sealing a structure. This foam is virtually waterproof, forms its own vapor barrier and adds structural strength.
Entrance into the air-structure is made through a double door airlock which keeps the air-pressure inside at a constant level. Approximately three inches of foam is applied. The foam is also the base for attaching the steel reinforcing rebar, Figure 55.

Figure 55. Building a Monolitic Dome. Step 3: Polyurethane insulation. (Source: [14], [17])

4. The steel reinforcing rebar is attached to the foam using a specially engineered layout of hoop (horizontal) and vertical steel rebar. Rebar is a steel bar with ridges that is used to strengthen concrete. In Monolithic Dome construction, rebar hangers that will hold the rebar are placed into the foam, following a pattern predetermined by the dome's size and shape. Small domes need small diameter bars with wide spacing. Large domes require larger bars with closer spacing. As in the construction of bridges, tunnels and roads, rebar reinforces the dome's concrete, Figure 56.

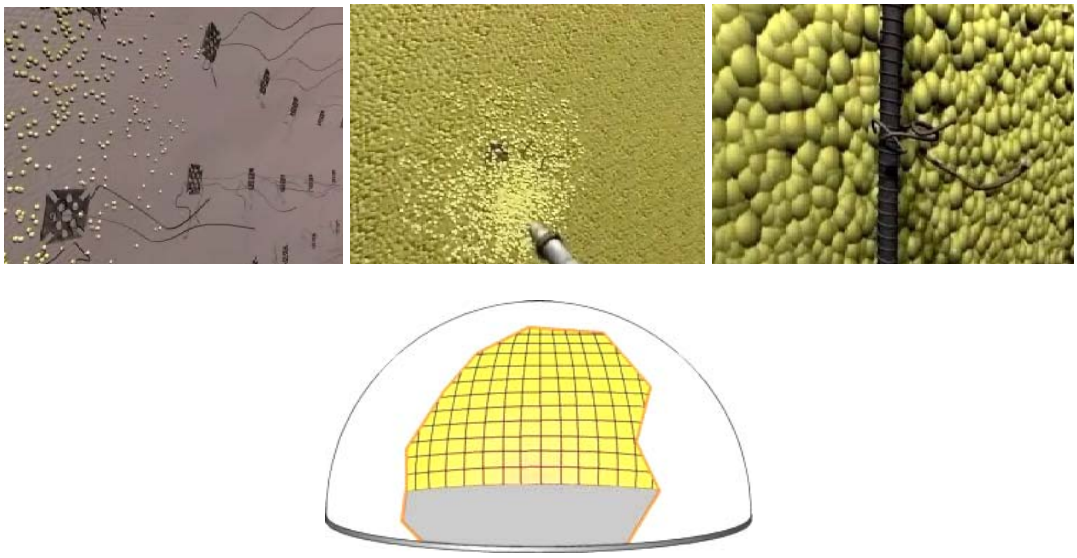

Figure 56. Building a Monolitic Dome. Step 4: Steel reinforcing. (Source: [14], [17])

5. A form of concrete called *shotcrete* is sprayed onto the interior surface of the dome, over the rebar and polyurethane. The shotcrete is a special mix of concrete that is spray-applied to a specific thickness, depending on the dome's size. Shotcrete covers the foam and embeds the rebar on the inside of the dome. The blower fans are shut off after the concrete is set, Figure 57.

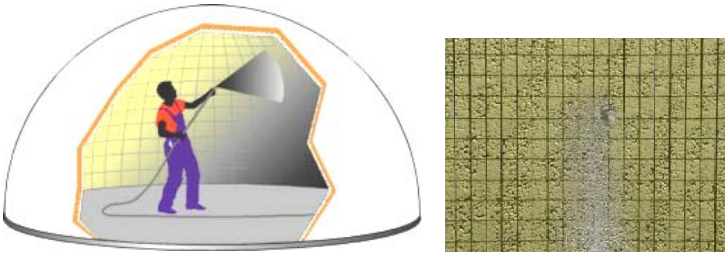

Figure 57. Building a Monolitic Dome. Step 5: Shotcrete layer. (Source: [14], [17])

Advantages of monolithic domes:
Monolithic domes are both efficient and incredibly strong structures; they take hurricane force, winds and earthquakes in their stride. Speed of construction and flexibility are key features. Bulk storage, schools, churches and homes can be built

using this system, by altering the airform, low profile, ellipsoid, hemispheres and even multiple domes can be constructed, in fact any shape that is inflatable could be built. Doors and windows of any shape can be easily incorporated into the structure. Being both well insulated and having a huge internal mass makes a monolithic dome one of the most heat efficient buildings you can build [12].

Problems with monolithic domes:
There are three main issues with monolithic domes:
1. Polyurethane foam, vinyl and concrete are not the most sustainable materials to build with. Polyurethane foam is petroleum based, can't be recycled easily and produces toxic smoke when it's burnt. The vinyl airform again is petroleum based and there are some questions over the lifespan of the airform. At least the concrete is pretty permanent, even if it has a large initial CO_2 footprint.
2. If the vinyl membrane is damaged in any way water can seep into the insulation beneath which will end up like a huge soggy sponge. Fire, vandalism even falling tree limbs are a worry for the monolithic dome owner. All it takes is someone with a knife to ruin an air-form; kids with air rifles or bows and arrows could easily make holes in it. Air-forms can be repaired or covered in aluminum to protect them but it does increase the cost considerably.
3. Monolithic domes are virtually hermetically sealed, this makes them great for storing materials that need a constant humidity, but when it comes human habitation; washing, cooking and bathing all produce water vapor which has to be removed from the building by dehumidifiers or forced air ventilation, as there isn't enough natural ventilation in this type of dome structure. The only way to get air movement through a dome structure is to have a hole covered with a cowl top dead centre of the dome.

2.4. Thin concrete shells

One kind of spatial structure, the thin concrete shell roof has been considered by both designers and the public to be among the most striking of structural systems, not only because of their superior aesthetics but also because of the ability to merge effortlessly into natural surroundings. Despite their rational use of material, thermal and acoustic insulation of thin concrete shell structures is naturally satisfactory. Further, no additional roofing is required. Thin concrete shells are also durable and demand minimal maintenance [13].

2.4.1. Decline of concrete shells

Thin concrete shells are economical regarding the consumption of material, in particular steel which is used only for reinforcement and usually at a low density. Hence they have been widely used for medium- and long-span roof structures from the 1920s. The shells of *Torroja*, *Candela* and *Nervi* were mainly constructed during the period when steel was often in short supply. However, after peaking in popularity in the fifties and sixties of the twentieth century, the use of reinforced concrete shells has gradually declined.

This is due to several factors; for instance, traditionally, shell construction is labor intensive, which makes it expensive in most developed countries owing to high labor costs. Figure 58 shows the buttress preparation before concrete casting of the *Kresge Auditorium Shell* (MIT, Cambridge, 1954). A large crew size was involved owing to the shell's steep geometry and the constraints of the working conditions. Another historical photograph of the same project (Figure 59) shows also the labor intensive nature of concrete shell construction.

Figure 58. Preparations for the concrete cast of Kresge Auditorium, MIT. (*Source: [13]*)

Figure 59. The Kresge Auditorium during construction. (*Source [13]*)

However, despite the acknowledged aesthetic appeal, due to the availability of a large variety of structural steel sections at competitive prices, together with many new long-span structural systems suited to steel construction, the demand for concrete shell structures was not sustained. The **high costs** associated with the construction and removal of temporary formwork and associated falsework for concrete casting (which is often used only once or for a limited number of times) also reduced the acceptability of thin concrete shells.

For instance, despite the fascinating look of the *Kresge Auditorium Shell* (Figure 60), the tremendous structure of formwork and the corresponding falsework (Figure 61) which was prepared for such a shell may also scare most of the architects and engineers as well as the clients today. More recently, the development of lightweight structures such as cable-net and membrane structures, coupled with the increasing ease in analyzing complex space grid structures offered by advances in computer technology also made concrete shells much less competitive than they had been a few decades ago.

Figure 60. The Kresge Auditorium, MIT. (Source: [13])

Figure 61. Supporting formwork and falsework for Kresge Auditorium, MIT. (Source: [13])

2.4.2 Thin concrete shells and space grid structures

In the past few decades, the proliferation of *space grid structures* all over the world has taken much of the potential market for *thin concrete shells*. The wider availability of structural steel and high-strength materials permit the construction of space grid structures of longer spans and more complex shapes. In addition, the wider use of powerful computers and the development of computer programs enable the analysis and design of space grids to be accurate and confident.

Some of the general *benefits* gained from the use of *space grid structures* are as follows. Firstly, the high redundancy of space grid structures means that, in general, failure of one or a limited number of elements does not necessarily lead to the overall collapse of the structure. Secondly, the naturally high modularity of space grid structures accelerates the fabrication and the assembly of members on site, resulting in savings in erection time. Further, the great freedom of choice of support locations leads to ease in space planning beneath the grid. Naturally, there are also some *disadvantages* with the use of space grid structures. The regular nature of the geometry makes the design appear

very 'busy' to some eyes, while the fire protection is difficult to achieve without excessive cost penalty if it is necessary.

Although thin concrete shells and space grids are at opposite ends of the structural spectrum, they can usually be compared, due to the similarity of their structural behavior. Although space grids consist of a large number of members dominantly in tension and compression, on the whole they behave much like thin continuum shells. In general, any applied load is distributed throughout the structure and to all the supports, with all elements contributing to the load carrying capacity. A space grid with an overall geometric shape following that of a similar thin shell, and equally supported and loaded, would clearly exhibit similar distributions of internal forces. The axial forces in the members of its top and bottom layers of a space grid would indicate the same distribution of tension and compression present within a shell.

Thin concrete shells and space grid structures are modern, efficient, light, versatile, and capable of covering a large column-free area. They are also comparable in cost.

Thin shells are complete in themselves, while space grids require an additional skin to complete their enclosure function. In terms of thickness, thin shells do not require the depth that space grids do.

2.4.3. Alternative ways of forming thin concrete shells

As described above, the problem of the high cost of forming plays a dominant role in the overall high cost of the construction of thin shells. Over the years, there have been several attempts aimed at reducing or eliminating the need for temporary formwork in constructing thin concrete shell roofs, but all have met with limited success. An excellent review of these attempts and other developments in thin concrete shell roof construction was given by *Medwadowski* [35], who concluded that forming "remains the great, unsolved problem of construction of concrete thin shell roofs. Any and all ideas should be explored, without prejudice." Two of the better recognized and more successful attempts are briefly reviewed below: inflated pneumatic forms, and precast concrete technology.

Inflated Pneumatic Forms

The application of *pneumatic forming* was an important improvement towards reducing the construction difficulties of curvilinear concrete shells. In this technique, the steel reinforcement and concrete are placed before the pneumatic form is inflated, and then covered with a PVC membrane. The concrete is spread uniformly when the membrane is fully raised. A well-known successful attempt for using inflated forms is **Binishells**.

The general construction process of a Binishell dome is shown in Figures Figure 62a to Figure 62d. There are several major advantages to this patented technique. Firstly, it is an automated construction system, with an extraordinary construction speed of about 7,700 m^3 volume per hour [36]. Secondly, the scaffolding and formwork are eliminated, resulting in considerable savings in the construction cost. Thirdly, though it requires

some expensive and sophisticated equipment, continued production of such circularbased, monolithic, reinforced concrete shells is cheap and fast. The Binishells were popular from the 1960s to 1980s; in fact, over 1,600 Binishells have been built in 23 countries over the past 40 years [36].

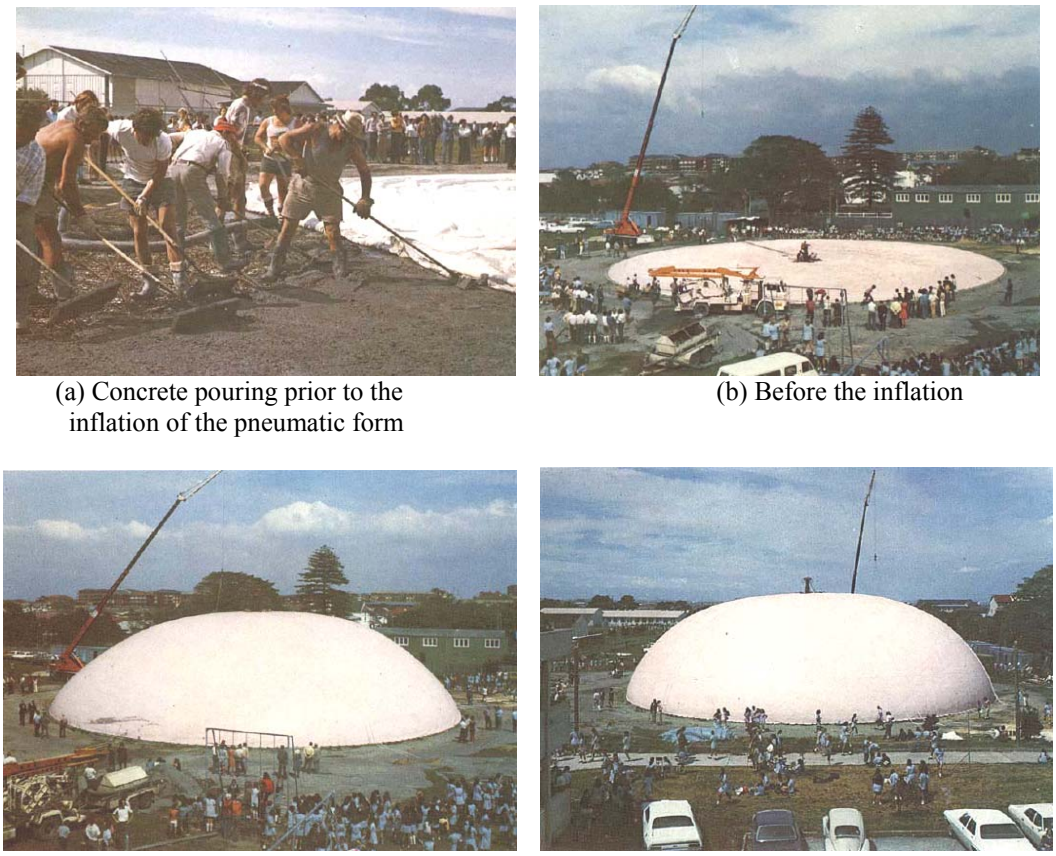

(a) Concrete pouring prior to the inflation of the pneumatic form

(b) Before the inflation

(c) During the inflation

(d) The fully inflated dome

Figure 62. General construction process of a Binishell dome. (*Source: [13]*)

In general, this method is limited to the construction of circular-based domes with a spherical or nearly spherical meridian. A major *disadvantage* of this method is that the shape and thickness of the dome and steel bar positions are difficult to control during the construction process. As shells, particularly these domes, depend on their shape for their buckling strength, even small shape deviations can be dangerous. The construction process of Binishells has proved to be sensitive to environmental disturbances. For instance, two days after erection, a 36m-diameter Binishell dome collapsed in 1975 [37], following a sudden thunderstorm that lowered the air temperature as well as the balloon pressure. A similar Binishell dome collapsed in Australia in August 1986, with the origin of failure being poor shape control [38].

Precast Concrete Technology

A concrete shell can be prefabricated in a factory in the form of either a large number of small *modular panels* or fewer large parts and then transported to the site for assembly into a shell. Joints between these panels are sealed by in-situ concrete casting. The precast concrete method for thin shell domes was particularly popular in the former Soviet Union.

Another well known application of the precast concrete technology to shell structures is the prefabricated forms which become a part of the completed shell. A good example of using this method involves the revolutionary reinforced concrete material, ferro-cement, with which *Nervi* designed and constructed many amazing shell structures during the 1920s to 1960s [39] [40]. Ferro-cement is a thin, flexible, elastic and very strong material composed of several layers of fine steel mesh with cement mortar.

For use in heavier structures, additional reinforcing bars are inserted in the center of the component. Figure 63 shows the prefabricated units for a four-sided dome designed by *Nervi*, where the protruding bars are for bonding with in situ concrete. By making the necessary forms of elements in ferro-cement, any desirable shape can be obtained but the timber forms are eliminated. Figure 64a to Figure 64c show the construction process of the *Palazzetto dello Sport* designed by *Nervi*, which reflects the efficiency of ferro-cement.

Figure 63. Process of manufacturing prefabricated units for a four-sided dome. (Source: [13], After Nervi 1957)

(a) Prefabricated elements on the ground

(b) Prefabricated elements of the ceiling, in place for pouring

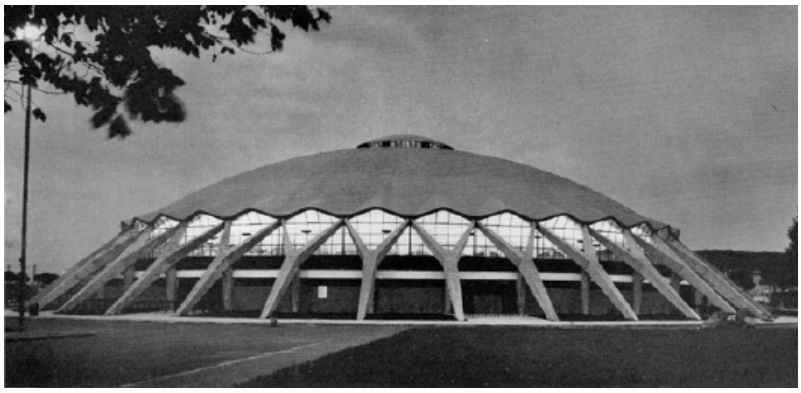

(c) An exterior view

Figure 64. Palazzetto dello Sport, Roma. (Source: [13], After Huxtable 1960)

Although it should not be considered obsolete as an option for shell designers, the *precast shell technique* has faded out gradually in the commercial market. One of the probable reasons is that, although this method eliminates the need for formwork, extra work for transportation and assembly is needed. It also requires heavy mechanical devices in the construction process. In general, the overall cost savings, if any, are limited.

3. NEW CONSTRUCTION METHOD AT VIENNA UNIVERSITY OF TECHNOLOGY

3.1. Introduction

Dome structures must provide strength, stiffness and stability. They must be capable of supporting applied loads and self weight without excessive deflection or displacements. Similar to an arch, a dome develops internal meridional forces that transfer loads to a support structure at its base. These forces are compressive and increase in magnitude from crown to the base for any dome loaded axisymmetrically by self weight.

However, in the dome additional forces, called hoop forces, are set up at right angle to these arching or meridional forces. As a result, though an arch is unstable without its keystone, a dome with an oculus is perfectly stable.

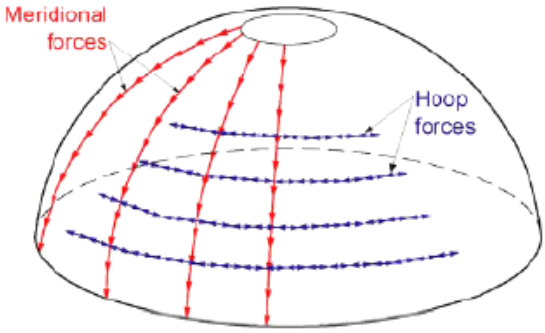

Figure 65. Forces developed in a dome. (Source: [10])

Nowadays, with several building methods shells with excellent qualities can be obtained. But these construction processes are usually complex, time consuming and expensive. Building shells with wooden doubly curved formworks is very time consuming and expensive, due to the increasing in labor costs. Other methods as inflating a pneumatic formwork which is covered with a freshly mixed concrete layer, also take too much time and costs. To reduce the construction time on site, **precast elements** can be used [21].

At the Institute for Structural Engineering at Vienna University of Technology a new construction method for building shells is under development. With this new method, a **doubly curved shell** is **built from a flat plate**. This new construction method consists on transforming a plate into a shell: the usage of precast elements, post tensioning and pneumatic formworks is combined.

Previously to this method with precast elements and post tensioning, an experiment with a concrete shell was carried out in the Institute. In this case a circular frame was previously built, then soft Styrofoam components were place and the concrete flat plate was made. These soft Styrofoam components were placed between concrete segments and therefore enable the plate to be deformed. Along the edge of the plate a tendon is placed. The erecting becomes possible by stressing the tendon so that the circular plate slowly lifts up and with the help of a pneumatic formwork to give the needed vertical

impulse. The concrete plate suffers cold deformation developing compression stresses in the bottom and tensile stresses in the upper zone of the cross section, so the shell curvature is limited and no hemispheric shapes can be obtained with this method. Moreover this tensile state in the concrete leads to the appearance of cracks in the surface of the shell.

In Figure 66, a concrete shell, with a diameter of 13m, built in June 2005 with this previous method can be seen.

Figure 66. Transforming a plate into a shell process. (Source: [21])

This construction method is not only suitable for concrete shells but also for ice shells. In December 2005 the Institute for Structural Engineering at Vienna University of Technology, constructed an ice dome with a diameter of 13m originating from one flat plate.

For applications on a large scale this previous building method was modified introducing the precast elements that need to be assembled on site. Normally concrete elements are connected by a grouting of overlapping steel reinforcement. If precast elements and sloped surfaces are used, this technology may entail structural problems. Therefore a new assembly method for precast elements was developed.

3.1.1. New assembly method for precast elements

During the manufacturing process the precast elements are equipped with ducts, where the appropriate tendons will pass through. Then these elements are transported to the site where the shell is going to be raised. On site, tendons are routed through the ducts of every individual element. Then the tendons are post-tensioned against the concrete, maintaining the final shell shape stable [21].

Due to this preload force the whole cross section experiences compressive stress. Therefore the structure, consisting of individual elements, acts as monolithic structure, as if fabricated in one piece.

This method can be used for plane, singly (Figure 67a) and also doubly curved surface structures (Figure 67b). For doubly curved shells it may be necessary to create a biaxial post-tension end state. This can be achieved by positioning two orthogonally arranged sets of tendons.

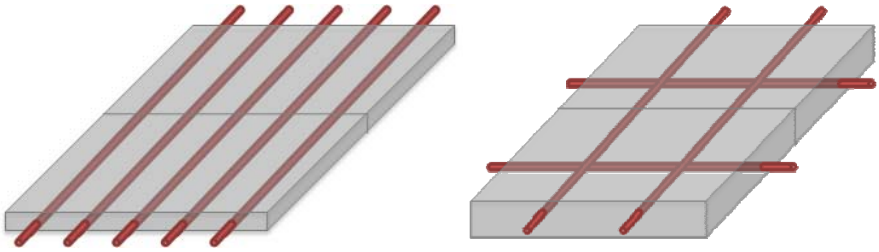

Figure 67. Steel tendons in (a) singly and (b) doubly curved surface structures.

Advantages of Post-Tensioning

The post-tensioning has 2 effects:

- On the one hand it joins the elements to each other and holds them firmly in place.
- On the other hand the post-tensioning has a positive effect on the load carrying behavior.

By the post-tensioning process a state of compressive stress is created in the concrete. Therefore the external load must first reduce this compressive stress before tensile stresses and cracks can appear.

Structures made of concrete which stay free of cracks have a higher extensional and bending stiffness. Post-tensioning causes that the cracking of concrete begins under a higher external load and therefore the structure experiences less deformation.

3.1.2. Shell formed by plane elements

A hemispheric is a non developable surface; this means that its surface cannot be flattened onto a plane without distortion. By dividing the sphere into matching elements, the final shape can be approached.

For this construction method the shell consists of individual plane elements. The shape of these elements has to be chosen according to the final shape of the shell.

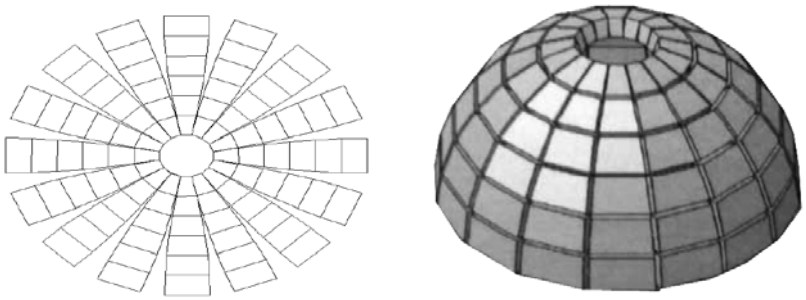

Figure 68. Hemispheric, non developable surface.

In these experiments the flat structure is composed by 16 longitudinal segments with 16 air spaces between them. Each of the longitudinal segments is formed by 6 elements. There are 96 elements forming the final shell shape, Figure 68.

Hemispherical shell radius

The calculation basis of the element geometry starts from the desired diameter in the flat plate initial position (D_{plate}), and the diameter of the hemispherical final shell shape (D_{shell}), Figure 69.

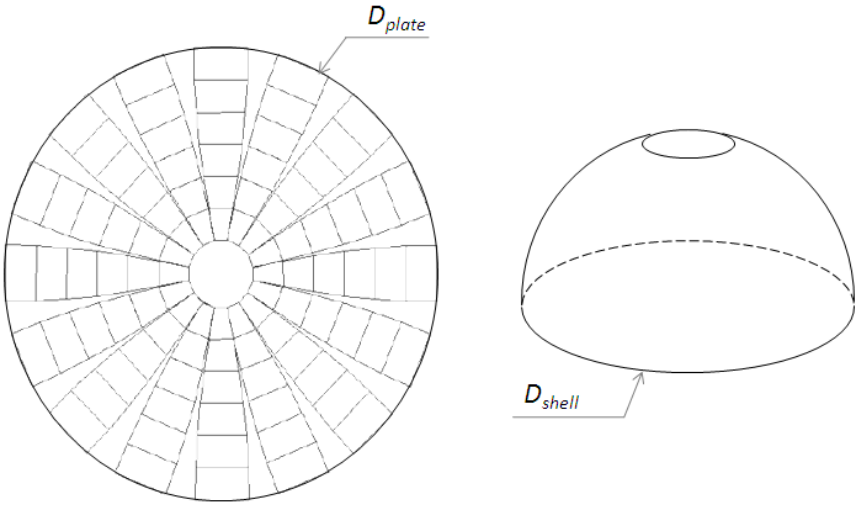

Figure 69. Flat plate and final shell diameter relationship.

Using simple geometrical knowledge the relationship between the two diameters can be obtained.

$$D_{plate} = \frac{2 \cdot \pi \cdot r_{shell}}{2} \qquad D_{plate} = \pi \cdot r_{shell} = \pi \frac{D_{shell}}{2} \tag{3}$$

Air separation and length of the outer piece border

This calculation is based on the comparison of a ring diameter formed by pieces and air spaces in the flat plate and the diameter of this same ring in the position in the final shell without any air spaces.

Outer plate perimeter $$U_{plate} = 2 \cdot \pi \cdot r_{plate} \quad (4)$$

Outer shell perimeter $$U_{shell} = 2 \cdot \pi \cdot r_{shell} \quad (5)$$

$$\Delta U = U_{plate} - U_{shell} = 2 \cdot \pi \cdot (r_{plate} - r_{shell}) \quad (6)$$

Air separation $$s = \frac{\Delta U}{16} \quad (7)$$

Length outer border $$s = \frac{U_{shell}}{16} \quad (8)$$

Air separation and length along the radius of the structure

The previous process is repeated for several points along the radius of the structure in order to obtain the approximated dimensions of each piece and the air separation between them. The edge of each piece has been defined by straight lines connecting the calculated points, Figure 70.

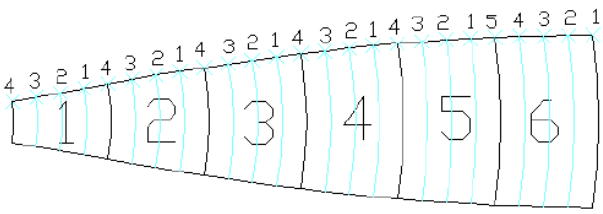

Figure 70. Numbering of the pieces and location of the points.

Curvature of the pieces

The longitudinal curvature of the pieces has been calculated in accordance with the hemispherical shape.

$$c = \frac{1}{r} \quad (9)$$

Technical drawings of the structure

In Figure 71 and Figure 72, the initial and final shapes and the distribution of the pieces which make up the shell can be seen.

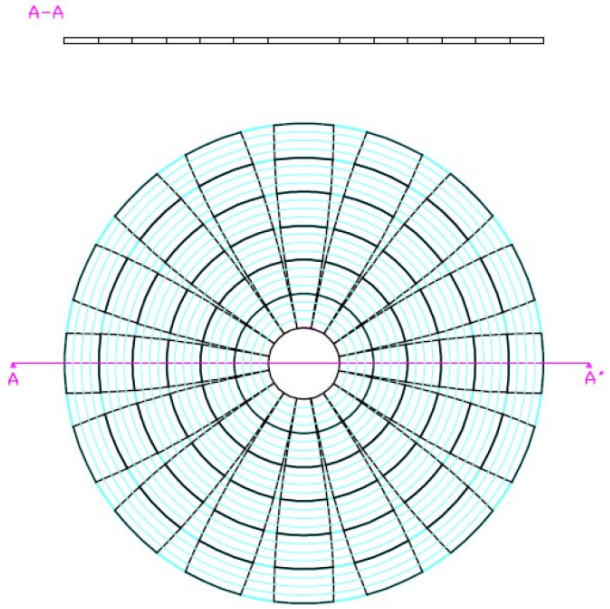

Figure 71. Floor plan and cross section of the flat structure. (Source: [22])

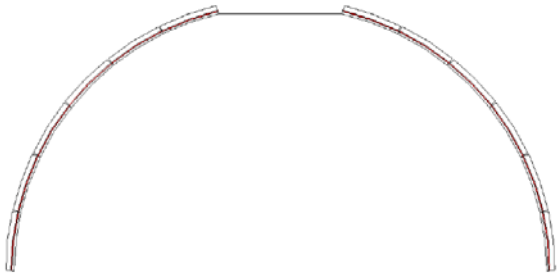

Figure 72. Cross section in the final position after the elevation. (Source: [22])

3.1.3. New construction method

The elements previously designed, are placed on a planar working surface and are assembled one by one by means of **tendons**. These tendons must allow the elements to open an interface on the outside of the shell.

In order to transform the plate into a shell a **pneumatic formwork** is used. The pneumatic formwork is placed underneath the plate. While air is inflating the pneumatic formwork, the plane plate is transformed into a shell. Afterwards the interfaces are filled with grouting material and post tensioning can be applied.

This construction method can not only be used for cupolas but also for other types of shells.

In Figure 73 the elements which are placed on the working surface can be seen. The red lines symbolize the tendons. There are tendons in radial direction holding the elements

together, as well as tendons in circumference direction which carry the horizontal forces.

Moreover, to help the final hemispheric shape formation while the pneumatic formwork is lifted up, many options can be used. One possibility is to place weights on the edge of the circular plate, as represented in Figure 73 with black rectangles. Another possibility is to fix the tendons in the working surface so that only movements in radial direction are possible. Also auxiliary constructions can be used [21]. These weight elements maintain the edges down in order to get the hemispheric shape of the shell. In the next sections can be seen that this elements are only used in the wooden models created in the laboratory and are not needed in the subsequent experiments.

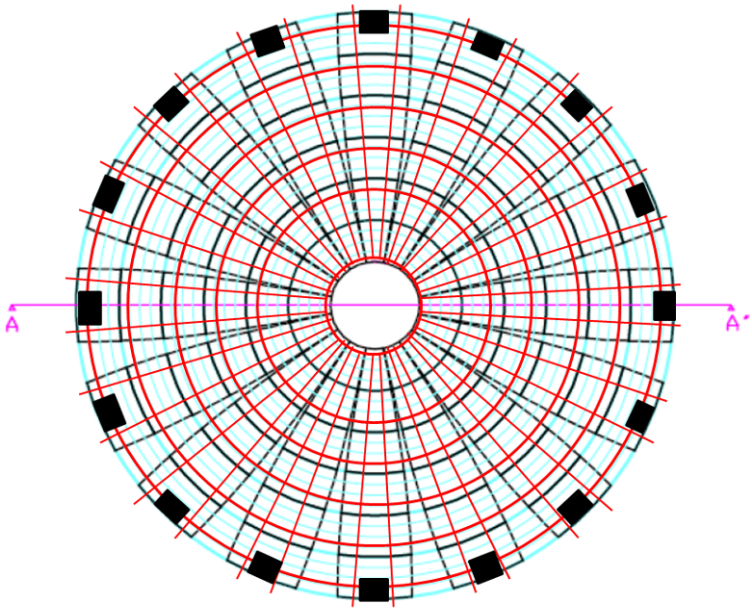

Figure 73. Flat structure with tendons and weights.

In Figure 74 is shown a sectional view of the circular plate, and in Figure 75, the same sectional view after the transformation.

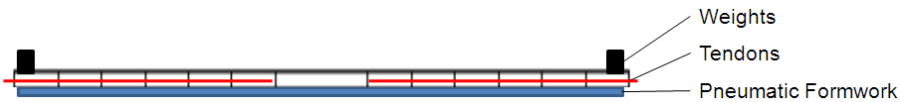

Figure 74. Cross section in the initial position before the elevation

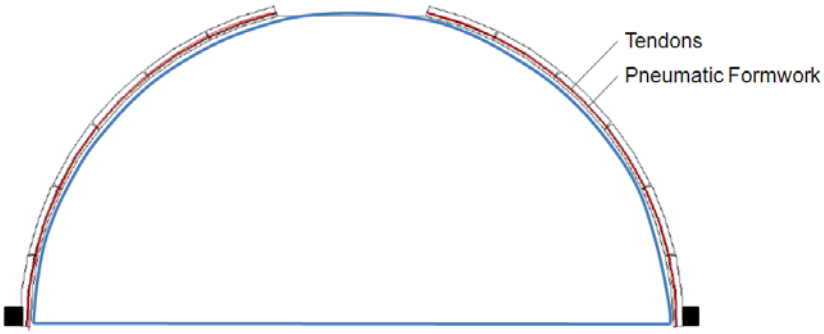

Figure 75. Cross section in the final position after the elevation

3.1.4. Wooden models

To demonstrate this new construction method, wooden models were created in order to find the best way to achieve the transformation operation of a flat plate into a shell successfully.

First Wooden Model

The model consists of 96 elements. In radial direction each elements contains 2 steel tendons. Moreover there are steel tendons in circumference direction. The diameter of the initial plate was of 2m, and the final shell formed had 1,28m of diameter and 0,64m of height [22].

The central ring had an anchorage system holding the meridian cables as shown in the Figure 76.

Figure 76. 1st Wooden model. Anchorage system in the central ring. (Source: [22])

A pneumatic formwork is placed under the elements. Weights are placed on the edge of the circular plate. In this model the weights are steel elements. The pneumatic formwork then is filled with air. Therefore the elements lifted and formed a shell, Figure 77.

a) Pneumatic formwork. b) Flat Plate above the pneumatic formwork.

c) The pneumatic formwork is filled with air d) Final dome shape.

Figure 77. 1st Wooden model. Raising process of the shell. (Source: [22])

Second Wooden model

Moreover a second wooden model was created. This model also consists of 96 elements, but the diameter of the plate, which is to be transformed into a shell, amounts to 4m, which is twice the diameter of the other wooden model [22].

One difference to the small wooden model, are **springs** which are placed at the ends of the tendons in the central ring, Figure 78. During the transformation process the interfaces between the elements open. In order to allow the elongation of the cables caused by the increase of the angle between the pieces, springs are placed on top of the central pieces. If the tendons need to increase their length to adopt the final semispherical shape, the springs will shorten. Through these springs controlled stresses can be generated in the tendons.

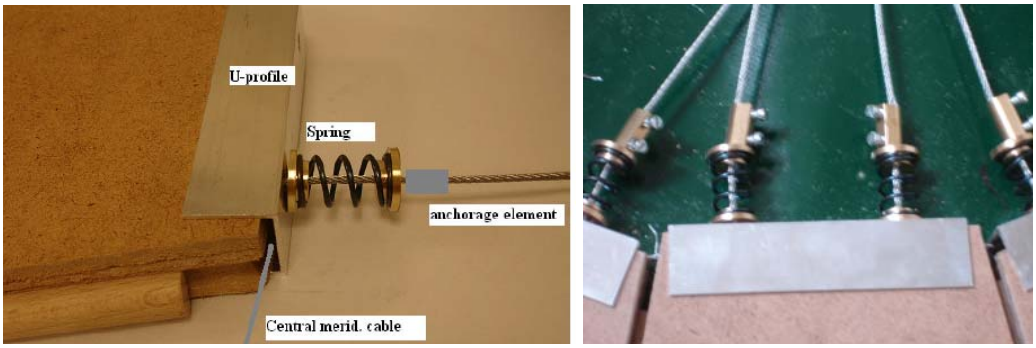

Figure 78. 2nd Wooden model. Central ring pieces with anchorage system in meridional direction. (Source: [22])

Another difference regarding the construction of this shell is the creation of **hinges** between the elements, Figure 79. This can be achieved by means of thin cylindrical elements in the joining. The edges of each element are provided with the correct shape to place in a rod. These rods are fixed to one side of the piece and just fit into the edge of the neighboring piece. This method facilitates the transfer of forces and decreases the relative movements among pieces. Moreover, through these hinges the elements can easily roll against each other whereby the shaping process is improved.

(a) Hinge in radial direction (b) Aluminum hinge in circumference direction

Figure 79. 2nd Wooden model. Hinges. (Source: [22])

These figures show the raising process of the shell: the pneumatic formwork and the transformation of the plane plate into a doubly curved shell, Figure 80.

Figure 80. 2st Wooden model. Raising process of the shell. (Source: [22])

3.1.5. Innovations and advantages

The innovative main points of this construction method is the combined usage of precast elements, pneumatic formworks and post tensioning.

Building shells with **precast elements** is an already known procedure, but in the past large doubly curved elements were produced. Therefore the transportation and the fittings were very difficult. With this new method the positioning of the elements is carried out by the pneumatic formwork. Moreover, the production of the precast elements is simple compared to other shells consisting of precast concrete, because all elements are plane and relatively small and there are only a limited number of different elements.

Pneumatic formworks have also been already used for shell structures. But with this method the complex process of covering an inflated pneumatic formwork with freshly mixed concrete is not necessary. Moreover the pneumatic formwork replaces a complicated doubly curved wooden or steel formwork.

The **post tensioning** is also remarkable. It holds the elements in place during the construction and, the post-tensioning cables can be used to improve the structural behavior of the shell structure after the construction [21].

3.2. Concrete shell construction

The concrete shell construction took place in Vienna, at the Institute for Structural Engineering at Vienna University of Technology.

The concrete shell built has the same design and shape as the wooden models. Only the diameter of the plane plate is increased to 13m. Therefore the dome will have a diameter of 8,3m and a height of 4,1m.

3.2.1. Previous planning

Shell Plans

In this initial phase in the project first the geometry of each element that would take part of the final shell shape was designed. The dome consists of only 6 differently shaped elements, Figure 81 and Figure 82.

It is remarkable that in two sides of the structure it is necessary to hold the circumference cables. For that, **cables winches** are used and placed in special elements, prepared for that mission with duct exits in the external face to attach the tendons to the engine, located as shown in Figure 83 and Figure 84.

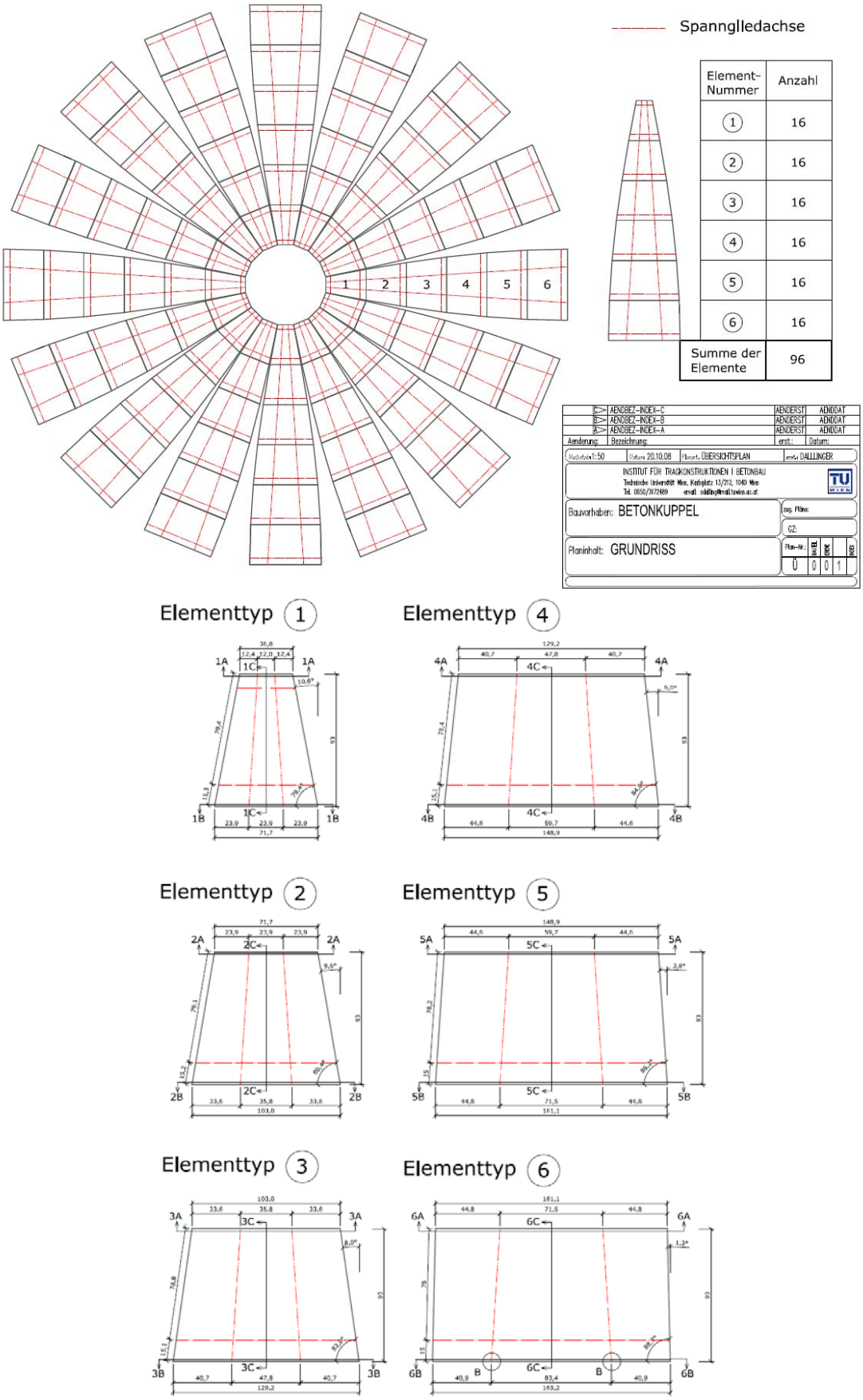

Figure 81. Concrete shell elements plans. (Source: [23])

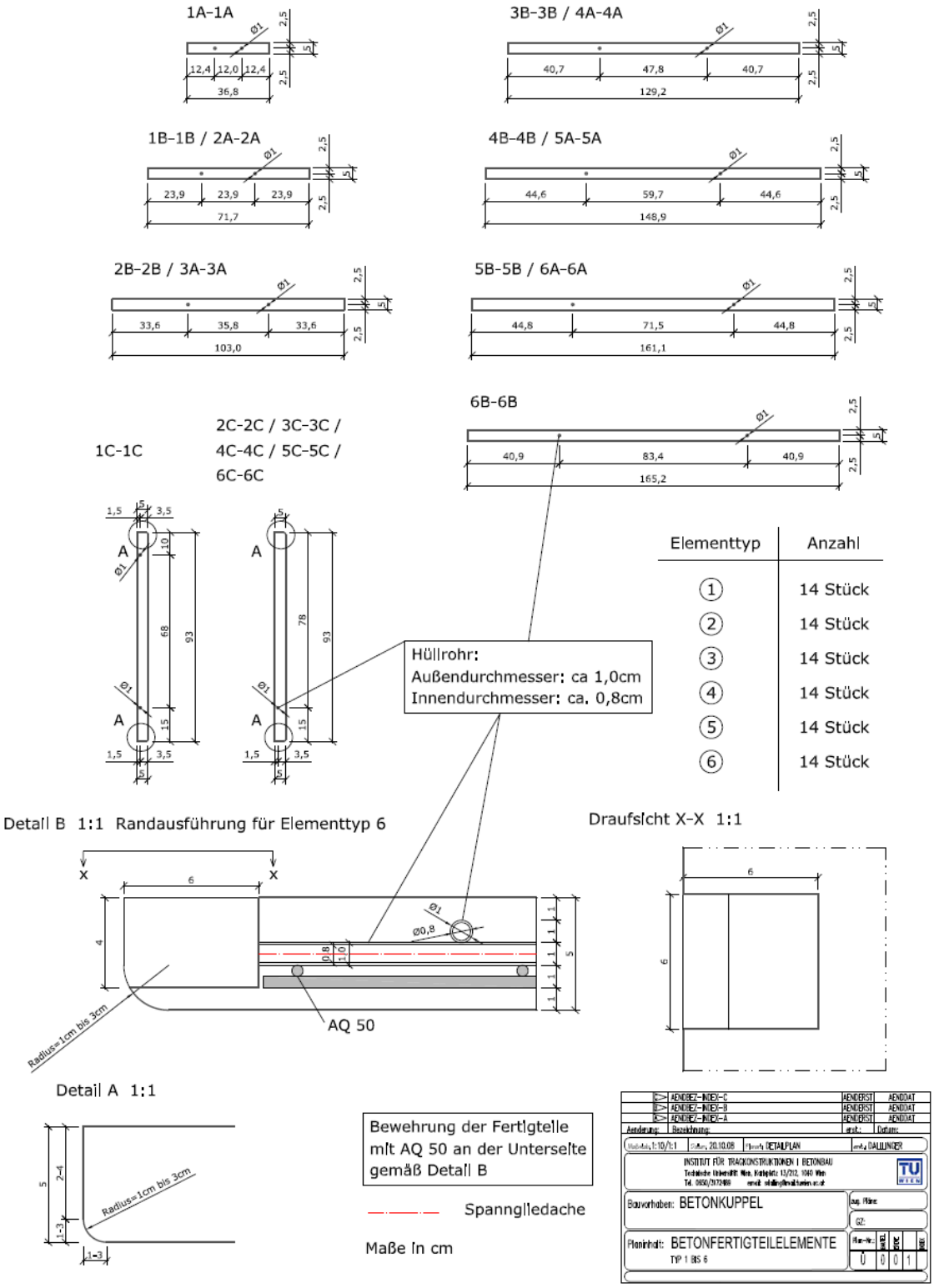

Figure 82. Concrete shell elements plans (II). (Source: [23])

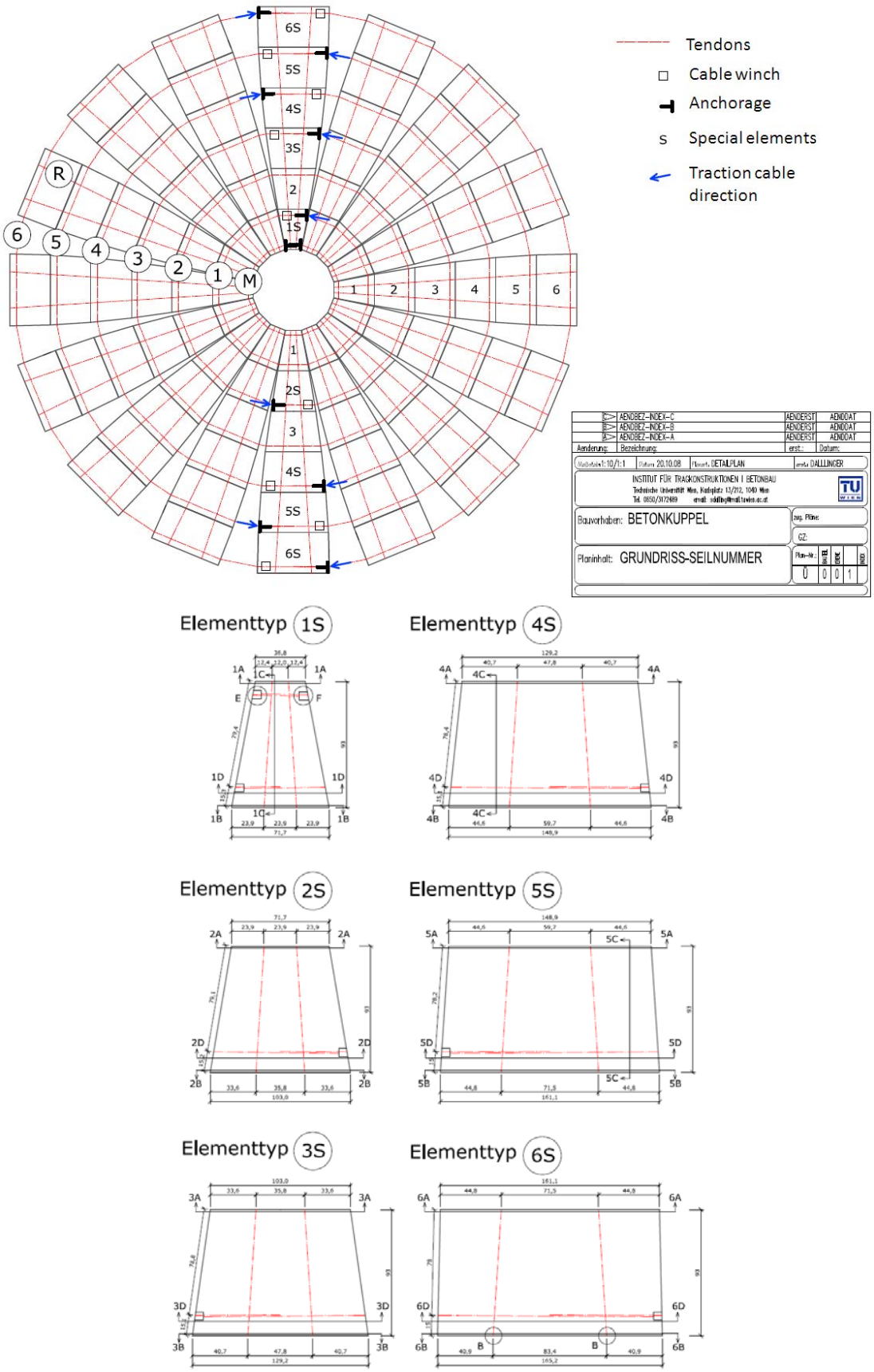

Figure 83. Concrete shell special elements plans. (Source: [23])

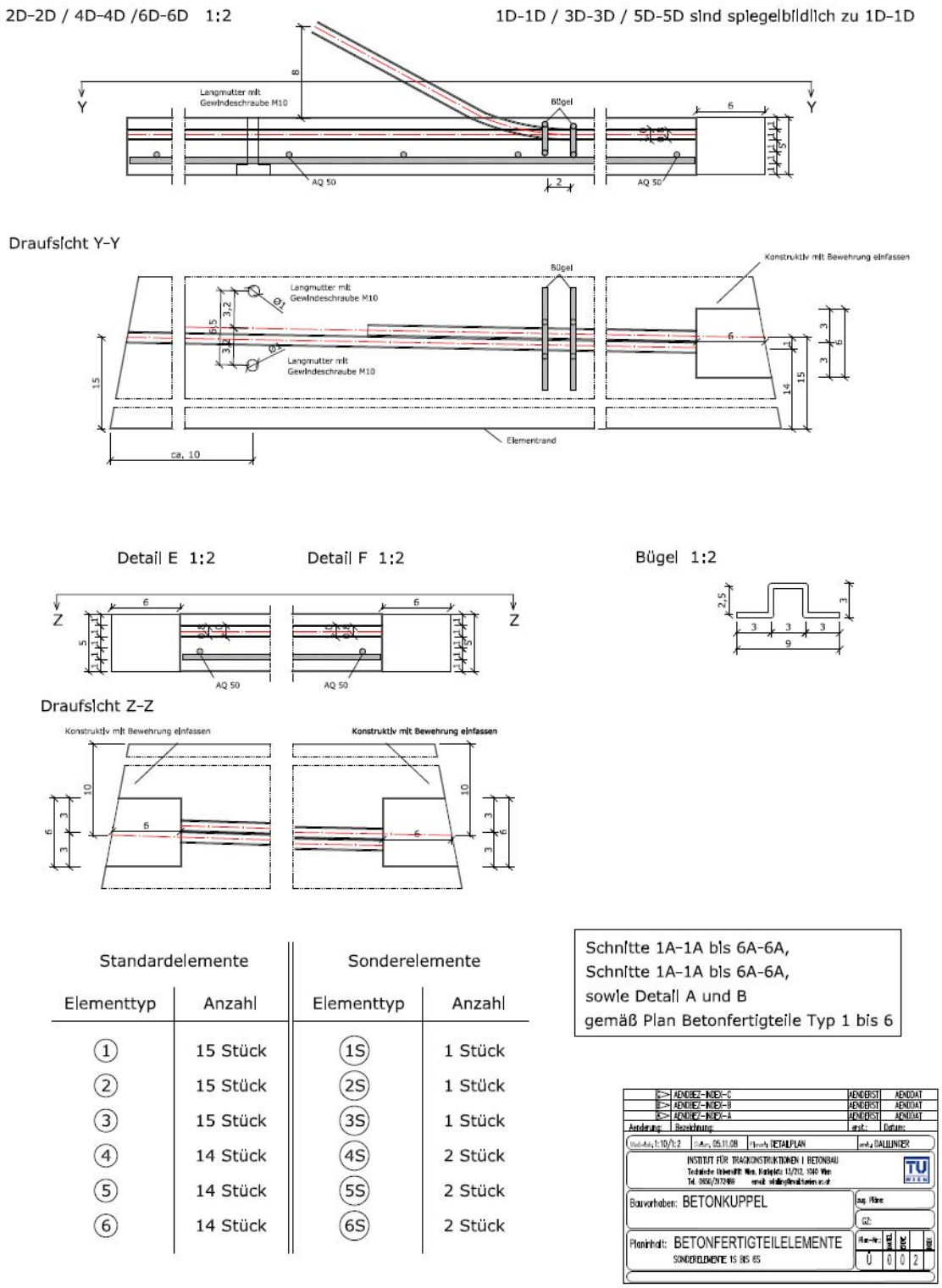

Standardelemente		Sonderelemente	
Elementtyp	Anzahl	Elementtyp	Anzahl
1	15 Stück	1S	1 Stück
2	15 Stück	2S	1 Stück
3	15 Stück	3S	1 Stück
4	14 Stück	4S	2 Stück
5	14 Stück	5S	2 Stück
6	14 Stück	6S	2 Stück

Figure 84. Concrete shell special elements plans (II). (Source: [23])

Precast elements

The tensile strength of concrete is only about 10% of its compressive strength. As a result, plain concrete members are likely to crack when loaded. In order to resist tensile stresses which plain concrete cannot resist, it can be reinforced with steel reinforcing bars. Reinforcing is selected assuming that the tensile zone of the concrete carries no load and that tensile stresses are resisted only by tensile forces in the reinforcing bars. The resulting reinforced concrete member may crack, but it can effectively carry the design loads.

The casting of the elements needed for this construction was entrusted to *Oberndorfer*, a pre-casting specialized factory [25].

In the casting process of the concrete elements, plastic conducts for the tendons were placed in the element's cross section, as can be seen in yellow in the Figure 85. There are two tendons in radial direction holding the elements together. As well as one tendon in circumference direction which carry the horizontal forces in each element.

Figure 85. Precast concrete elements.

Pneumatic formwork

To build the pneumatic formwork the following materials were used: PVC coil, glue *Plastigum 77*, fiber material for the base and tape.

Cutting the 16 segments and the base and top circles was the first step. A fiber layer was placed on the base to avoid the formation of non desirable ice during the shell construction process in cold environmental conditions, Figure 86.

Figure 86. Pneumatic formwork: cutting the elements.

To join the 16 radial segments, specific plastic glue was used. To speed up the sticking process a wooden box model representing one radial segment formed by 6 elements was built. All 16 segments cut were joined leaning on the wooden model, Figure 87.

Figure 87. Pneumatic formwork: wooden model.

The radial elements were joined to the base as shown in Figure 88. Pasting the two faces, element and base, one on top of the other was an easier and faster method.

Figure 88. Pneumatic formwork: joining segments to the base.

The pneumatic formwork was successfully inflated in the laboratory to check its strength, Figure 89.

Figure 89. Pneumatic formwork: inflating the formwork.

As can be seen afterwards in section 3.2.3, in the concrete shell building process the pneumatic formwork collapsed in the base and was not able to raise the two last rings of the structure. For this reason another pasting method to join the elements must be developed.

A second pneumatic formwork was built. Focusing on the base, the joining of the radial segments with the base was done as shown in the Figure 90. In this way it took much more time than before, but a better strength was obtained. Also a ring was pasted in the base enclosure to guarantee the appropriate enclosure. This leads to a stronger pneumatic formwork to hold the structure weight, Figure 91.

Figure 90. Pneumatic formwork: joining the elements and reinforcement.

Figure 91. Pneumatic formwork: final inflated shape.

Tendons

The tendons were entrusted to *Teufelberger*. In the *Catalogue Stahl- und Faserseile* its main characteristics can be seen in Table 1 [26].

The steel cables are formed by four main elements, Figure 92:

- Wire: It is the basic component of steel cable, which is manufactured in various diameters, according to the final use of the cable.
- Cord: It consists of a number of wires according to their construction, which are rolled spirally around a center in one or more layers.
- Core: It is the central axis of the cable where the cords strand. This core can be made of steel, natural fiber or polypropylene.
- Cable: The final product consists of several cords, which are helical coiled around the core.

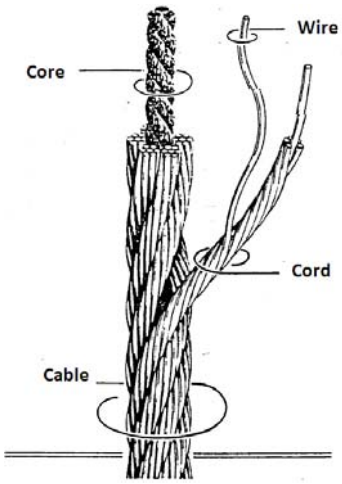

Figure 92. Cable elements.

The cable used is the *42N*, with 5mm of diameter. The maximum traction force that can support the cable is of 14,8KN, so the traction resistance for a 5mm diameter is of 188,44N/mm^2.

Table 1. Cable selection. ***Teufelberger, Catalogue Stahl- und Faserseile.*** **(Source: [26])**

42 N

SPEZIFIKATIONEN **EN 12385-4***

6 x 7 N mit Fasereinlage (FC) Kreuzschlag
Aufbau: FC + 6 (1+6)
Anzahl der Drähte in den Außenlitzen: 42

* ehem. DIN 3055

Einsatzgebiete
- Zugseil
- Materialseilbahn
- Bauwinden
- Abspannseile

Seil-Ø mm	Art.Nr.	Bezeichnung	MBK kN	Oberfläche	Nennfestigkeit der Drähte	kg/m	Alupresskl. Größe	AC	STC	Preis Euro/100m
2,00	4681105	42N 1AX	2,4	verzinkt	1770	0,01	2	1	S	29,91
2,50	4681149	42N 1AX	3,3	verzinkt	1770	0,02	3	1	S	35,76
3,00	4681291	42N 1AX	5,3	verzinkt	1770	0,03	3	1	S	40,66
4,00	4681493	42N 1AX	9,4	verzinkt	1770	0,05	4	1	S	60,96
5,00	4681749	42N 1AX	14,8	verzinkt	1770	0,10	5	1	S	75,38
6,00	4682029	42N 1AX	21,2	verzinkt	1770	0,13	6	1	S	101,60
8,50	4682887	42N 1CX	37,6	verzinkt	1770	0,25	9	3	N	188,00
9,50	4183191	42N 1AX	53,2	blank	1770	0,31	10	3	N	213,00
10,00	4703192	42N 1AX	58,8	verzinkt	1770	0,35	10	1	N	237,46

3.2.2. Anchorage elements

Two types of anchorage elements, cable closure and rope clip, were tested in the laboratory in order to ensure that the maximum traction force fulfills the requirements needed in the structure. Finally, taking into account the shell element's design, the cable closures were used.

<u>Anchorage element: Cable Closure.</u>

The elements chosen from *Seilerei Wüstner* catalogue, company specialized in cables anchorage systems [27], Figure 93.

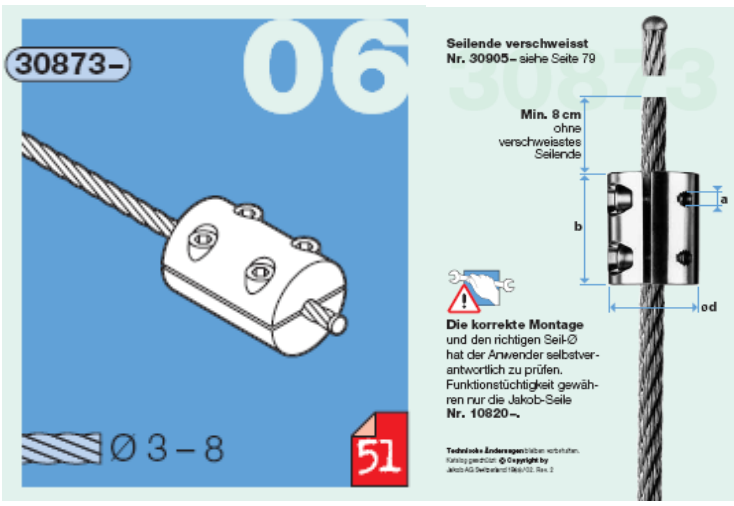

Figure 93. Anchorage element: cable closure. ***Seilerei Wüstner.*** **(Source: [27])**

As can be seen in Table 2, the maximum axial force supported by the element is 70% of the force supported by the steel cable. As can be seen in Table 1, the maximum traction force that can support the cable is of 14,8KN. So the maximum axial forced supported by the element is 13,16KN. This element was subjected to some tests to ensure this value, and it was found that it does not support as much force as it is specified by the manufacturer. This is discussed later on in this section.

Table 2. Cable closure geometrical parameters. (Source: [27])

KLEMMRING 2TEILIG

1.4404
AISI 316

Bruchkraft: 70% der Seil-Mindestbruchkraft / Patent/ DBGM angemeldet

mm

30873–	ø mm	a	b	ø d
0300	3,0	M4	27	22
0400	4,0	M4	27	22
0500	5,0	M6	42	28
0600	6,0	M6	42	28
0800	8,0	M6	42	28

The anchorage elements to hold the tendons in the structure were tested in the laboratory. First with only one element and then with two elements in series configuration.

As can be seen in subsequent graphs, force versus displacement, obtained in the tensile tests; the results in the beginning of the graph are not representative. In this period of time the displacement of the tensile testing bench is represented until the elements are tight and the tensile force is really applied, when the representative data are obtained.

Test 1: One element

A traction test bench was used to carry on the experiments in the laboratory. The cable closure elements were screwed on as tight as possible, Figure 94.

Figure 94. Cable closure. Test 1: one element.

After the test was carried on, the two elements were able to support 16KN, Figure 95, so each element could support 8KN of traction force.

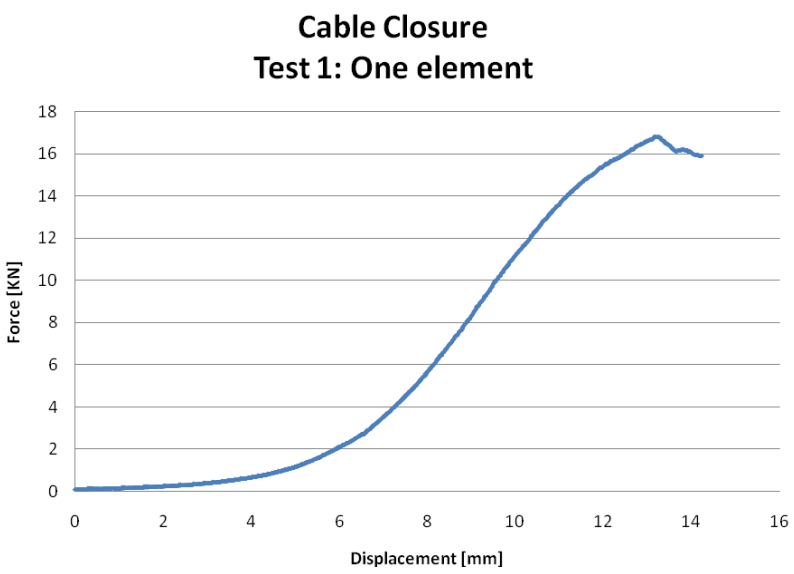

Figure 95. Cable closure, test 1 results: one element.

Test 2: Two elements in series

Now two elements in series configuration were placed in each side of the cable, Figure 96.

Figure 96. Cable closure. Test 2: two elements in series.

In this case, the four elements were able to support 24KN, Figure 97, so each block of two elements in series configuration could support 12KN of traction force.

The two elements in series configuration were tightened to the steel cable leaving a small gap between them, so can be seen in the Figure 97 a change on curvature (when there is 6mm of displacement) when the slide occurs.

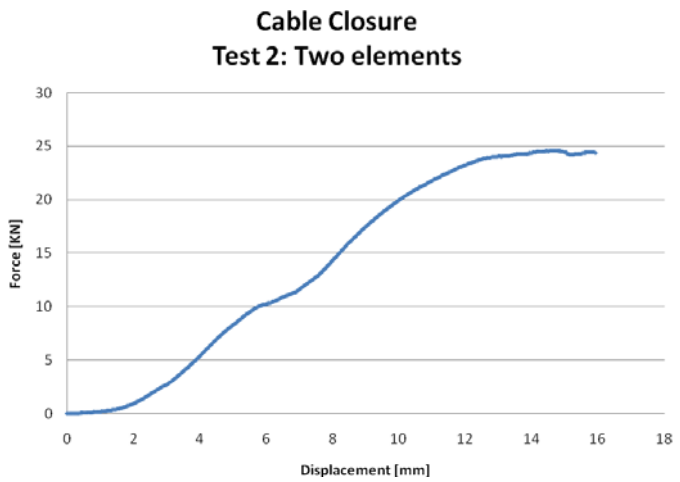

Figure 97. Cable closure, test 2 results: two elements.

As can be seen the element do not reach the 13,16KN specified in their characteristic catalogue. Each element only was able to carry 6KN in the tests carried. This can be due to the difficulty in screwing on properly the four screws in the element. For future researches this elements can be tested with different screw qualities in order to improve their behavior.

Anchorage element: rope clips

The elements were chosen from *Stabilit* catalogue: *10 Seil-Klemmen* , small ones 2-4 mm (Article number: 0-19-174-4) and big ones 3-5 mm (Article number: 0-19-177-5), for cables from 3 to 5mm of diameter,
Figure 98 [26].

(a) Small clips (b) Big clips.

Figure 98. Rope clips

Table 3. Rope clips geometrical parameters. (Source: [26])

DRAHTSEILKLEMME EN 13411-5 (DIN 1142)

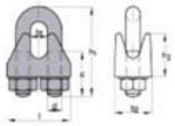

SPEZIFIKATIONEN: verzinkt

Nenngröße = max. Seil-Ø in mm	Art.Nr.	erf. Anzahl	Maß b2 in mm	Maß h1 in mm	Maß l in mm	Aufmachung in Stück	AC	STC	Preis/Stk. Euro
5,0	3011052	3	13	25	25	100	2	S	0,23
6,5	3011062	3	16	32	30	100	2	S	0,33
8,0	3011082	4	20	41	39	50	2	S	0,48
10,0	3011102	4	20	46	40	50	2	S	0,56
13,0	3011132	4	28	64	55	100	2	S	1,48
16,0	3011162	4	32	76	64	50	2	S	2,29
19,0	3011192	4	32	83	68	50	2	S	2,38
22,0	3011222	5	34	96	74	50	2	S	3,55
26,0	3011262	5	38	111	84	50	2	S	6,86

DRAHTSEILKLEMME

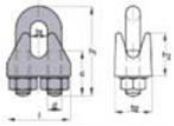

SPEZIFIKATIONEN: ähnlich DIN 741/schwarz

Nenngröße = max. Seil-Ø in mm	Art.Nr.	erf. Anzahl	Maß b2 in mm	Maß h1 in mm	Maß l in mm	Aufmachung in Stück	AC	STC	Preis/Stk. Euro
3,0		3	10	20	21	100	2	N	1,79
5,0		3	11	24	23	100	2	N	2,14
6,5		3	12	28	26	100	2	N	2,53
8,0		4	14	34	30	100	2	N	3,32
10,0		4	18	42	34	50	2	N	5,59

The two different sizes of rope clips were tested.

Small Rope Clips

Test 1: One element

This element was tested in the laboratory with a single cable configuration, Figure 99.

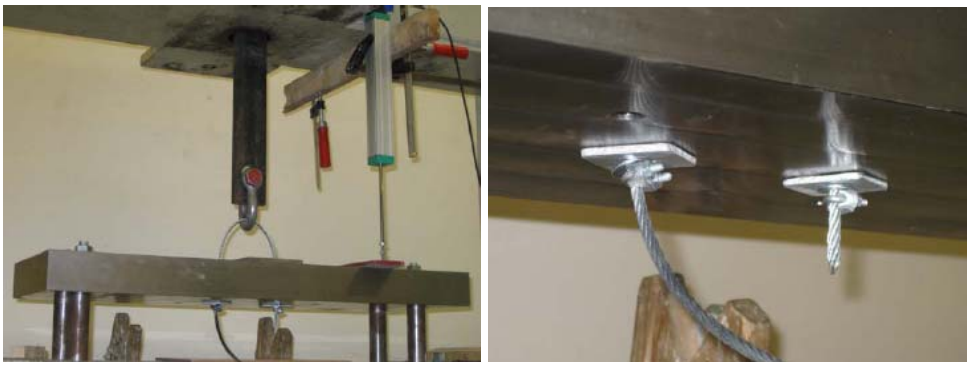

Figure 99. Small rope clips Test. One element each side.

In this case, the two elements were able to support 3KN, Figure 100, so each element could support 1,5KN of traction force. This value does not fulfill our requirements, is not strong enough.

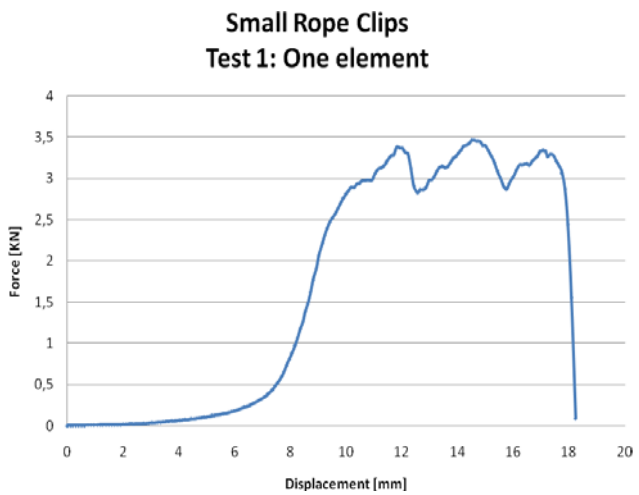

Figure 100. Small rope clips, test1: one element.

In Figure 100 the variations or changes in curvature when the element reaches the maximum force value are due to the slip of the element (negative slope) until it gets the enough friction again (inflexion point) and the element works again agaist tensile force (positive slope).

Big Rope Clips

This element was tested in the laboratory with a single and double cable configuration, as well as with series configurations with two and three elements.

Test 1: One element in single cable

In the first test one element and a single cable configuration was used, Figure 101.

Figure 101. Big rope clips Test. One element each side.

In this case, the two elements were able to support 5 KN, Figure 102, so each element could support 2,5KN of traction force. Again the change in curvature is due to the slide of the element. Also can be seen clearly the displacement of the test tensile bench in the beginning of the experiment.

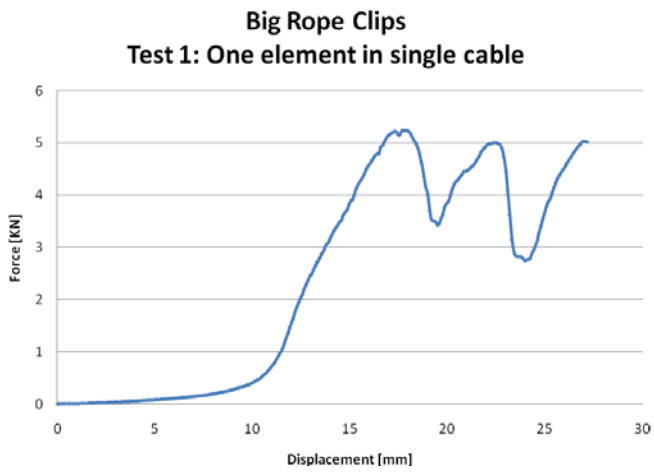

Figure 102. Big rope clips, test1: one element.

Test 2: Two elements in single cable

In the second test two elements in series and a single cable configuration was used, Figure 103.

Figure 103. Big rope clips Test. Two element each side.

In this case, the four elements were able to support 11 KN, Figure 104, so each pair of elements could support 6,5KN of traction force.

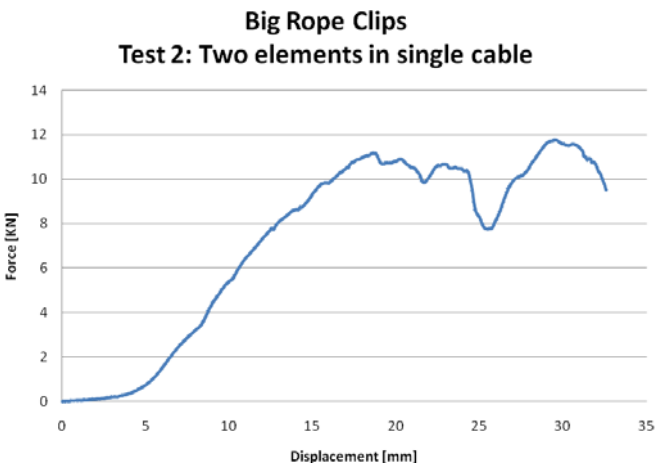

Figure 104. Big rope clips, test 2: two elements in single cable.

Test 3: One element in double cable

Now one element and a double cable configuration was used, Figure 115.

Figure 105. Big rope clips Test. One element in double cable.

In this case, the two elements were able to support only 4 KN, Figure 106, so each element could support 2 KN of traction force.

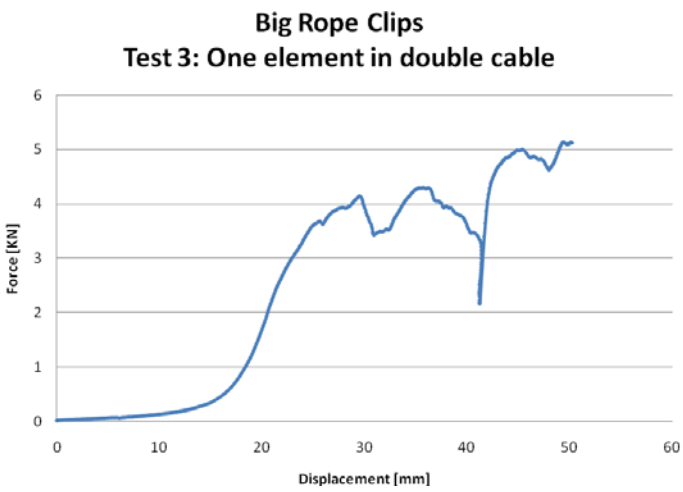

Figure 106. Big rope clips, test 3: one element in double cable.

Test 4: Three elements in double cable

In this case three elements and a double cable configuration was used, Figure 107.

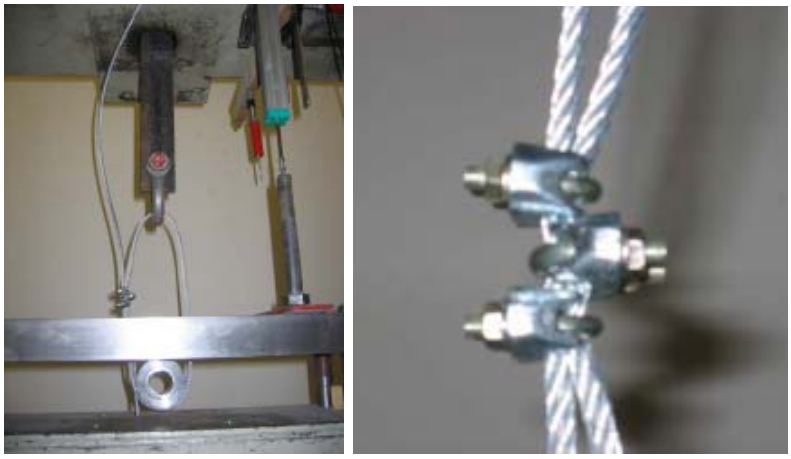

Figure 107. Big rope clips Test. Three elements in double cable.

The steel cable broke in the test close to the elements, so the cable collapsed and was not able to support the tension, Figure 108.

Figure 108. Failure of the steel cable.

In this case, the three elements were able to support 25 KN, Figure 109, so each element could support 8,3 KN of traction force.

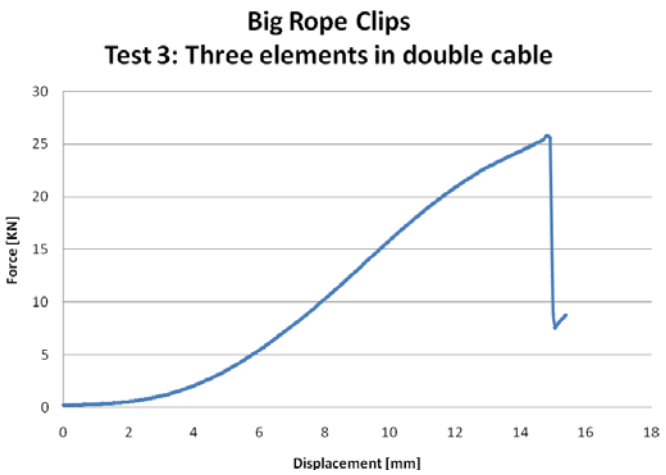

Figure 109. Big rope clips, test 4: three elements in double cable.

To sum up, it can be seen that the rope clips enclosure elements work much better maintaining together two cables instead of one. Moreover the use of more than one element in series configuration improves greatly the behavior. So this will be taken into account in futures designs.

In our case an element to maintain tight only one cable was needed, so the cable closure elements were chosen in this construction.

3.2.3. Construction process

First the pneumatic formwork was placed on the plane work surface, folded properly. Then it was covered with a plastic thin layer. This plastic layer was previously marked with the correct position of each element of the flat plane, allowing and speeding up the subsequent collocation of the elements in the plane, Figure 110.

Figure 110. Pneumatic formwork, plastic layer and precast elements.

The elements were positioned in their places with the help of a crane. The process starts with the smaller elements (elements type 1) in the internal ring, then the second ring (elements type 2), and advance element by element following a spiral path, Figure 111.

Figure 111. Allocation of the elements in the plane.

The cables are allocated in the conducts step by step when every element is positioned, Figure 112.

Figure 112. Cables allocated in the conducts element by element.

The central ring had an anchorage system with a spring, Figure 113, holding the meridian cables as shown in the figure with the cable closure elements previously selected in section 3.2.2.

Figure 113. Anchorage system in the central ring with a spring in all meridional tendons.

In element 6, at the base of the dome, there is also an anchorage system holding each one of the tendons in radial direction. In the installation, the correct play must be left in order to allow the tendon acquire its curved shape while the elements are raising one after another to get the final dome shape, Figure 114.

Figure 114. Anchorage systems in elements 6 type in all meridional tendons.

Now the cable winches are anchored in the right place and direction, Figure 115. The right position can be seen in the previous plans, in Figure 83.

Figure 115. Cable winches anchored.

When everything is correctly attached the pneumatic formwork can start working. The pneumatic formwork raises the structure ring by ring, Figure 116.

Figure 116. Raising process. Concrete Shell.

In this experiment the last two rings did not raise to reach the final shape. The pneumatic formwork used was the one from Figure 89, whose joints were not reinforced enough. So the pneumatic formwork did not support the pressure of the elements and collapsed in the base enclosures. This is why another pneumatic formwork, Figure 91, was built taking special care in the base reinforcement. Calculations about the pneumatic formwork load capacity are presented in Section 5.2.

3.3. Ice shell construction

This new construction method can also be applied to ice shells. The key elements of the construction method are the same as shown before. There are only small differences in working with ice instead of concrete.

3.3.1. Ice as construction material

Ice is a beautiful material present in nature associated mainly to winter and cold temperatures. However, considering the strength properties, ice is a rather weak material compared to conventional construction materials as concrete or wood [24].

Pure liquid water is transformed to its solid state, ice, at a temperature of 0°C when the pressure is at one atmosphere. Interestingly, the density of liquid water at the freezing point is 0.99984 g/cm^3 but decreases to 0.9168 g/cm^3 when that water organizes itself into crystalline ice at 0°C. This density difference is due the large open spaces within the crystal lattice of ice. The increased volume of the solid lattice causes pure water to expand by approximately 9% upon freezing, resulting in ruptured pipes or damaged engines when the process occurs in a closed vessel. Ice is one of a very few solid substances that is lower in density than the corresponding liquid state.

To enable the freezing of water a constant temperature below -2ºC is a requirement to build the ice shells. In the northern hemisphere this temperature requirement will only be met during the winter months November to March and it will strongly depend on altitude and location. Warmer short periods will not harm the ice shell due to the long winter nights and also due to the possibility to increase the thickness of the ice during cold periods.

Therefore, ice as a construction material is either used as a decorative material on a supporting structure or it is applied in structures with very low stress states due to self weight and wind forces.

Igloos and *Japanese structures* were used for the storage of vegetables and stake during the winter. Small ice shells were also built in *Isler* by hanging textile membranes from supports, spraying the membranes with fresh water and removing the supporting struts after the freezing of water.

Larger ice shells with spans up to 30m were constructed in 2000 by *Kokawa*. Kokawa's ice domes were built on air inflated membrane which was covered by snow with the aid of snow ploughs and then sprayed with water, Figure 117 [34].

Figure 117. Kokawa's ice dome. (Source: [34])

3.3.2. Ice shell in the laboratory

First an ice shell in the laboratory was built. The final shell had a diameter of 4,8m and 0,9m height, Figure 118. In this case a previous method was used, Styrofoam segments where placed between the ice segments as was explained in Section 3.1. All the shell was surrounded with an unbounded tendon marked in red [24].

A flat ice plate with 32 Styrofoam segments was produced, Figure 118a. The circle in the plan was approximated by a polygonal line with 31 straight parts and a concrete anchor block for the post tensioning tendons. Along the circumference scaffolding had to be provided in order to form the boundary of the ice shell with a thickness of 40 mm, Figure 118b. Along the edge of the ice plate an unbounded tendon was placed and two stressing anchorages were provided at the anchor block. Figure 118c shows a section through the ice shell which was obtained by stressing the tendon. During the transformation from flat plane to shell the diameter was reduced from 5,2m to 4,8m.

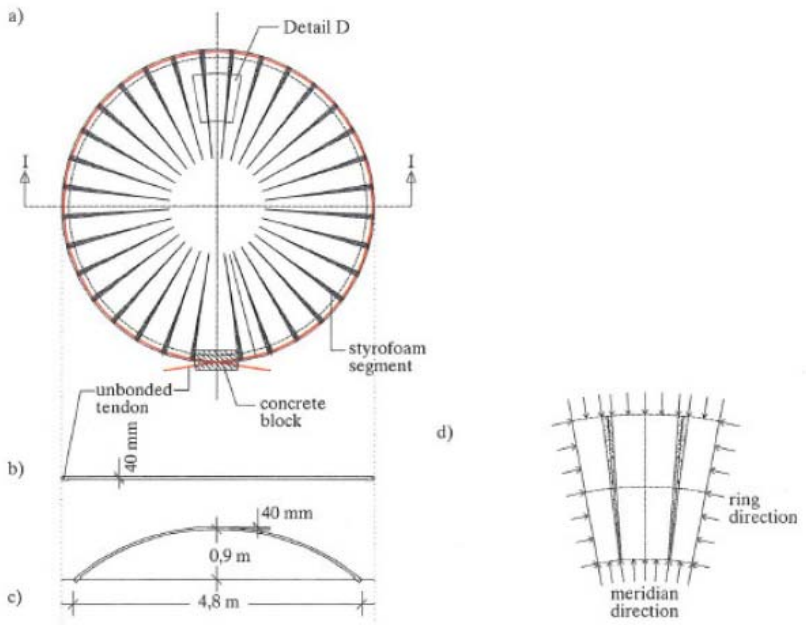

Figure 118. (a) Plan view of ice plate, (b) Section of ice plate, (c) Section of ice shell, (d) Detail D. (Source: [24])

This experiment was carried out in the laboratory of the Institute for Structural Engineering after its suitable fitting out. The Figure 119 and Figure 120 show the transforming process of this ice plate into an ice shell.

Figure 119. Raising process of the ice shell. (Source: [24])

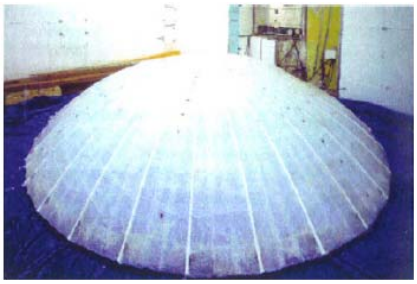

Figure 120. Completed ice shell in laboratory. (Source: [24])

3.3.3. Small ice shell

The construction of the ice shell with the new method based on planar elements took place in Obergurgl, a village in the Alps in Tyrol, Austria, situated almost 2000 meter above the sea level, Figure 121.

Figure 121. Austria map, Obergurgl location. (Source: azerb.com)

First the pneumatic formwork was placed on the plane working surface. Then a frame is situated alongside the circumference of the circular plate. Afterwards water, which will freeze to ice, is sprayed inside the frame. So a circular plate of ice is generated.

After the hardening of the ice, those parts of the ice which are superfluous for the transformation into a shell will be removed, Figure 122. Through the removal of the superfluous material, interfaces in radial direction are created. Also the ducts are created cutting the paths, placing the ducts and filling the gaps, to ensure the ducts, with water again.

The interfaces in circumference direction are produced by cutting into the ice. These cuttings are predetermined breaking points. Therefore the ice will break along these cuts during the transformation process.

Now the cable winches are anchored in the right place and direction in the special elements.

Figure 122. Circular plate of ice formation, cutting the elements.

The pneumatic formwork raises the elements to form the shell,
Figure 123. When the final shape was obtained the tendons were tight and the cable winches were removed. Also a door was built removing three elements near the base, Figure 124.

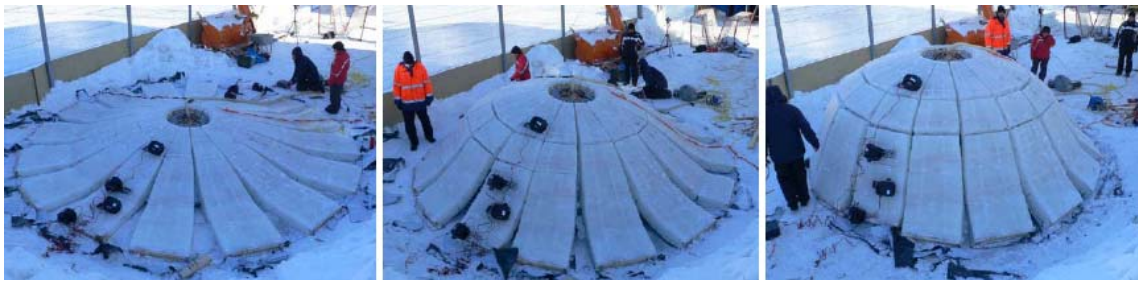

Figure 123. Raising process in the small ice shell.

Figure 124. Door built in the small ice shell

3.3.4. Big ice shell in Obergurgl

The construction of this big ice shell took place also in Obergurgl. The process in this case was the same carried out by constructing the small one, Figure 125 and Figure 126.

Figure 125. Circular plate formation in the big ice shell.

Figure 126. Raising process in the big ice shell.

The last ring of the structure did not rise properly due to the fracture in the wood frame in the central ring. This was probably caused because the frame was formed in December 2008 but there was not enough cold to continue with the experiment, so the rest of the process was made in January 2009. In this long period the wood frame got damage with the humidity from the snow falls during Christmas time.

Other way for creating the ducts, where the cables are placed, can be tested in the future. The frame is situated alongside the circumference of the circular plate. First a layer of water is sprayed inside the frame. When it freezes into ice the conducts are placed in the right position over the ice layer previously created. Then a second layer of water is sprayed inside the frame. After the hardening of the ice, those parts of the ice which are superfluous for the transformation into a shell will be removed.

4. ANALYTICAL AND NUMERICAL ANALYSIS OF A SHELL

In this section of the project the structural behavior of a concrete and an ice shell is going to be studied by using two main methods: analytical formulas and finite element analysis. The results obtained in both analyses will be compared.
Three different load cases will be studied:

- Dead load.
- Snow effect.
- Wind effect.

The analysis in this section is carried out on a hemispheric shape and not on the final shape formed by 96 planar elements. This approximation allows us to obtain results with more simple calculation methods.

4.1. Shell parameters

4.1.1. Geometrical parameters of the shell

A hemispherical shell with constant thickness is a revolution structure. Due to its axisymmetry it is only necessary to study the points which belong to one meridian. All the points situated in the same shell ring will have the same properties, forces, stresses and displacements.

The main points taken into account in our study are the edges of the planar elements. In these points the resultant forces and the stresses are calculated analytically and with finite element analysis.

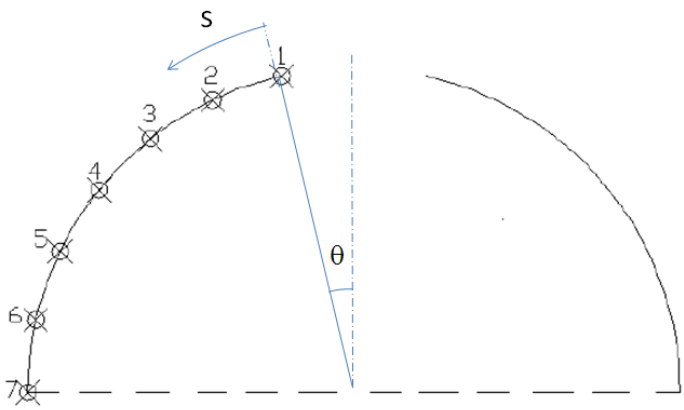

Figure 127. Position of the analyzed points

The ordinate length of the meridians, s, and the meridional angle, θ, can be easily obtained, explained later on in this section, for all the points in this study, Figure 127. The values for each point are shown in Table 4 (see Annex I).

Table 4. Position of the analyzed points.

Shell Point	θ [º]	θ [rad]	s[rad]
1	12,8571	0,2244	0,0000
2	25,7143	0,4488	0,9319
3	38,5714	0,6732	1,8639
4	51,4286	0,8976	2,7958
5	64,2857	1,1220	3,7277
6	77,1429	1,3464	4,6597
7	90,0000	1,5708	5,5916

4.1.2. Material properties of the shell

Two different types of shells will be studied: concrete and ice shells. The main physical properties of the shell materials are exposed in the following Table 5:

Table 5. Material properties of the shell

Properties	Concrete	Ice
Density [Kg/m^3]	2400	916,7
Poisson's ratio	0,2	0,33
Young's modulus [GPa]	28,4	9,5
Shell Thickness [m]	0,05	0,2

4.1.3. Loads and boundary conditions

Three different load cases will be studied:
Case 1. Dead load.
Case 2. Snow effect.
Case 3. Wind effect.

The vertical displacements in the base of the shell are not allowed, and the displacements in the horizontal plane are free. Therefore only vertical reactions will be obtained.

4.2. Analytical analysis formulation

Symbols

For the analytical analysis some symbols are used in this section [28].

Dimensional parameters

θ	—	Meridional angle
φ	—	Perimetrical angle
r	[L]	Radius
s	[L]	Ordinate length of the meridians
t	[L]	Shell thickness

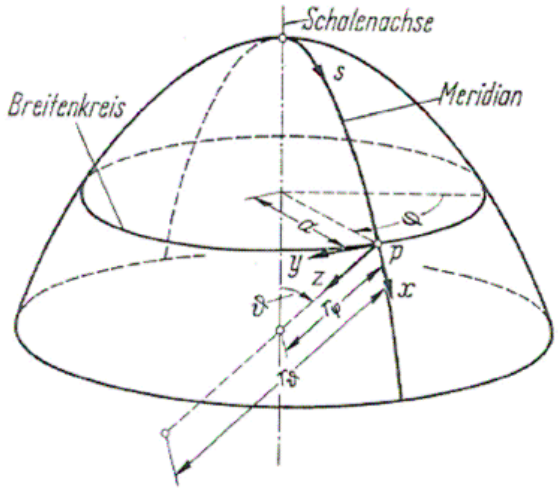

Figure 128. Dimensional parameters. (Source: [28])

Deformations

u	[L]	Translational displacement in x-direction
w	[L]	Translational displacement in z-direction
$\overline{w}$	[L]	Translational displacement perpendicular to shell axis
χ	—	Elongation of the meridian tangent
E	[K/L^2]	Modulus of elasticity
μ	—	Poisson´s ratio

$$x = \sqrt[4]{3\left(1-\mu^2\right)\frac{r^2}{t^2}}$$ Dimensionless shell parameter (9)

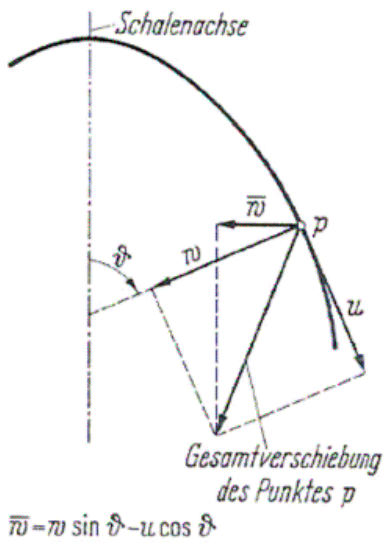

Figure 129. Deformations. (Source: [28])

Load types, load components and stresses resultants

p_E	[K/L^2]	Self-weight of the shell per unit of middle surface
p_S	[K/L^2]	Snow pressure per unit of middle surface
p_x	[K/L^2]	
p_y	[K/L^2]	Surface load components
p_z	[K/L^2]	
N_θ	[K/L]	Normal forces
N_φ	[K/L]	
T	[L/L]	Tangential force
M_θ	[KL/L]	Moments
M_φ	[KL/L]	
Q	[K/L]	Shear force

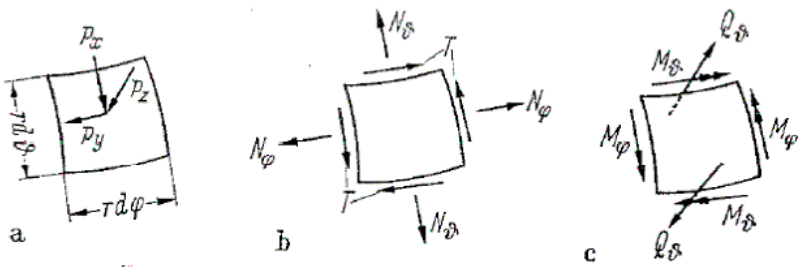

Figure 130. Load components and resultant forces. (Source: [28])

Stresses calculation

To calculate the stresses in all load cases the following formulas are used:

$$\sigma_\theta = \frac{N_\theta}{A} + \frac{M_\theta z}{I_\theta} \tag{10}$$

$$\sigma_\varphi = \frac{N_\varphi}{A} + \frac{M_\varphi z}{I_\varphi} \tag{11}$$

In our load cases the structure won't suffer moments and the stress calculated is per unit length (being t the shell thickness), so the formulas are reduced to the following:

$$\sigma_\theta = \frac{N_\theta}{t} \text{ [N/m}^2\text{]} \tag{12}$$

$$\sigma_\varphi = \frac{N_\varphi}{t} \text{ [N/m}^2\text{]} \tag{13}$$

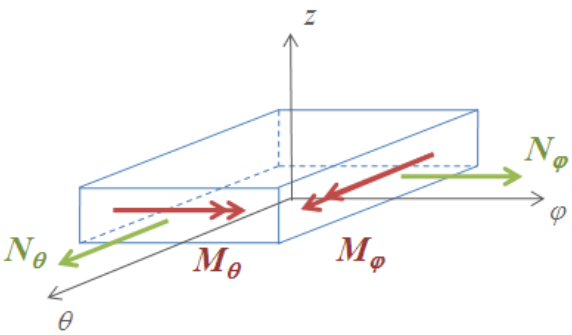

Figure 131. Shell element with local axis.

The formulas which have been used to calculate the **resultant forces** depend on the type of load applied. We differ between three types of loads in our study.

4.2.1. Case 1: Dead load

To calculate the self weight is the easiest case in our study, it can be obtained with the following formulas, Figure 132 [28].

Normal forces

$$N_\theta = -p_E r \frac{\cos\theta_0 - \cos\theta}{\sin^2\theta} \text{ [N/m]} \tag{14}$$

$$N_\varphi = p_E r \left(\frac{\cos\theta_0 - \cos\theta}{\sin^2\theta} - \cos\theta \right) \text{ [N/m]} \tag{15}$$

$$T = 0 \tag{16}$$

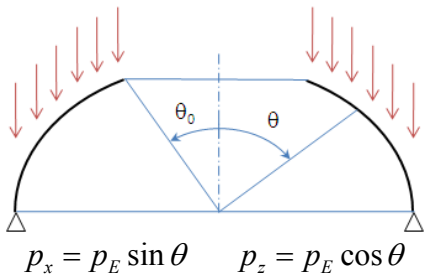

Figure 132. Forces caused by a distributed load over the shell. (Source: [28])

Self-weight of the shell per unit of middle surface

$$p_E = \rho(\frac{Kg}{m^3}) \cdot g(\frac{N}{Kg}) \cdot t(m) \quad \text{[N/m}^2\text{]} \tag{17}$$

ρ [Kg/m^3] Material density
$g = 9.8$ m/s^2 Gravity

4.2.2. Case 2: Snow effect.

To calculate the snow effect, the simplest case is supposed, snow perpendicular to the ground, Figure 133[28].

Normal forces

$$N_\theta = -p_s \frac{r}{2}\left(1 - \frac{\sin^2\theta_0}{\sin^2\theta}\right) \tag{18}$$

$$N_\varphi = p_s \frac{r}{2}\left(1 - \frac{\sin^2\theta_0}{\sin^2\theta} - 2\cos^2\theta\right) \tag{19}$$

$$T = 0 \tag{20}$$

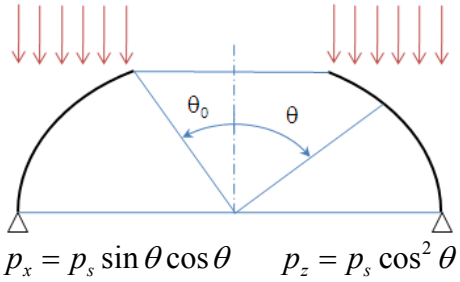

Figure 133. Forces caused by a distributed load. (Source: [28])

p_s [N/m^2] Snow pressure per unit of middle surface

From *Eurocode* (Actions on structures, Part 1-3: General Actions Snow loads, [29]) the snow pressure can be calculated considering some parameters as the altitude.

Snow load on roofs, *s*

$$s = \mu_i C_e C_t s_k \tag{21}$$

s	snow load on roofs [KN/m^2]
μ_i	roof shape coefficient
s_k	snow load characteristic value on the ground, depending on the altitude [KN/m^2]
C_e	exposure coefficient (generally taken equal to 1)
C_t	thermal coefficient (for normal standards of thermal insulation, taken equal to 1.

- Roof shape coefficient μ_i

Shape coefficients are needed for an adjustment of the ground snow load to a snow load on the roof taking into account effects caused by non-drifted and drifted snow load arrangements.

There are three different possibilities of snow load that must be taken into account in the coefficients:
- Snow equally and uniform distributed when there are no wind conditions.
- Snow not uniformly distributed, due to local obstacles or snow accumulated from other inclined roofs.
- Snow from the higher part of the building due to slicing, impediments in the structure for snow slicing.

For cylindrical roofs the roof shape coefficient is selected as follows, Figure 134, Figure 135.

For $\beta \leq 60^{o}$, $\mu_1 = 0{,}8$

$\mu_2 = 0{,}2 + 10h/l$, with the restriction $\mu_2 \leq |2{,}0|$

$\mu_3 = 0{,}5\mu_2$

For $\beta > 60^{o}$, $\mu_1 = \mu_2 = \mu_3 = 0$ (22)

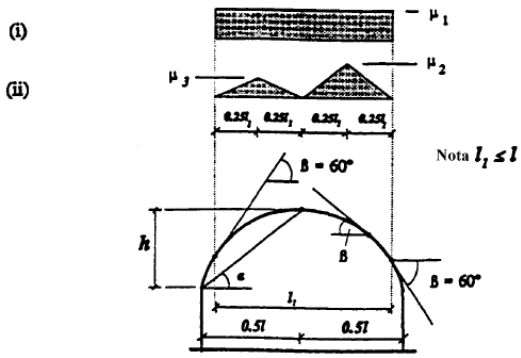

Figure 134. Roof shape coefficient for snow loads in cylindrical roofs.

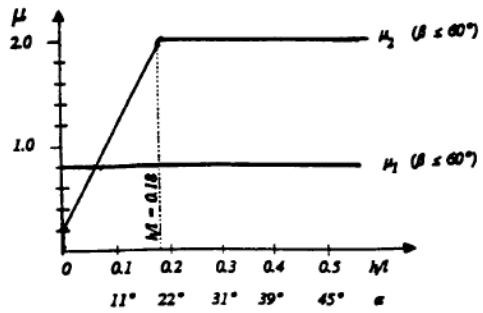

Figure 135. Roof shape coefficient for snow loads in cylindrical roofs, as function of *h/l* relationship.

In our case $\beta \leq 60^{o}$, so $\mu_1 = 0{,}8$. We only take into account the first coefficient, a snow equally and uniform distributed load when there are no wind conditions.

The roof shape coefficient depends on the roof angle. For our case: $\mu_i = 0{,}8$

- Snow load on the ground s_k

The characteristic value depends on the climatic region. Austria belongs to the Alpine Region as can be seen in Figure 136.

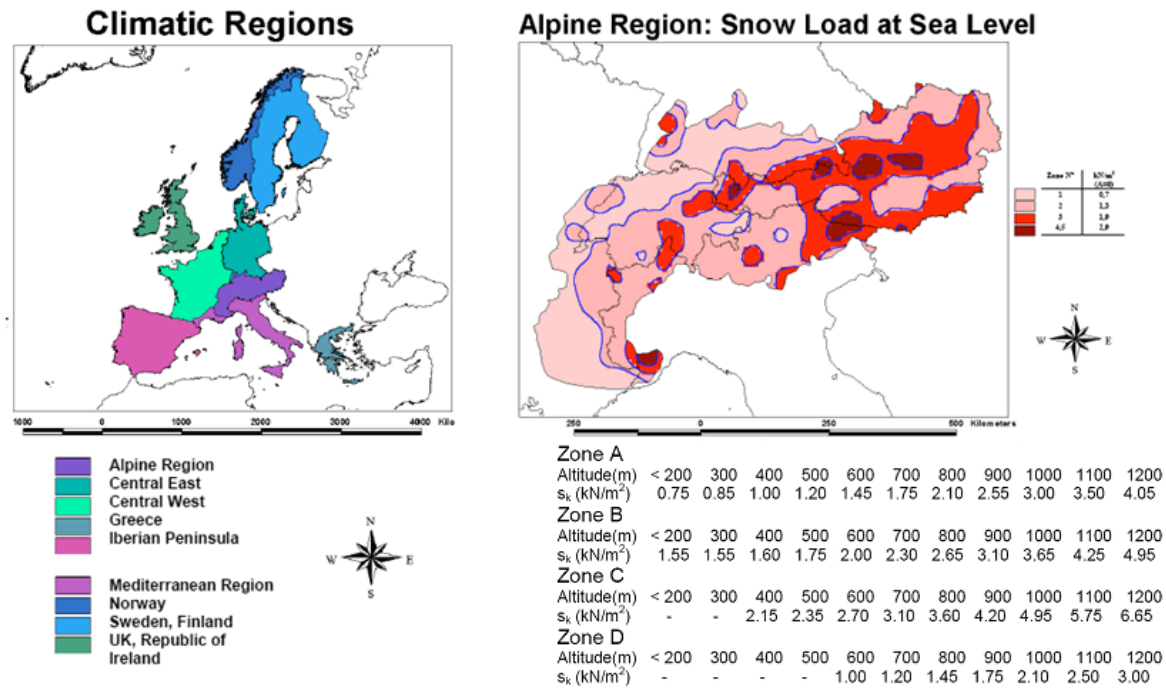

Figure 136. Snow load. (Source: [29])

The values obtained from *Eurocode* and *Önorm* are sum up in the Table 6.

Table 6. Snow load values. (Source:[30])

Location in Austria	Altitude (m)	Zone	s_k (KN/m^2)	$s = 0.8 s_k$
Wien (Stephansplatz)	171	2 (B)	1.36	1.088
Tirol (Obergurgl)	1910	2 (B)	7.00	5.600

So the following formula will be used:

$$p_s = 0.8 s_k \tag{23}$$

4.2.3. Case 3: Wind effect.

From *Eurocode* (Actions on structures, Part 1-4: General Actions Wind loads, [31]) the wind pressure can be calculated in several ways following a more difficult process.

Symbols

q_b	reference mean (basic) velocity pressure
q_p	peak velocity pressure
z	height above ground
c_d	dynamic factor
c_s	size factor
v_b	basic wind velocity
c_{dir}	directional factor
c_{season}	season factor
z	height above the terrain
$v_m(z)$	mean wind velocity
$c_r(z)$	roughness factor
$c_o(z)$	orography factor
z_0	roughness length
k_r	terrain factor
z_{min}	minimum height
z_{max}	maximum height
$I_v(z)$	turbulence intensity
ρ	air density
$c_e(z)$	exposure factor
w_e	wind pressure acting on the external surfaces
$q_p(z_e)$	peak velocity pressure
z_e	reference height for the external pressure
c_{pe}	pressure coefficient for the external pressure
w_i	wind pressure acting on the internal surfaces
z_i	reference height for the internal pressure
c_{pi}	pressure coefficient for the internal pressure
c_{pe}	external pressure coefficients for buildings and parts of buildings
$c_s c_d$	structural factor
c_f	force coefficient for the structure or structural element
F_w	wind force acting on a structure
A_{ref}	reference area of the structure or structural element
$c_{f,x}$	alongwind force coefficient of spheres
Re	Reynolds number
K	roughness
b	diameter
v	kinematic viscosity of the air ($\nu = 15 \cdot 10\text{-}6\ m^2/s$)

Representations of wind actions *([31] Eurocode 3.2)*

The wind action is represented by a simplified set of pressures or forces whose effects are equivalent to the extreme effects of the turbulent wind.

Models *([31] Eurocode 3.5)*

The effect of the wind on the structure (i.e. the response of the structure), depends on the size, shape and dynamic properties of the structure. This part covers dynamic response due to along-wind turbulence in resonance with the along-wind vibrations of a fundamental flexural mode shape with constant sign.
The response of structures should be calculated from the peak velocity pressure, q_p, at the reference height in the undisturbed wind field, the force and pressure coefficients and the structural factor $c_s c_d$. q_p depends on the wind climate, the terrain roughness and orography, and the reference height. q_p is equal to the mean velocity pressure plus a contribution from short-term pressure fluctuations.

Wind velocity and velocity pressure *([31] Eurocode 4.1, 4.3)*

The wind velocity and the velocity pressure are composed of a mean and a fluctuating component.

The fundamental value of the basic wind velocity, $v_{b,0}$, is the characteristic 10 minutes mean wind velocity, irrespective of wind direction and time of year, at 10 m above ground level in open country terrain with low vegetation such as grass and isolated obstacles with separations of at least 20 obstacle heights. The value of the basic wind velocity, $v_{b,0}$, is given in the *ÖNORM B 1991-1-4*, [32].

The fundamental value of the basic wind velocity in the locations in Austria under study are showed in Table 7.

Table 7. Wind velocity and velocity pressure.

Location in Austria	Altitude (m)	$V_{b,0}$ (m/s)	$q_{b,0}$ (KN/m^2)
Wien (Stephansplatz)	1910	27	0,46
Tirol (Obergurgl)	171	27,6	0,48

The ***basic wind velocity*** shall be calculated from expression:

$$v_b = c_{dir} \cdot c_{season} \cdot v_{b,0} \tag{24}$$

where:

v_b is the basic wind velocity, defined as a function of wind direction and time of year at 10 m above ground of terrain category II

$v_{b,0}$ is the fundamental value of the basic wind velocity

c_{dir} is the directional factor. The recommended value is 1,0.

c_{season} The value of the season factor, c_{season}. The recommended value is 1,0.

So we can reduce the basic wind velocity expression 24 to:

$$v_b = v_{b,0} \tag{25}$$

The ***mean wind velocity*** $v_m(z)$ at a height z above the terrain depends on the terrain roughness and orography and on the basic wind velocity, v_b, and should be determined using expression:

$$v_m(z) = c_r(z) \cdot c_0(z) \cdot v_b \tag{26}$$

where:
$c_r(z)$ is the roughness factor.
$c_o(z)$ is the orography factor, taken as 1,0.

The ***roughness factor***, $c_r(z)$, accounts for the variability of the mean wind velocity at the site of the structure due to: the height above ground level and the ground roughness of the terrain upwind of the structure in the wind direction considered.
The recommended procedure for the determination of the roughness factor at height z is given by Expression 27 and is based on a logarithmic velocity profile.

$$c_r(z) = k_r \cdot \ln\left(\frac{z}{z_0}\right) \quad \text{for} \quad z_{\min} \le z \le z_{\max}$$

$$c_r(z) = c_r(z_{\min}) \quad \text{for} \quad z \le z_{\min} \tag{27}$$

where:
z_0 is the roughness length
k_r terrain factor depending on the roughness length z_0.
z_{min} minimum height defined in Table 4.1
z_{max} maximum height, is to be taken as 200 m.

z_0, z_{min} depend on the terrain category. Recommended values are given in Table 8 depending on five representative terrain categories.

Table 8. Terrain categories and terrain parameters. (Source: [31], Table 4.1)

Terrain category		z_0 m	z_{min} m
0	Sea or coastal area exposed to the open sea	0,003	1
I	Lakes or flat and horizontal area with negligible vegetation and without obstacles	0,01	1
II	Area with low vegetation such as grass and isolated obstacles (trees, buildings) with separations of at least 20 obstacle heights	0,05	2
III	Area with regular cover of vegetation or buildings or with isolated obstacles with separations of maximum 20 obstacle heights (such as villages, suburban terrain, permanent forest)	0,3	5
IV	Area in which at least 15 % of the surface is covered with buildings and their average height exceeds 15 m	1,0	10
The terrain categories are illustrated in Annex A.1.			

Terrain category III

Area with regular cover of vegetation or buildings or with isolated obstacles with separations of maximum 20 obstacle heights (such as villages, suburban terrain, permanent forest)

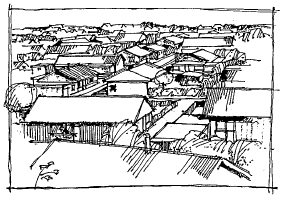

We are in case III:

$z_0 = 0{,}3m$, $z_{\min} = 5m$, $z_{\max} = 200m$

$z = 4{,}153m$, so $z \le z_{\min} = 5m$

$c_r(z) = c_r(5)$

In our case:

$$v_m(z) = c_r(5) \cdot v_{b,0} \tag{28}$$

Wind turbulence

The turbulence intensity $I_v(z)$ at height z is defined as the standard deviation of the turbulence divided by the mean wind velocity.

In or case, case III, $z \le z_{\min} = 5m$,

$$I_v = I_v(z_{\min}) = I_v(5) \tag{29}$$

Peak velocity pressure, *([31] Eurocode 4.8)*

The peak velocity pressure $q_p(z)$ at height z, which includes mean and short-term velocity fluctuations, should be determined.

$$q_p(z) = [1 + 7I_v(z)] \cdot \frac{1}{2} \cdot \rho \cdot v_m{}^2(z) = c_e(z) \cdot q_b \tag{30}$$

where:

ρ is the air density, which depends on the altitude, temperature and barometric pressure to be expected in the region during wind storms, we suppose $\rho = 1{,}25 Kg/m^3$

$c_e(z)$ is the exposure factor given in Expression 31.

$$c_e(z) = \frac{q_p(z)}{q_b} \tag{31}$$

q_b is the basic velocity pressure given in Expression 32.

$$q_b = \frac{1}{2} \cdot \rho \cdot v_b{}^2 \tag{32}$$

For ***flat terrain*** where $c_0(z)=1,0$, the exposure factor $c_e(z)$ is illustrated in Figure 137 as a function of height above terrain and a function of terrain category as defined in Table 8.

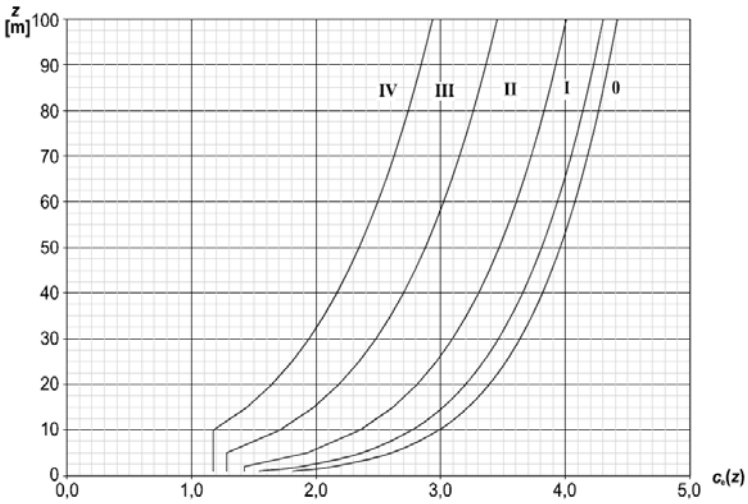

Figure 137. Ilustrations of the exposure factor $c_e(z)$ for c_0=1.0, k_i=1.0. (Source: [31], Figure 4.2)

From the graph $c_e(4{,}153)=1{,}28$

We suppose flat terrain:

$$q_p(z)=c_e(z)\cdot q_b=c_e(z)\cdot\frac{1}{2}\cdot\rho\cdot v_b^{\,2}=c_e(z)\cdot\frac{1}{2}\cdot\rho\cdot v_{b,0}^{\,2}=1{,}28\cdot\frac{1}{2}\cdot\rho\cdot v_{b,0}^{\,2} \qquad (33)$$

$$\rho=1{,}25Kg/m^3$$

So we have:

$$q_p(z)=0{,}64\cdot\rho\cdot v_{b,0}^{\,2} \qquad (34)$$

In Table 9 the peak velocity values are shown.

Table 9. Peak velocity values.

Location in Austria	$V_{b,0}$ (m/s)	$q_p(z)$ (N/m^2)
Wien (Stephansplatz)	27	583,2
Tirol (Obergurgl)	27,6	609,4

Wind pressure on surfaces, *([31] Eurocode 5,7)*

The wind pressure acting on the ***external surfaces***, w_e , should be obtained from Expression 35.

$$w_e=q_p(z_e)\cdot c_{pe} \qquad (35)$$

where:
$q_p(z_e)$ is the peak velocity pressure.
z_e is the reference height for the external pressure.
c_{pe} is the pressure coefficient for the external pressure.

The wind pressure acting on the ***internal surfaces*** of a structure, w_i , should be obtained from Expression 36.

$$w_i = q_p(z_i) \cdot c_{pi} \tag{36}$$

where:
$q_p(z_i)$ is the peak velocity pressure.
z_i is the reference height for the internal pressure.
c_{pi} is the pressure coefficient for the internal pressure.

The ***external pressure coefficients*** c_{pe} for buildings and parts of buildings depend on the size of the loaded area A, which is the area of the structure, that produces the wind action in the section to be calculated. The external pressure coefficients are given for loaded areas A of 1 m^2 and 10 m^2 in the tables for the appropriate building configurations as $c_{pe,1}$, for local coefficients, and $c_{pe,10}$, for overall coefficients, respectively.
Values for $c_{pe,1}$ are intended for the design of small elements and fixings with an area per element of 1 m^2 or less such as cladding elements and roofing elements. Values for $c_{pe,10}$ may be used for the design of the overall load bearing structure of buildings.

The recommended procedure for loaded areas up to 10 m^2, the value of $c_{pe,10}$ is taken as it is shown in the Figure 138.

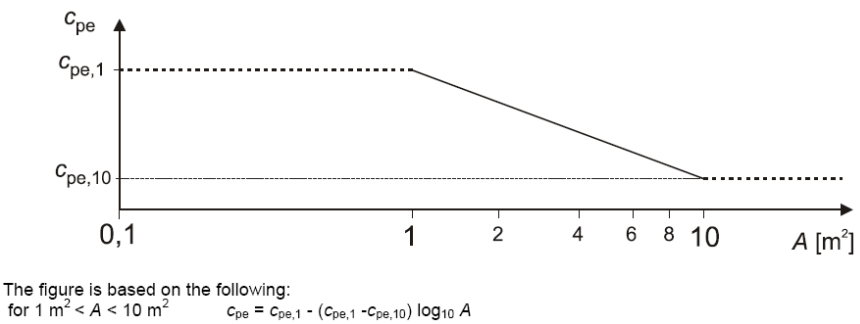

Figure 138. External pressure coefficient for buildings with a loaded area *A* between 1m^2 and 10m^2. (Source: [31], Figure 7.2)

For domes with circular base $c_{pe,10}$ can be seen in Figure 139.

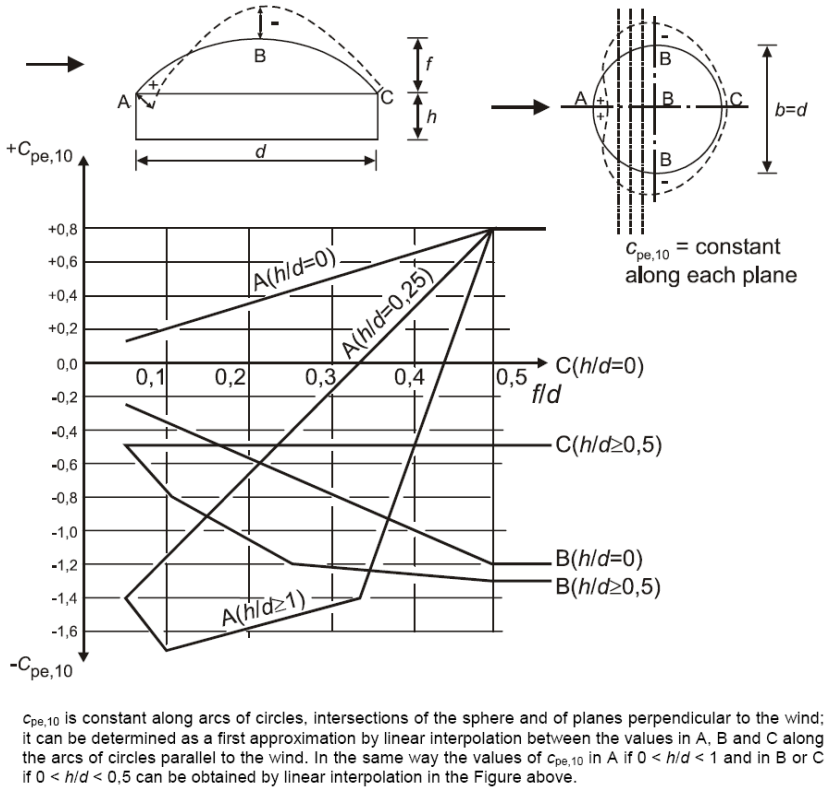

$c_{pe,10}$ is constant along arcs of circles, intersections of the sphere and of planes perpendicular to the wind; it can be determined as a first approximation by linear interpolation between the values in A, B and C along the arcs of circles parallel to the wind. In the same way the values of $c_{pe,10}$ in A if $0 < h/d < 1$ and in B or C if $0 < h/d < 0,5$ can be obtained by linear interpolation in the Figure above.

Figure 139. Recommended values of external pressure coefficients $cp_{e,10}$ for domes with circular base. (Source: [31], Figure 7.12)

In our case:

$f/d = 1$
$h/d = 0$

A $c_{pe,10} = 0,8$

B $c_{pe,10} = -1,2$

C $c_{pe,10} = 0$

Wind forces, *([31] Eurocode 5)*

The wind forces for the whole structure or a structural component can be determined by calculating forces using force coefficients.
The wind force F_w acting on a structure or a structural component may be determined directly by using Expression 37.

$$F_w = c_s c_d \cdot c_f \cdot q_p(z_e) \cdot A_{ref} \tag{37}$$

$c_s c_d$ is the structural factor. For buildings with a height less than 15 m the value of $c_s c_d$ may be taken as 1.
c_f is the force coefficient for the structure or structural element.
$q_p(z_e)$ is the peak velocity pressure at reference height z_e
A_{ref} is the reference area of the structure or structural element.

In our case:

$$F_w = c_f \cdot q_p(z_e) \cdot A_{ref} \tag{38}$$

Spheres, *([31] Eurocode 7.10)*

The alongwind force coefficient $c_{f,x}$ of spheres should be determined as a function of the Reynolds number *Re*, and the equivalent roughness *k/b* (see Table 10).

Table 10. Equivalent surface roughness *k*. (Source: [31], Table 7.13)

Type of surface	Equivalent roughness *k* mm	Type of surface	Equivalent roughness *k* mm
glass	0,0015	smooth concrete	0,2
polished metal	0,002	planed wood	0,5
fine paint	0,006	rough concrete	1,0
spray paint	0,02	rough sawn wood	2,0
bright steel	0,05	rust	2,0
cast iron	0,2	brickwork	3,0
galvanised steel	0,2		

Pressure coefficients of sections depend upon the Reynolds numbers *Re* defined by Expression 38.

$$\mathrm{Re} = \frac{b \cdot v(z_e)}{\upsilon} \tag{39}$$

b is the diameter
v is the kinematic viscosity of the air (v = 15·10-6 m^2/s)
$v(z_e)$ is the peak wind velocity defined in Note 2 of Figure 7.27at height z_e

The values of $c_{f,x}$ may be given in the National Annex. Recommended values based on measurements in low turbulent flow are given in Figure 141, is based on the Reynolds number with $v = \sqrt{\frac{2 \cdot q_p}{\rho}}$ and q_p given.

The values in Figure 141 are limited to values $z_g > b/2$, where z_g is the distance of the sphere from a plain surface, *b* is the diameter (see Figure 140). For $z_g < b/2$ the force coefficient $c_{f,x}$ is be multiplied by the factor 1,6.

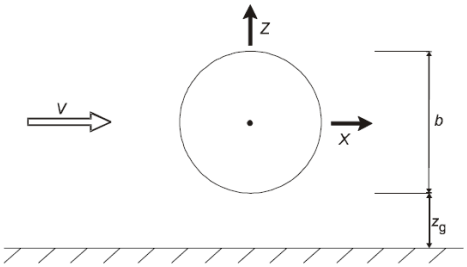

Figure 140. Sphere near a plain surface. (Source: [31], Figure 7.31)

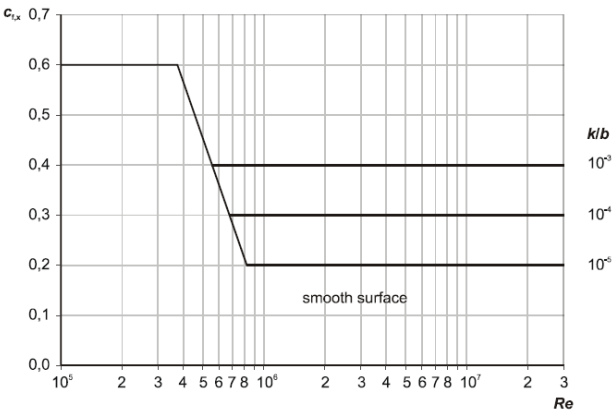

Figure 141. Alongwind force coefficient of a sphere. (Source: [31], Table 7.30)

In our case $z_g < b/2$, $0 < 4{,}153m$, so the force coefficient $c_{f,x}$ is multiplied by the factor 1,6.

With Expression 39 the values from Table 11. Reynolds values. and Table 12 are obtained.

Table 11. Reynolds values.

Location in Austria	$v_{b,0}$ (m/s)	$q_p(z)$ (N/m^2)	$v(z_e)$ (m/s)	Re
Wien (Stephansplatz)	27	583,2	30,55	$1{,}71 \cdot 10^7$
Tirol (Obergurgl)	27,6	609,4	31,22	$1{,}73 \cdot 10^7$

Table 12. Force coefficients.

Location in Austria	*Material*	*k*	*k/b*	*Re*	$c_{f,x}$	$c_{f,x} \cdot 1{,}6$
Wien (Stephansplatz)	Concrete	0,2	$2{,}4 \cdot 10^{-5}$	$1{,}7 \cdot 10^7$	0,2	0,32
Tirol (Obergurgl)	Ice					

$$c_{f,z} = +0{,}6 \qquad \text{for} \qquad z_g < \frac{b}{2}$$

In both cases the reference area A_{ref} should be obtained by Expression 40.

$$A_{ref} = \pi \frac{b^2}{4} \tag{40}$$

The reference height should be taken as:

$$z_e = z_g + \frac{b}{2} \tag{41}$$

In our case $z_e = z_g + \frac{b}{2} = \frac{b}{2}$

To sum up:

$$q_p(z) = 0{,}64 \cdot \rho \cdot v_{b,0}{}^2 \qquad (42)$$

Wind pressure on surfaces, from Expression 35.

$$z_e = \frac{b}{2} = z \text{, the dome radius}$$

$$q_p(z_e) = q_p(z)$$

Table 13. Coefficients c_{pe} in a spherical shape structure.

c_{pe}	
$c_{pe(A)}$	0,8
$c_{pe(B)}$	-1,2
$c_{pe(C)}$	0
$c_{pe((C+B)/2)}$	-0,6

Finally the pressure values for our structure are different depending on the location respect to wind, Figure 142, the values obtained with previous coefficients in Expression 35 are summed up in Table 14.

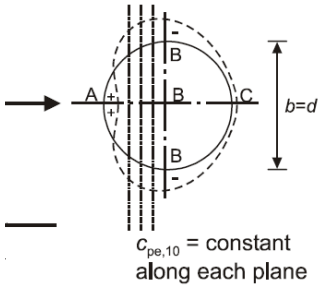

Figure 142. Pressure distribution due to wind load.

Table 14. Pressure values in surfaces of the shell.

Location in Austria	$q_p(z)$ (N/m^2)	$w_{e(A)}$ (N/m^2)	$w_{e(B)}$ (N/m^2)	$w_{e((B+C)/2)}$ (N/m^2)
Wien (Stephansplatz)	583,2	466,56	-699,84	-349,92
Tirol (Obergurgl)	609,4	487,52	-731,28	-365,64

4.3. FEM analysis with ABAQUS

In this section the finite elements analysis program ABAQUS is used to manage all numerical calculations. The version ABAQUS 6.6-2 is used.

4.3.1. ABAQUS overview

ABAQUS is a highly sophisticated, general purpose finite element program, designed primarily to model the behavior of solids and structures under externally applied loading. ABAQUS includes the following features:

- Capabilities for both static and dynamic problems.
- The ability to model very large shape changes in solids, in both two and three dimensions.
- An element library.
- A sophisticated capability to model contact between solids.
- An advanced material library, including the usual elastic and elastic – plastic solids; models for foams, concrete, soils, piezoelectric materials, and many others.
- Capabilities to model a number of phenomena of interest, including vibrations, coupled fluid/structure interactions, acoustics, buckling problems, and so on.

The main strength of ABAQUS, however, is that it is based on a very sound theoretical framework. While no computer program can ever be guaranteed free of bugs, ABAQUS is among the more trustworthy codes based on continuum mechanics formulations.

For this reason, ABAQUS is used by a wide range of industries, including aircraft manufacturers, automobile companies, oil companies and microelectronics industries, as well as national laboratories and research universities.

ABAQUS is written and maintained by Hibbitt, Karlsson and Sorensen, Inc (HKS), which has ABAQUS tutorial headquarers in Pawtucket, RI. The company was founded in 1978 (by graduates of Brown's Ph.D. program in solid mechanics), and today has several hundred employees with offices around the world [33].

4.3.2. Steps in running ABAQUS

A) Create a model

- Defining the model geometry
- Defining the material properties
  - Create material
  - Creating and assigning section properties
- Creating an assembly

- Creating the mesh
- Defining steps
- Prescribing boundary conditions and loads

B) Analysis
- Defining and submitting a job
- Postprocessing
  - Visualization of results

4.3.3. Data preparation. Units.

ABAQUS does not use any particular units. Input parameters are simply numbers as far as ABAQUS is concerned. There is no units associated with ABAQUS. The user has to choose an appropriate set of units.

In our case units from International System will be used.

Table 15. Units used in ABAQUS.

Quantity	SI
Length	m
Force	N
Mass	Kg
Stress	Pa (N/m^2)
Energy	J
Density	Kg/m^3

4.4. Concrete shell analysis

The concrete shell analyzed has the same geometrical structure as explained in previous sections. Its main characteristics: radius, angle of each element, thickness, and density, can be show in Table 16.

Table 16. Concrete shell analysis parameters.

Concrete shell parameters	
r [m]	4,153
θ_0 [º]	12,8571
θ_0 [rad]	0,2244
t [m]	0,05
x	11,8726
$\rho_{Concrete}$ [Kg/m^3]	2400

The shell parameter x is calculated with the Equation 9.

4.4.1. Case 1. Dead load.

The self weight load will be analyzed analytically and with finite elements tool ABAQUS.

Analytical Analysis

Following the assessments and formulas from section 4.2.1, and the parameters from Table 16, the loads can be obtained.

$$p_E = \rho \cdot g \cdot t = 2400\left(\frac{Kg}{m^3}\right) \cdot 9{,}8\left(\frac{N}{Kg}\right) \cdot 0{,}05(m) = 1176 N/m^2$$

Using the formulas, for each point we obtain the following results for forces and stresses (see Annex I).

Table 17. Concrete shell. Dead load analytical results.

Shell Points	N_θ [N/m]	N_φ [N/m]	σ_θ [N/m^2]	σ_φ [N/m^2]
1	0,00	-4761,47	-0,08	-95229,47
2	-1918,73	-2481,54	-38374,62	-49630,73
3	-2425,97	-1392,44	-48519,34	-27848,83
4	-2807,97	-237,11	-56159,32	-4742,27
5	-3255,24	1136,18	-65104,71	22723,58
6	-3866,14	2779,36	-77322,71	55587,19
7	-4761,48	4761,48	-95229,56	95229,56

ABAQUS FEM Analysis

In ABAQUS first of all the geometry of the shell is drawn, as showed in Figure 143. For that a new part must be created in the CAE file. In this case 3D modeling space is selected, deformable type, and shell shape elements of revolution type are used, with an approximate size of 200 elements. Moreover the material properties and thickness of the shell are defined. The dead load (self weight) is defined as a vertical force, $F_2 = -9{,}81N$. Two boundary conditions are defined: the vertical displacement is not allowed, $u_2 = 0$; and a point of the base of the shell is fixed to the ground, $u_1 = u_2 = u_3 = 0$. The load and boundary conditions are showed in Figure 144.

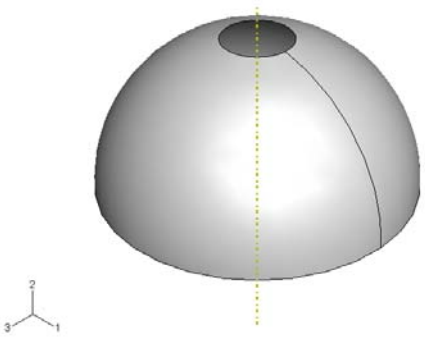

Figure 143. Shell geometry drawing in Abaqus.

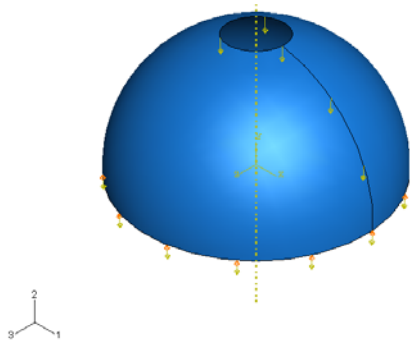

Figure 144. Loads and boundary conditions.

Afterwards the mesh is defined with a global size of 0.1. The global size must be small enough so coherent and accurate results can be obtained.

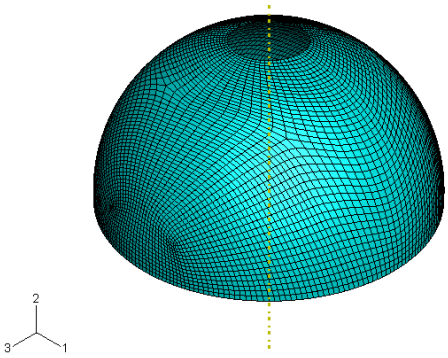

Figure 145. Shell meshed.

The forces obtained are shown in the following figures, the meridional forces, N_θ in Figure 146; and the hoop forces, N_φ in Figure 147. The radial forces can be seen in Figure 148.

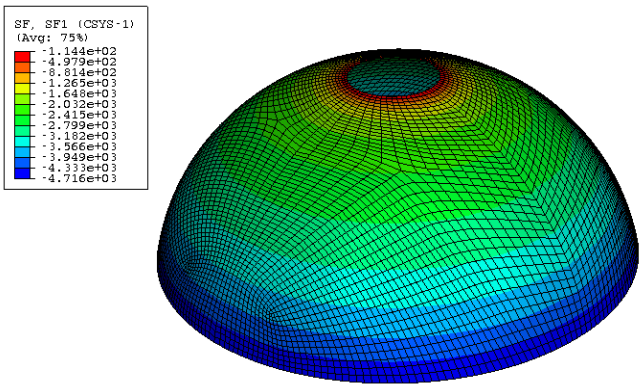

Figure 146. Shell meridional forces (N_θ, [N/m]). (Concrete Shell, Case 1).

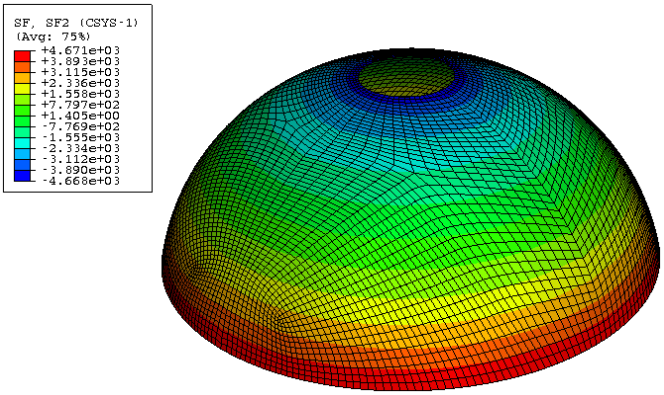

Figure 147. Shell hoop forces (N_φ, [N/m]). (Concrete Shell, Case 1).

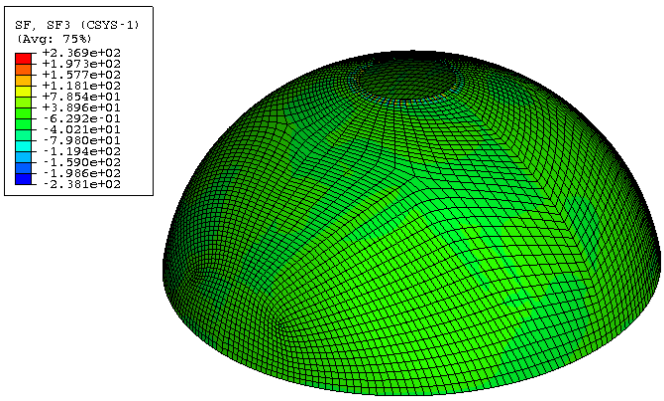

Figure 148. Shell radial forces (N_φ, [N/m^2]). (Concrete Shell, Case 1).

The Von Misses stresses obtained are shown in the following figures, the meridional stresses, σ_θ in Figure 150; and the hoop stresses, σ_φ in Figure 151.

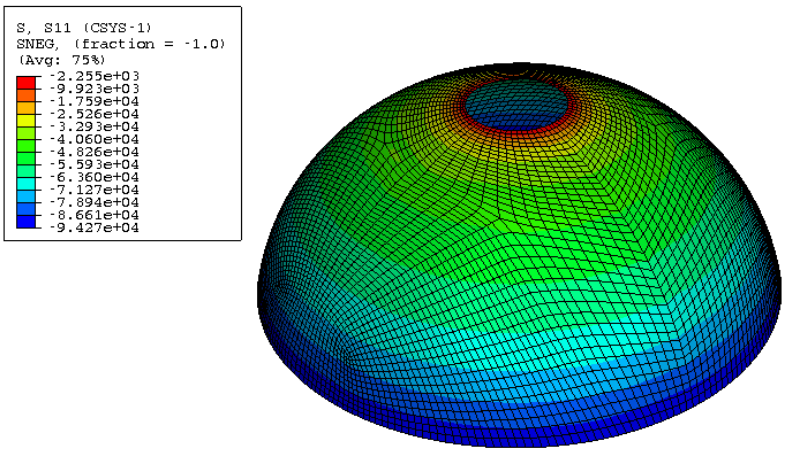

Figure 149. Shell meridional stresses (σ_θ, [N/m^2]). (Concrete Shell, Case 1).

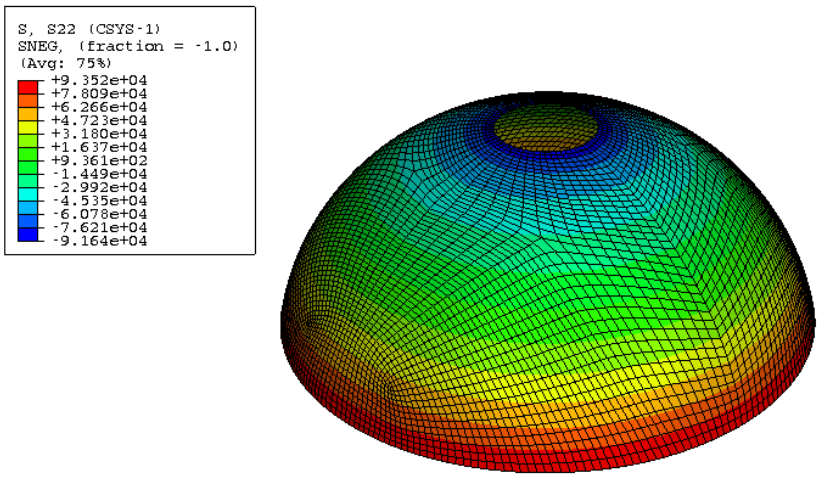

Figure 150. Shell hoop stresses (σ_φ, [N/m^2]). (Concrete Shell, Case 1).

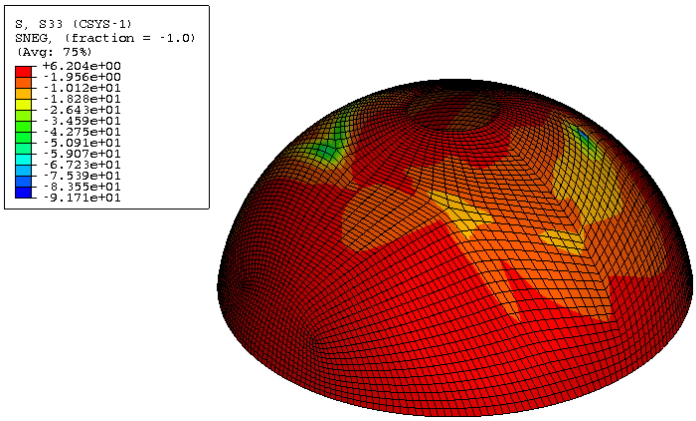

Figure 151. Shell radial stresses (σ_r, [N/m^2]). (Concrete Shell, Case 1).

As we can see in the figures the meridional stresses are in compression along all the meridian of the shell. The hoop stresses are in traction in the upper zone of the shell and in compression in the lower one.

The numerical values obtained are summed up in the following Table 18.

Table 18. Concrete shell. Dead load ABAQUS results.

Shell Points	N_θ [N/m]	N_φ [N/m]	σ_θ [N/m^2]	σ_φ [N/m^2]
1	-22,44	-4513	-5540,44	-87433
2	-1893,47	-2524,12	-36440,70	-48659,20
3	-2409,94	-1456,49	-46786,80	-27594,70
4	-2790,53	-333,46	-54449,60	-5219,04
5	-3238,12	1063,96	-64085,60	22055,50
6	-3854,17	2730,57	-76704,70	54993,70
7	-4678,75	4580,45	-93400,00	91726,80

Comparison Analysis

Comparing the obtained values from analytical analysis, Table 17, and ABAQUS, Table 18; can be seen in the following figures the comparatives between the two different methods used.

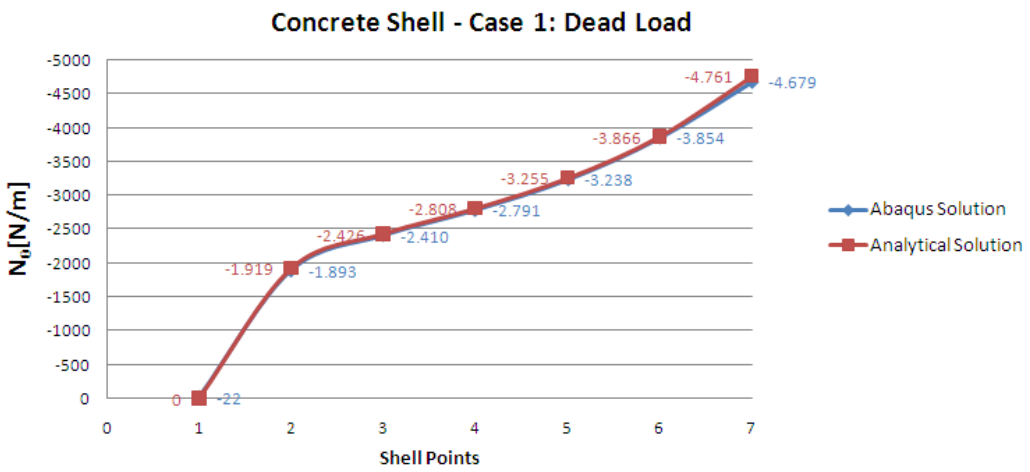

Figure 152. Concrete Shell – Case 1: Dead Load. Meridional forces comparative.

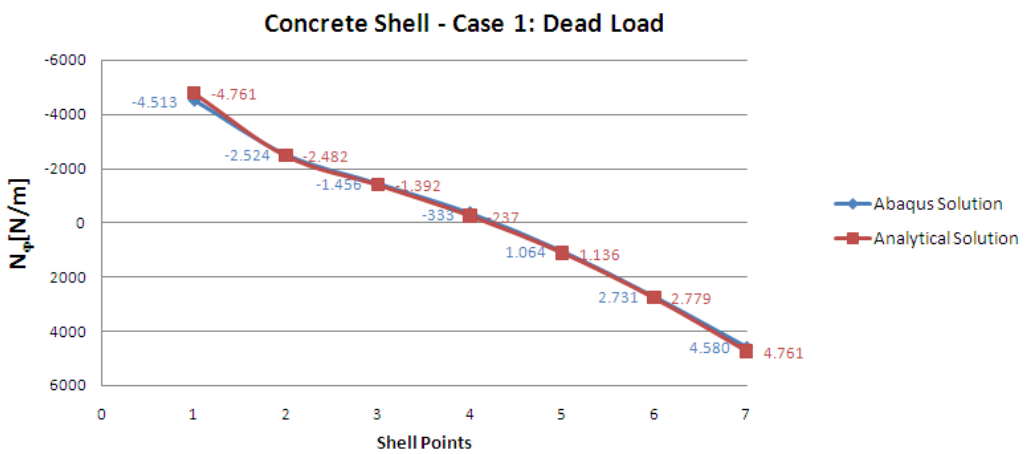

Figure 153. Concrete Shell – Case 1: Dead Load. Hoop forces comparative.

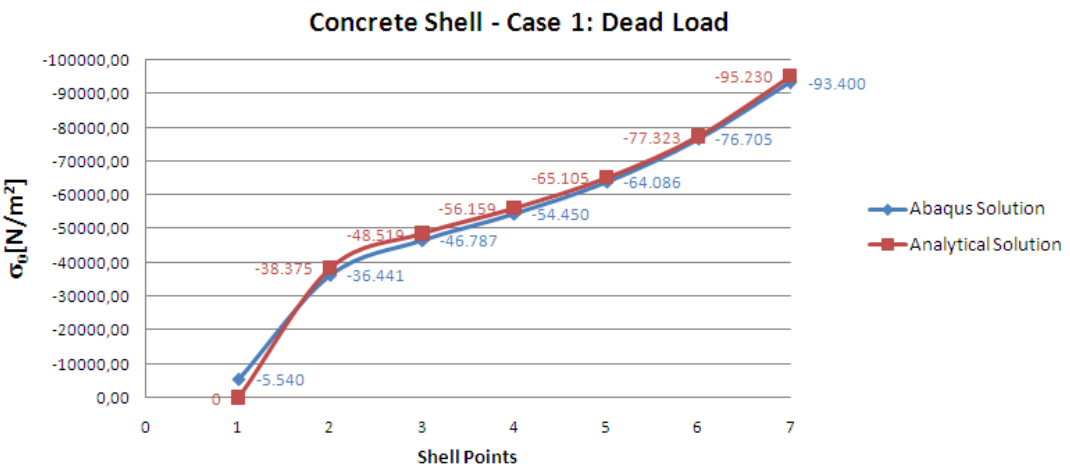

Figure 154. Concrete Shell – Case 1: Dead Load. Meridional stresses comparative.

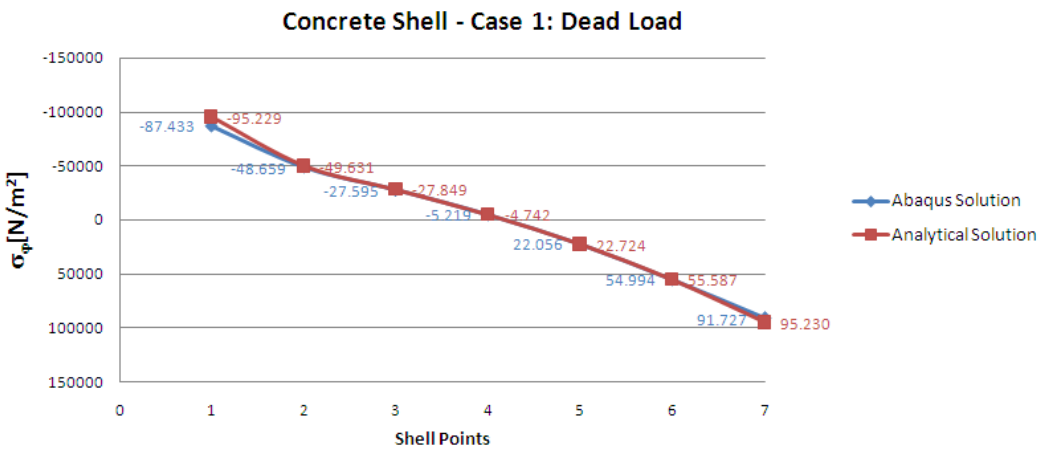

Figure 155. Concrete Shell – Case 1: Dead Load. Hoop stresses comparative.

It can be affirmed that our numerical model was enough accurate in comparison with the ABAQUS model. We have only a relative difference between the two models less than 4%.

4.4.2. Case 2. Snow effect.

The snow load will be analyzed only analytically due to some difficulties in the use of ABAQUS with this type of load. The snow load distribution can be seen in Figure 156.

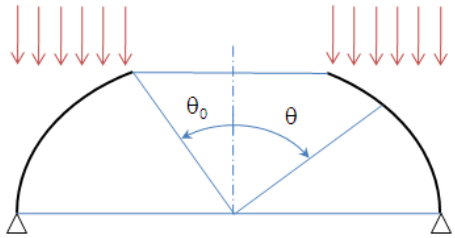

Figure 156. Snow load distribution.

The snow load is obtained using the formulas from section 4.2.2, and the parameters from Table 5.

$$p_E = \rho \cdot g \cdot t = 2400\left(\frac{Kg}{m^3}\right) \cdot 9{,}8\left(\frac{N}{Kg}\right) \cdot 0{,}05(m) = 1176 N/m^2$$

$$p_s = 0.8 s_k = 0{,}8 \cdot 1360 = 1088 N/m^2$$

For all the critical points in the structure the snow load was calculated and summed to the self weight load, Table 19 (see Annex II).

Table 19. Concrete shell. Snow load analytical results.

Shell Points	Dead load		Snow load		TOTAL load	
	N_θ [N/m]	N_φ [N/m]	N_θ [N/m]	N_φ [N/m]	N_θ [N/m]	N_φ [N/m]
1	0,00	-4761,47	0,00	-4294,73	0,00	-9056,20
2	-1918,73	-2481,54	-1665,00	-2002,84	-3583,73	-4484,38
3	-2425,97	-1392,44	-1971,46	-790,49	-4397,43	-2182,94
4	-2807,97	-237,11	-2076,22	319,72	-4884,19	82,60
5	-3255,24	1136,18	-2121,42	1270,80	-5376,66	2406,98
6	-3866,14	2779,36	-2141,54	1917,80	-6007,67	4697,16
7	-4761,48	4761,48	-2147,37	2147,37	-6908,84	6908,84

Shell Points	Dead load		Snow load		TOTAL load	
	σ_θ [N/m^2]	σ_φ [N/ m^2]	σ_θ [N/ m^2]	σ_φ [N/ m^2]	σ_θ [N/ m^2]	σ_φ [N/ m^2]
1	-0,08	-95229,47	-0,08	-85894,52	-0,16	-181123,99
2	-38374,62	-49630,73	-33300,03	-40056,78	-71674,64	-89687,50
3	-48519,34	-27848,83	-39429,27	-15809,90	-87948,61	-43658,73
4	-56159,32	-4742,27	-41524,43	6394,32	-97683,75	1652,06
5	-65104,71	22723,58	-42428,43	25415,95	-107533,14	48139,53
6	-77322,71	55587,19	-42830,75	38356,06	-120153,46	93943,25
7	-95229,56	95229,56	-42947,30	42947,30	-138176,86	138176,86

The relationship between the snow and the dead load can be seen in Figure 157 and Figure 158. The meridional stress component due to the weight is higher than the snow load. In point 2 (upper ring) the dead and snow loads are similar, but the dead load increases more until point 7 (lower ring) were its value double the snow load. In the hoop stresses a similitude in the values of the two components, weight and snow, is observed in all over the shell.

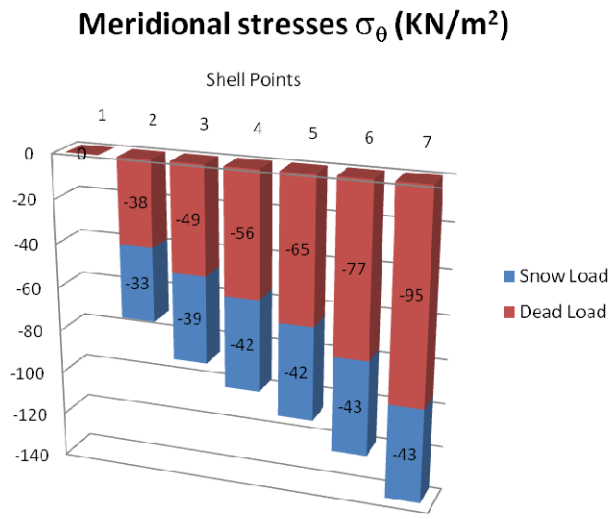

Figure 157. Case 2. Meridional stresses. Concrete shell.

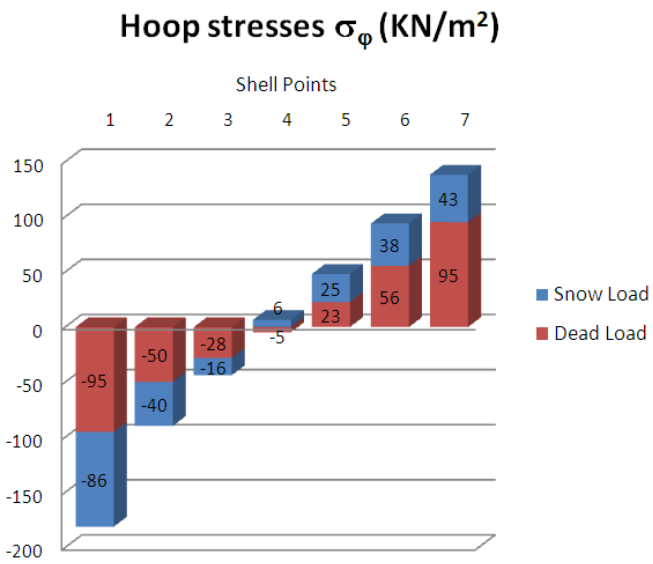

Figure 158. Case 2. Hoop stresses. Concrete shell.

4.4.3. Case 3. Wind effect.

The wind load will be analyzed only with ABAQUS. The analytical calculations would be too complicated because the wind load is not symmetrically applied in the hemispheric.

Following the *Eurocode*, to calculate the wind effect on the shell structure, equations from section 4.2.3 are used. The wind load model showed in Figure 159 is introduced in ABAQUS to check the structure behavior.

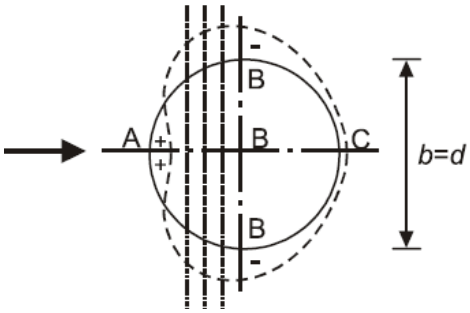

Figure 159. Pressure distribution due to wind load.

As can be seen in Figure 159, three different zones are distinguished in wind effect calculation. Zone A includes the surface that receives directly the wind pressure load perpendicular to its surface. Zone B and C suffer a suction effect due to the wind load.

Each zone has its own coefficient, Table 20.

Table 20. Coefficients c_{pe} in a spherical shape structure.

c_{pe}	
$c_{pe(A)}$	0,8
$c_{pe(B)}$	-1,2
$c_{pe(C)}$	0
$c_{pe((C+B)/2)}$	-0,6

As it was stated in section 4.2.3, finally the pressure values for our structure in Wien are shown in the following Table 21.

Table 21. Pressure values in surfaces of the shell in Wien.

Location in Austria	$q_p(z)$ (N/m^2)	$w_{e(A)}$ (N/m^2)	$w_{e(B)}$ (N/m^2)	$w_{e((B+C)/2)}$ (N/m^2)
Wien (Stephansplatz)	583,2	466,56	-699,84	-349,92

Following this model, the shell was divided in three different surfaces, Figure 159. Surface 1 where the wind pressure hits directly perpendicular to its surface. Surface 2

that absorbs and release the main part of the wind pressure load and surface 3 in the top of the structure near to the central ring whole.

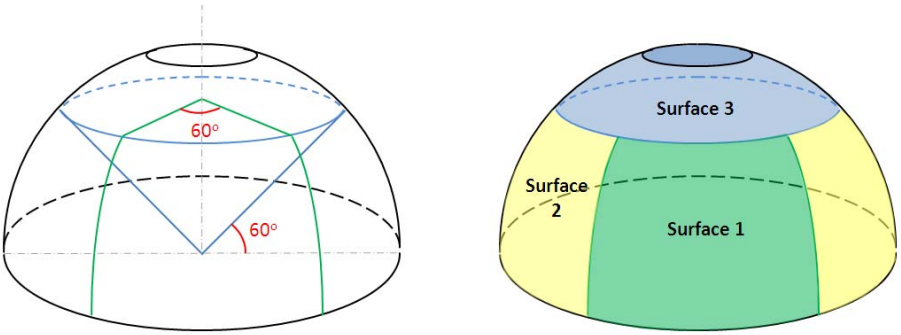

Table 22. Shell division in three surfaces.

In ABAQUS the boundary conditions and loads, self weight and wind, were applied. The wind pressure loads were applied separately in every surface, Figure 160.

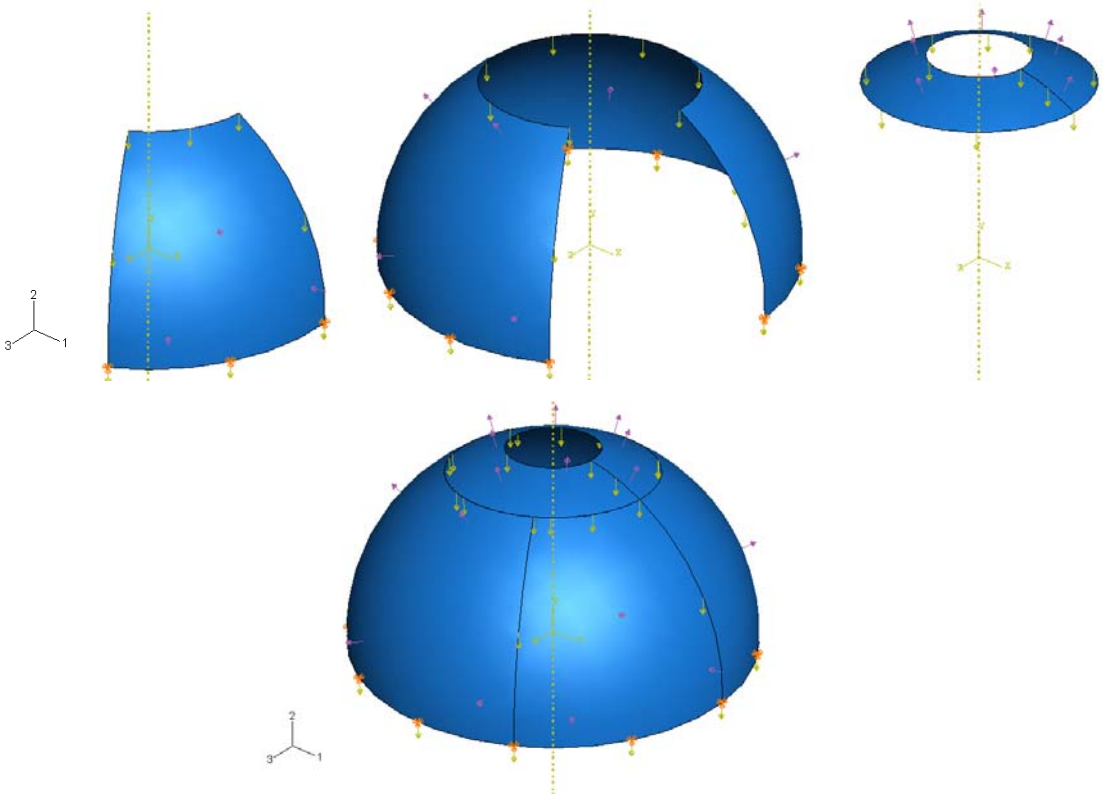

Figure 160. Wind pressure loads in ABAQUS.

The finite element program run properly giving the expected non symmetrical results. As can be seen in Figure 161, the pressure load applied in surface one produce compression stresses (negative values) in surface one. The highest stresses are reached in surface one in the base of the shell, with a maximum value of 127 KPa.

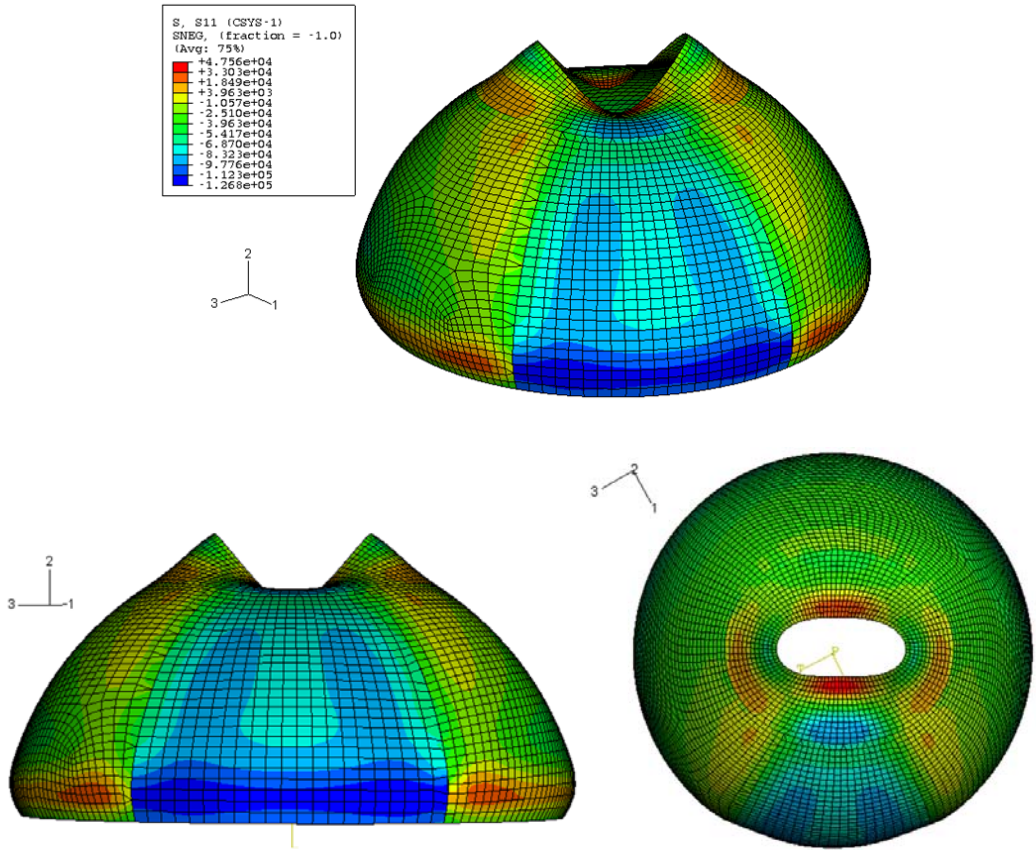

Figure 161. Shell meridional stresses (σ_θ, [N/m]). (Concrete Shell, Case 3).

The highest positive or tensile stresses are reached in the central ring in the red zones of Figure 161, with a maximum value of 475 KPa.

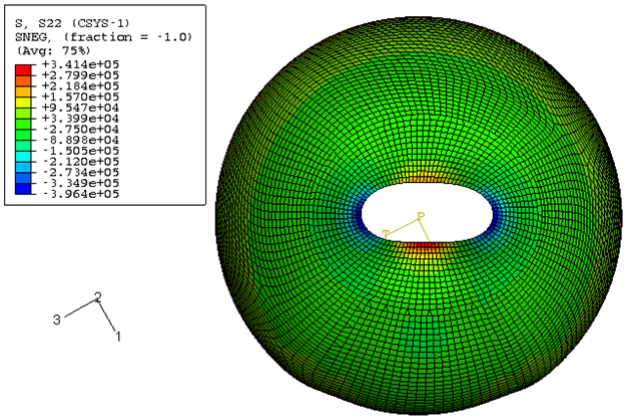

Figure 162. Shell hoop stresses (σ_φ, [N/m]). (Concrete Shell, Case 3).

The radial stresses can be neglected, Figure 163.

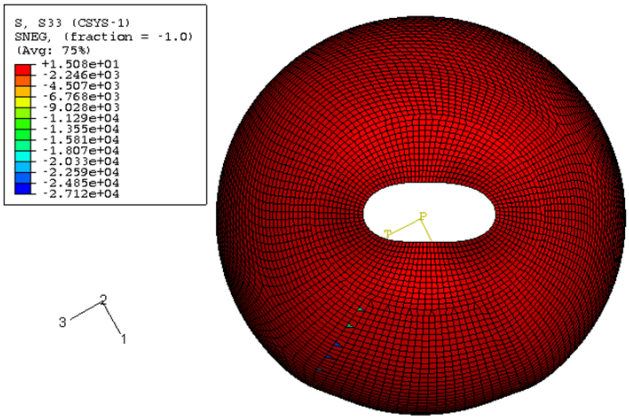

Figure 163. Shell radial stresses (σ_φ, [N/m^2]). (Concrete Shell, Case 3).

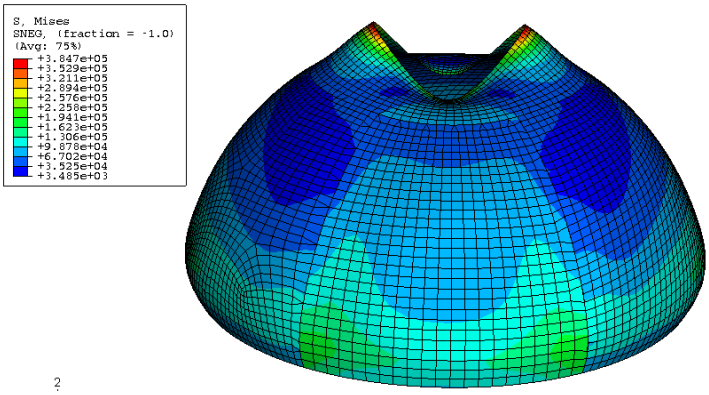

Figure 164. Wind load. General Von Misses Stresses

The higher displacements are in meridional direction in the central ring as was clearly notice in the deformed shape of the shell with the loads, Figure 165Figure 166.

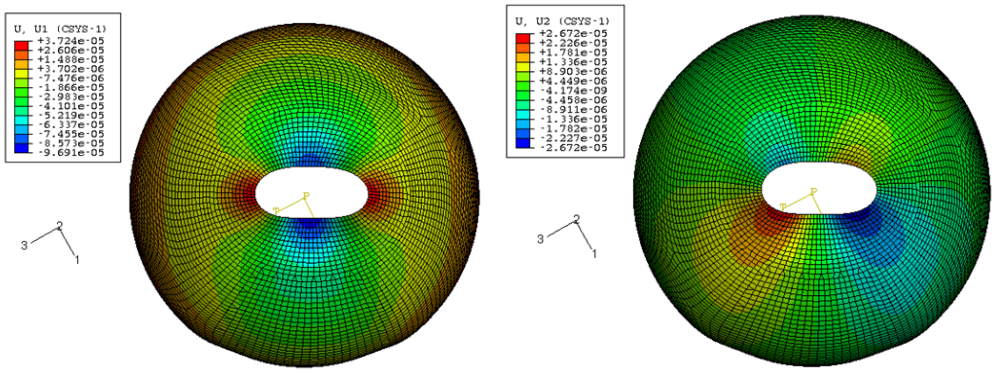

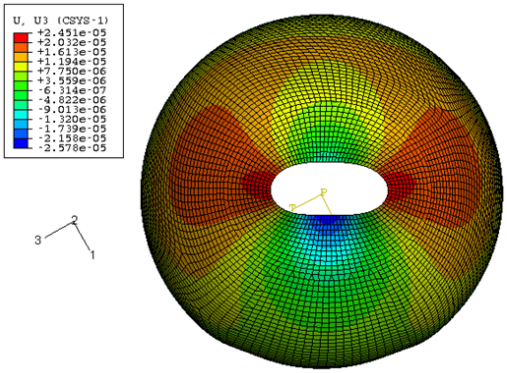

Figure 165. Shell displacements (u_1, u_2, u_3, [m]). (Concrete Shell, Case 3).

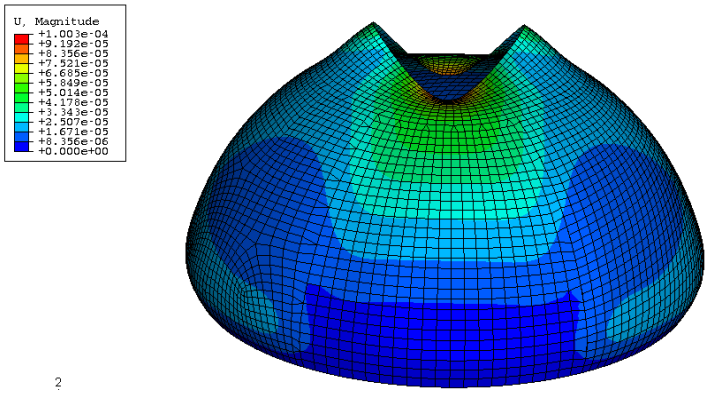

Figure 166. General shell displacements [m]. (Concrete Shell, Case 3).

4.5. Ice shell analysis

The ice shell analyzed has the same geometrical structure as the concrete one, explained in previous sections. Its main characteristics: radius, angle of each element, thickness, and density, can be show in Table 23.

Table 23. Ice shell analysis parameters.

Parameters	
r [m]	4,153
θ_0 [º]	12,8571
θ_0 [rad]	0,2244
t [m]	0,2
x	5,8268
ρ_{Ice} [Kg/m^3]	916,7

4.5.1. Case 1. Dead load.

As the concrete shell, the self weight load will be analyzed analytically and with finite elements tool ABAQUS.

Analytical Analysis

$$p_E = \rho \cdot g \cdot t = 916{,}7\left(\frac{Kg}{m^3}\right) \cdot 9{,}8\left(\frac{N}{Kg}\right) \cdot 0{,}2(m) = 1796{,}73 N/m^2$$

Using the formulas, for each point we obtain the following results for forces and stresses (see Annex I).

Table 24. Ice shell. Dead load analytical results.

Shell Points	N_θ [N/m]	N_φ [N/m]	σ_θ [N/m^2]	σ_φ [N/m^2]
1	-0,01	-7274,74	-0,03	-36373,69
2	-2931,50	-3791,37	-14657,50	-18956,87
3	-3706,47	-2127,42	-18532,37	-10637,09
4	-4290,10	-362,27	-21450,52	-1811,35
5	-4973,46	1735,89	-24867,29	8679,46
6	-5906,81	4246,40	-29534,05	21231,99
7	-7274,74	7274,74	-36373,72	36373,72

Abaqus FEM Analysis

The forces obtained are shown in the following figures, the meridional forces, N_θ in Figure 167; and the hoop forces, N_φ in Figure 168. The radial forces can be seen in Figure 169.

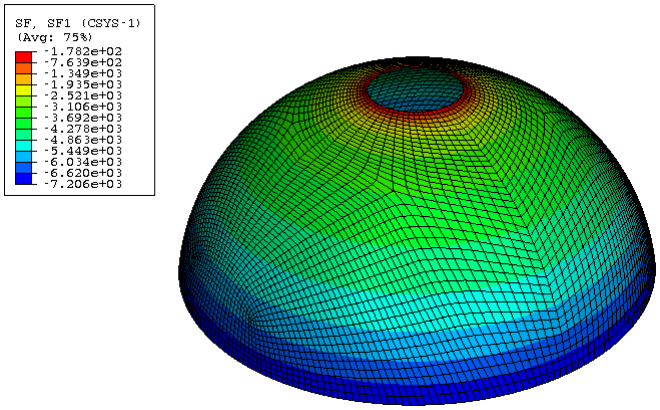

Figure 167. Shell meridional forces (N_θ, [N/m]). (Ice Shell, Case 1).

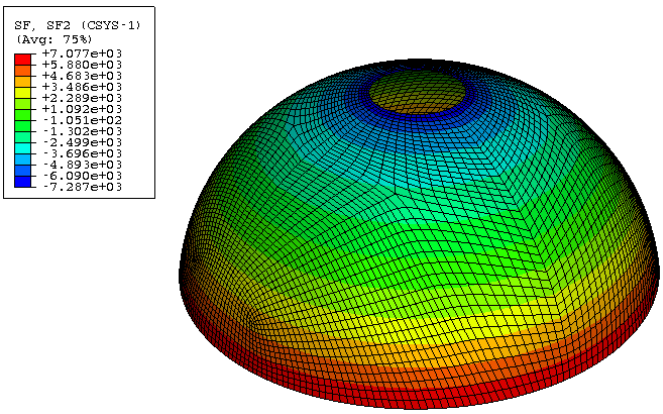

Figure 168. Shell hoop forces (N_φ, [N/m]). (Ice Shell, Case 1).

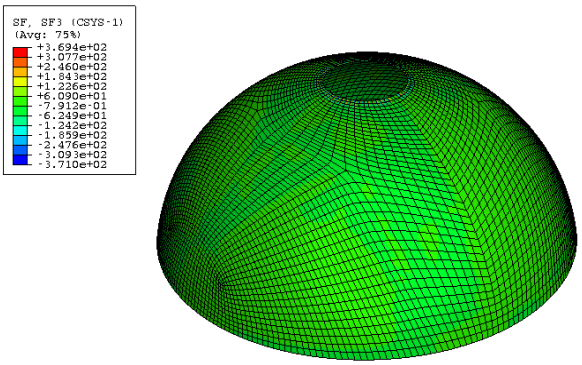

Figure 169. Shell radial forces (N_φ, [N/m^2]). (Ice Shell, Case 1).

The Von Misses stresses obtained are shown in the following figures, the meridional stresses, σ_θ in Figure 170; and the hoop stresses, σ_φ in Figure 171.

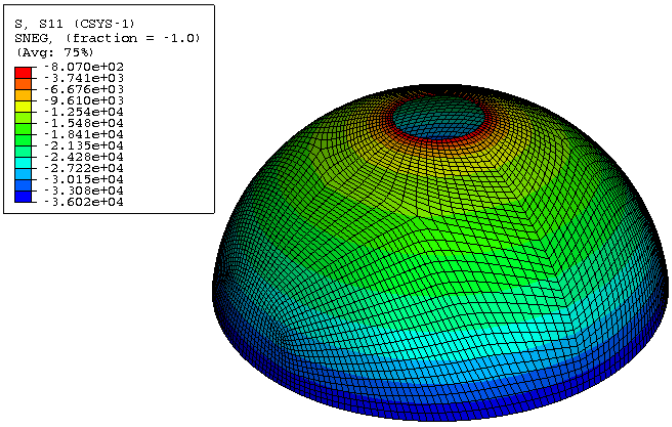

Figure 170. Shell meridional stresses (σ_θ, [N/m^2]). (Ice Shell, Case 1).

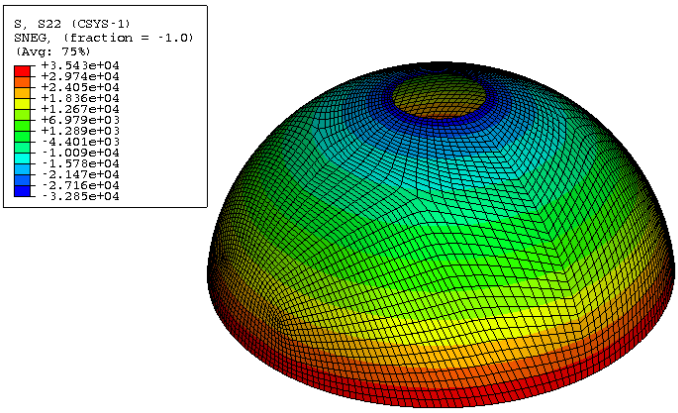

Figure 171. Shell hoop stresses (σ_φ, [N/m^2]). (Ice Shell, Case 1).

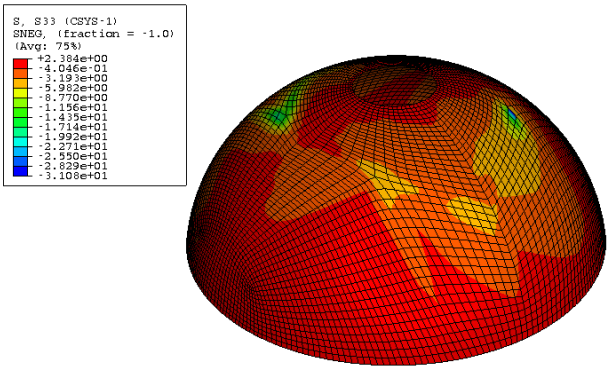

Figure 172. Shell radial stresses (σ_φ, [N/m^2]). (Ice Shell, Case 1).

The values obtained are summed up in the following table.

Table 25. Ice shell. Dead load ABAQUS results.

Shell Points	N_θ [N/m]	N_φ [N/m]	σ_θ [N/m^2]	σ_φ [N/m^2]
1	-431,741	-7040,06	-1953,53	-31604,9
2	-2900,04	-3819,48	-12321,80	-16406,2
3	-3674,61	-2202,22	-15843,90	-8512,12
4	-4248,59	-499,466	-19128,40	-401,501
5	-4940,46	1626,17	-23318,20	9553,62
6	-5885,13	4169,7	-28801,20	21565,9
7	-7143,15	6945,61	-35679,00	34863,2

Comparison Analysis

Comparing the obtained values from analytical analysis, Table 24, and ABAQUS, Table 25; can be seen in the following figures the comparatives between the two different methods used.

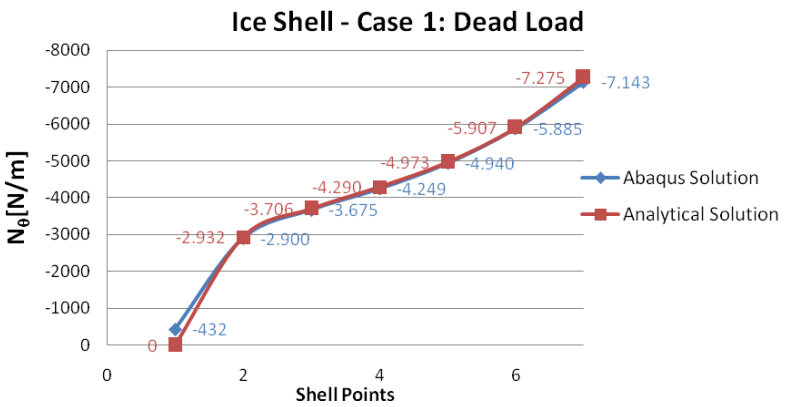

Figure 173. Ice Shell – Case 1: Dead Load. Meridional forces comparative.

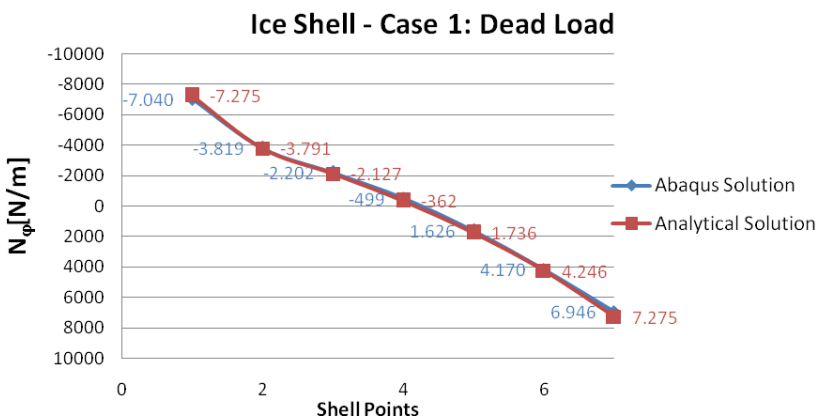

Figure 174. Ice Shell – Case 1: Dead Load. Hoop forces comparative.

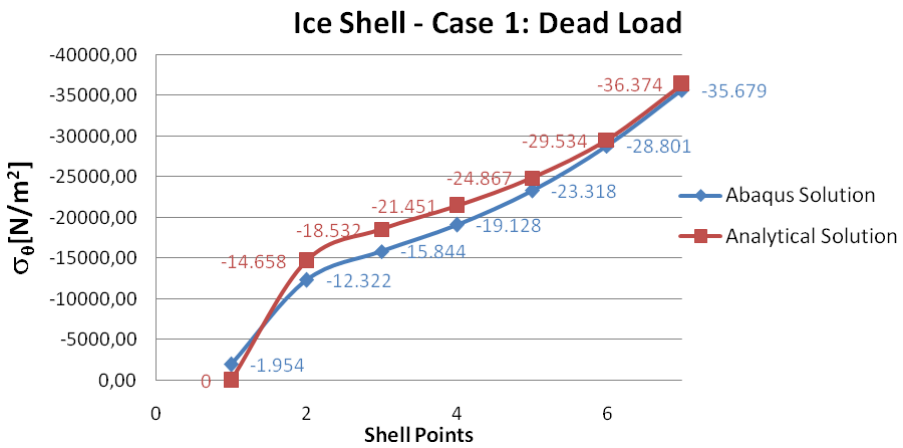

Figure 175. Ice Shell – Case 1: Dead Load. Meridional stresses comparative.

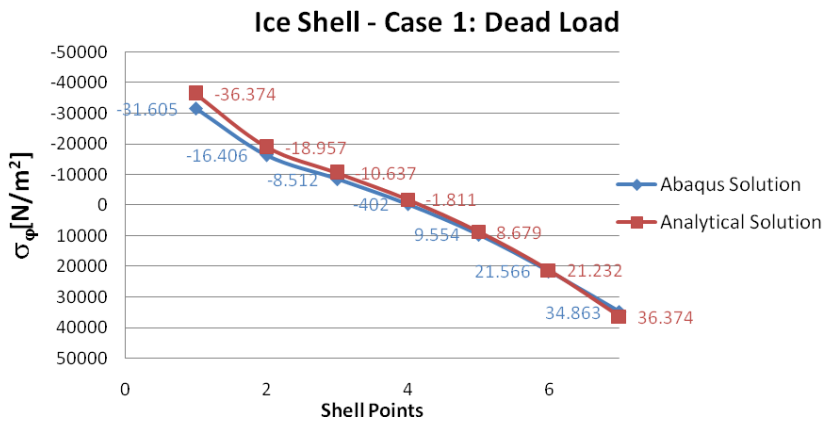

Figure 176. Ice Shell – Case 1: Dead Load. Hoop stresses comparative.

The values obtained with both methods are quite similar, as with the concrete shell.

4.5.2. Case 2. Snow effect.

The snow load will be analyzed only analytically following the same analysis process as with the concrete shell (see Annex II).

$$p_E = \rho \cdot g \cdot t = 916{,}7\left(\frac{Kg}{m^3}\right) \cdot 9{,}8\left(\frac{N}{Kg}\right) \cdot 0{,}2(m) = 1796{,}7 N/m^2$$

$$p_s = 0.8 s_k = 0{,}8 \cdot 7000 = 5600 N/m^2$$

Table 26. Ice shell. Snow load analytical results.

Shell Points	Dead load		Snow load		TOTAL load	
	N_θ [N/m]	N_φ [N/m]	N_θ [N/m]	N_φ [N/m]	N_θ [N/m]	N_φ [N/m]
1	-3778,28	-7274,74	-0,02	-22105,21	-3778,30	-29379,95
2	-1786,57	-3791,37	-8569,86	-10308,73	-10356,43	-14100,10
3	-3805,11	-2127,42	-10147,24	-4068,72	-13952,35	-6196,14
4	-3346,61	-362,27	-10686,44	1645,60	-14033,04	1283,33
5	-5203,93	1735,89	-10919,08	6540,87	-16123,01	8276,76
6	-6103,64	4246,40	-11022,62	9871,04	-17126,26	14117,44
7	-7461,83	7274,74	-11052,61	11052,61	-18514,44	18327,36

Shell Points	Dead load		Snow load		TOTAL load	
	σ_θ [N/m^2]	σ_φ [N/ m^2]	σ_θ [N/ m^2]	σ_φ [N/ m^2]	σ_θ [N/ m^2]	σ_φ [N/ m^2]
1	-18891,39	-36373,69	-0,10	-110526,04	-18891,49	-146899,73
2	-8932,84	-18956,87	-42849,30	-51543,65	-51782,14	-70500,51
3	-19025,54	-10637,09	-50736,19	-20343,62	-69761,74	-30980,71
4	-16733,04	-1811,35	-53432,18	8227,99	-70165,21	6416,64
5	-26019,64	8679,46	-54595,41	32704,35	-80615,05	41383,80
6	-30518,20	21231,99	-55113,09	49355,22	-85631,29	70587,21
7	-37309,14	36373,72	-55263,07	55263,07	-92572,21	91636,79

The relationship between the snow and the dead load can be seen in Figure 167 and Figure 168. In this case the meridional stress component due to the snow load is higher than the dead load. In the hoop stresses the snow load also dominates the dead load. This can be due to the higher coefficients for the snow load due to the higher altitude in Obergurgl, a village in the Alps in Tyrol, Austria.

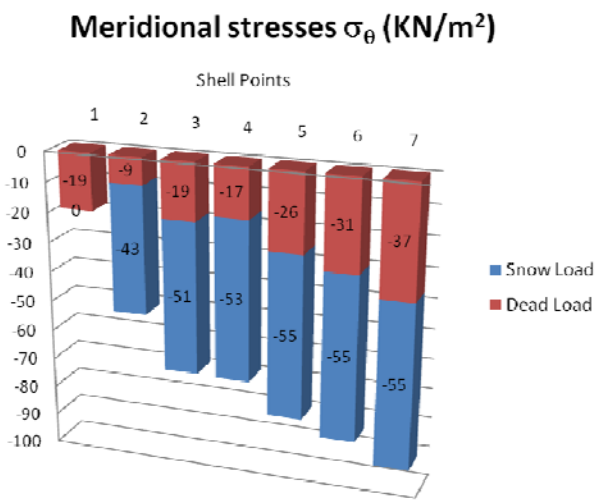

Figure 177. Case 2. Meridional stresses. Ice shell.

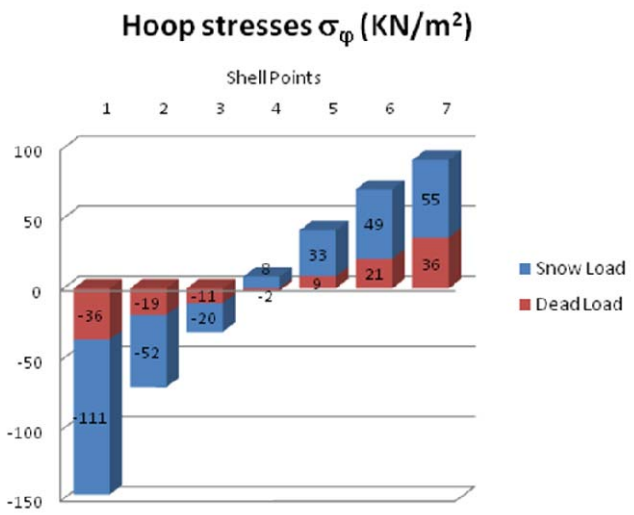

Figure 178. Case 2. Hoop stresses. Ice shell.

4.5.3. Case 3. Wind effect.

As it was stated in section 4.2.3, finally the pressure values for our structure in Obergurgl are shown in the following table.

Table 27. Pressure values in surfaces of the shell in Obergurgl.

Location in Austria	$q_p(z)$ (N/m^2)	$w_{e(A)}$ (N/m^2)	$w_{e(B)}$ (N/m^2)	$w_{e((B+C)/2)}$ (N/m^2)
Tirol (Obergurgl)	609,4	487,52	-731,28	-365,64

In this case, as with the concrete shell, the highest stresses are reached in the surface one in the base of the shell, with a maximum value of 546KPa, Figure 179, higher than in the concrete shell.

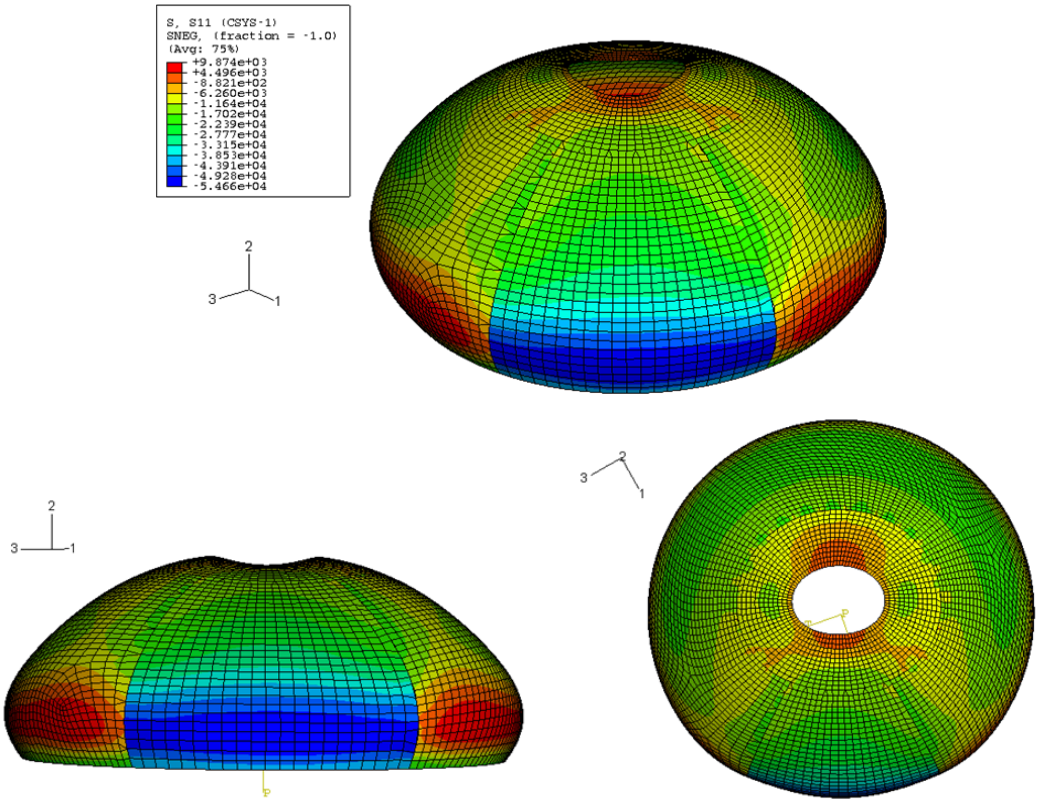

Figure 179. Shell meridional stresses (σ_θ, [N/m]). (Ice Shell, Case 3).

The highest positive or tensile stresses are reached in the central ring in the red zones of Figure 179, with a maximum value of 987 KPa.

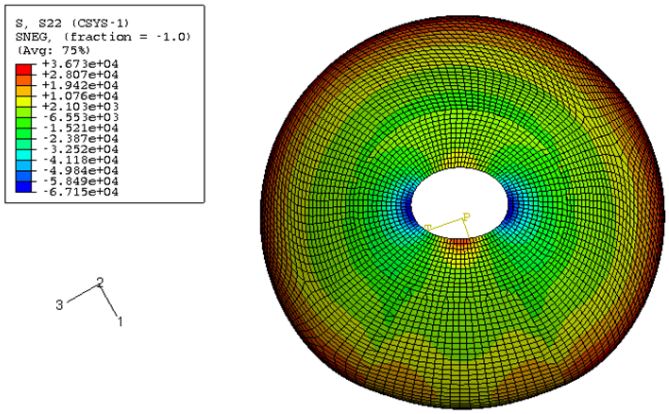

Figure 180. Shell hoop stresses (σ_φ, [N/m]). (Ice Shell, Case 3).

The radial stresses can be neglected, Figure 181.

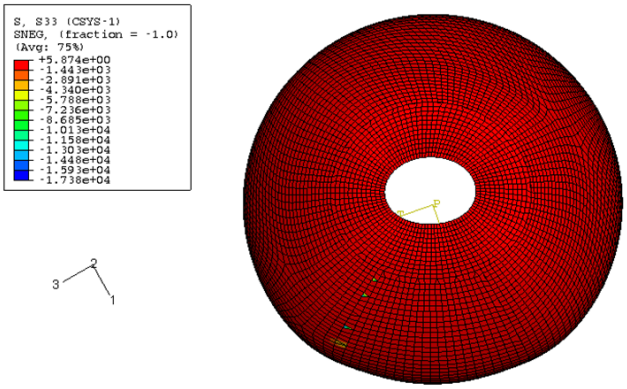

Figure 181. Shell radial stresses (σ_φ, [N/m^2]). (Ice Shell, Case 3).

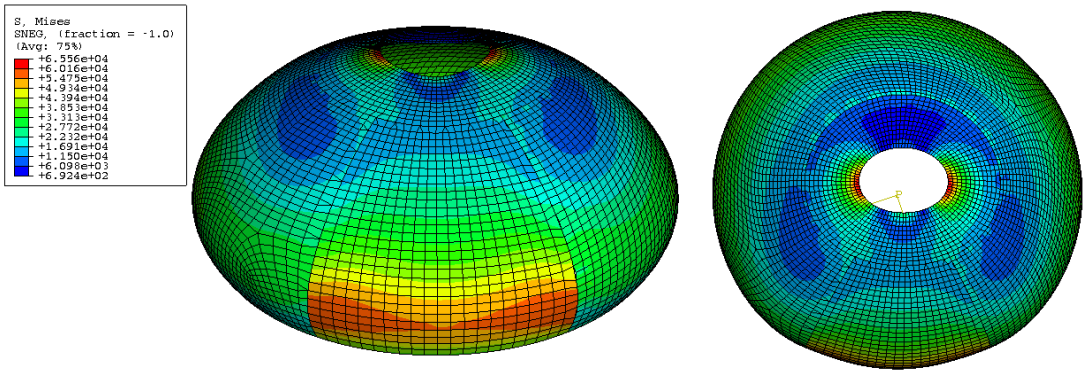

Figure 182. Wind load. General Von Misses Stresses

In this case the higher displacements are in the radial direction in the central ring, see the following figures.

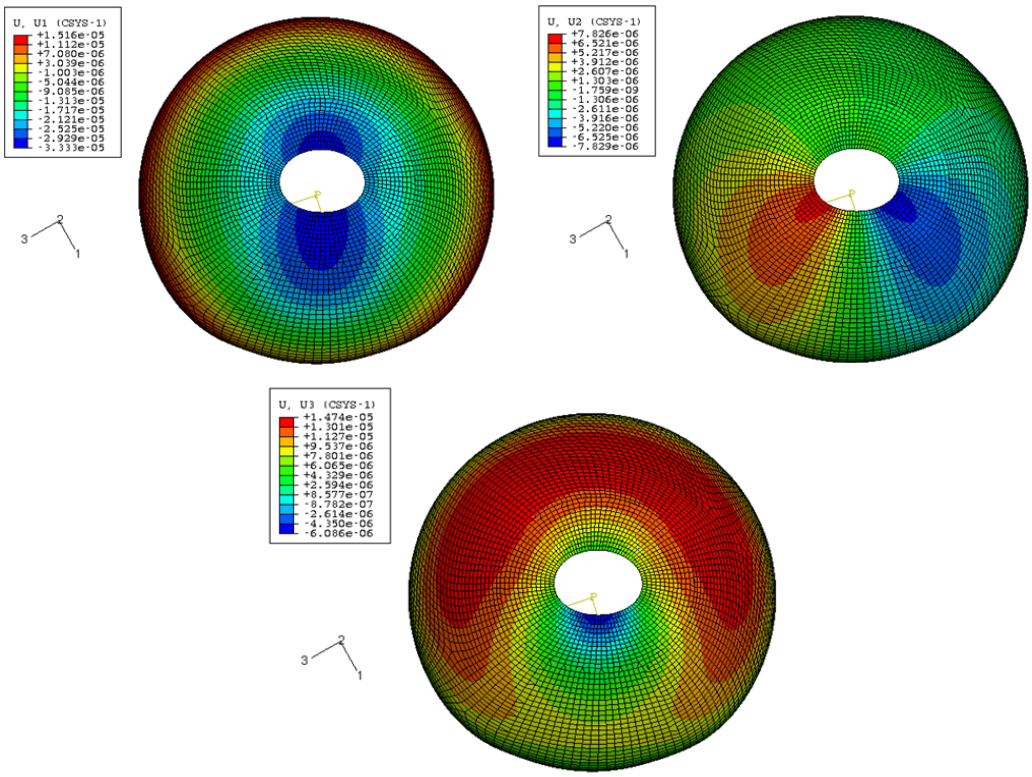

Figure 183. Shell displacements (u_1, u_2, u_3, [m]). (Ice Shell, Case 3).

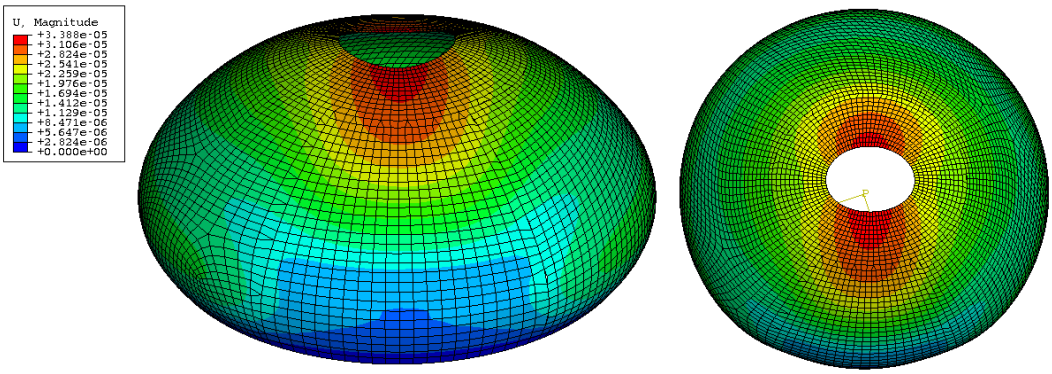

Figure 184. General shell displacements [m]. (Ice Shell, Case 3).

4.6. Shell with a door analysis

In this section the stresses in a shell with a door are calculated using finite elements analysis, with ABAQUS tools. The door geometry corresponds to three elements in one segment of the shell as can be seen in Figure 185.

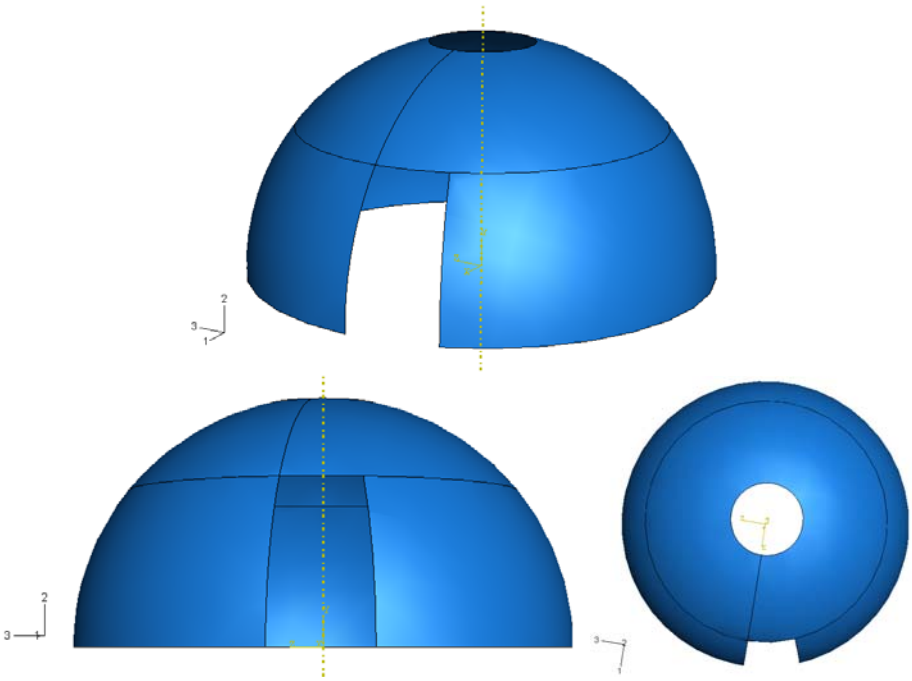

Figure 185. Views of the shell with a door.

Only dead load is applied to this model. Moreover the vertical displacement is not allowed in the base of the shell. Also a mesh size of 0.1 is used in the door analysis.

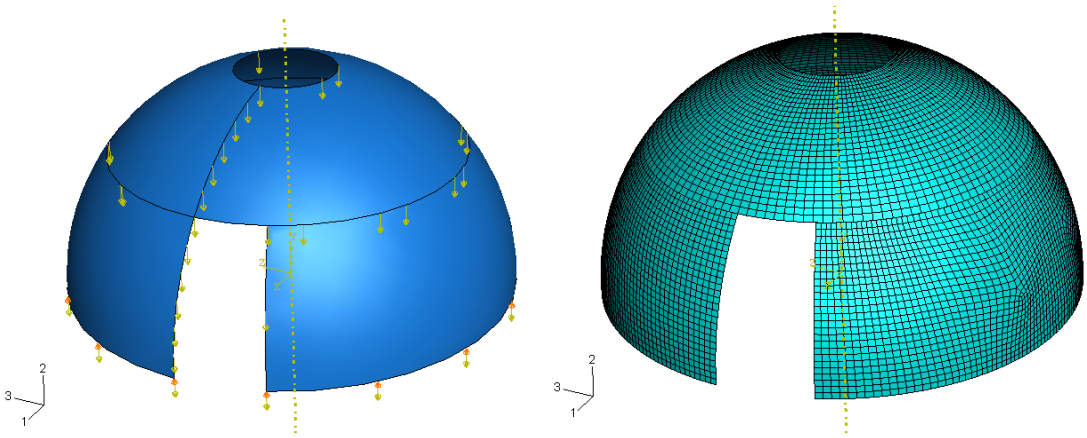

Figure 186. Shell with a door model: dead load, boundary conditions, and meshing.

As in previous sections two different cases are studied, the concrete and the ice shell with its own thicknesses.

4.6.1. Concrete shell

The concrete shell analyzed has the same geometrical structure as explained in previous sections. Its main characteristics: radius, angle of each element, thickness, and density, were shown in Table 16. Concrete shell analysis parameters..

The Von Misses stresses obtained are shown in the following figures, the meridional, the hoop, and the radial stresses, Figure 187. The radial stresses are neglected.

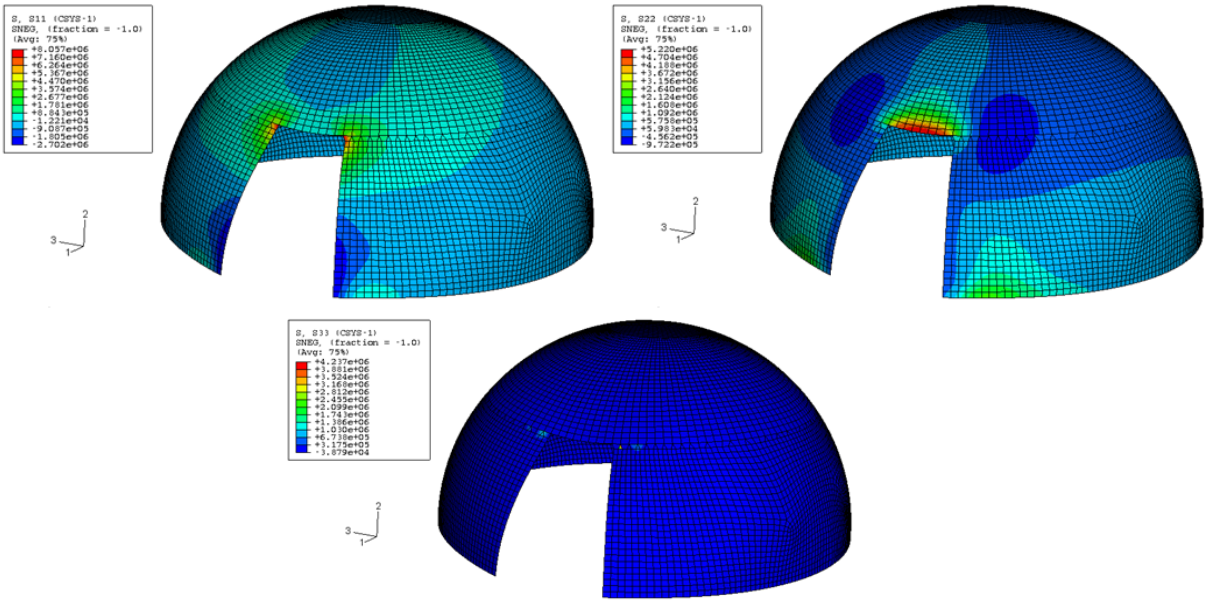

Figure 187. a. meridional stresses (σ_θ, [N/m^2]), b. hoop stresses (σ_φ, [N/m^2]), c. radial stresses (σ_r, [N/m^2]).

Now the stresses in the shell with a door are not spherical symmetrically distributed as when the door was not created. The values obtained in the edges of the elements, the red points in Figure 188, are shown in Table 28. As can be seen the highest stress point is the four, placed in the corner of the upper frame in the door.

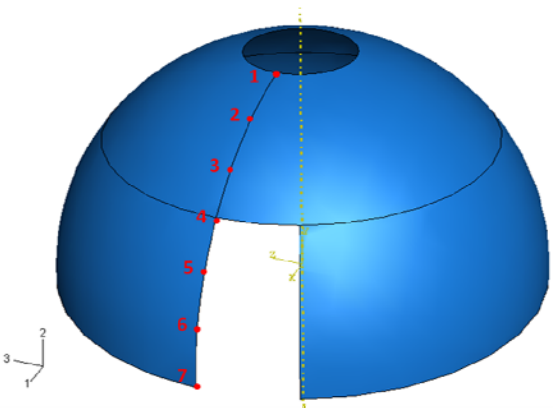

Figure 188. Points in the edges of the elements.

Table 28. Stresses in the edges of the elements. Concrete Shell.

Shell Point	σ_θ (KPa)	σ_φ (KPa)
1	-24	58
2	-249	163
3	-504	220
4	4108	3024
5	811	1
6	-2008	-19
7	-2501	11

The stresses concentration in the upper frame of the door is remarkable, so a deeply analysis in that area is performed. Two different messes are used to check the grade of accuracy in the finite element analysis. The first mess with a size of 0.1and the second one of 0.08, Figure 189.

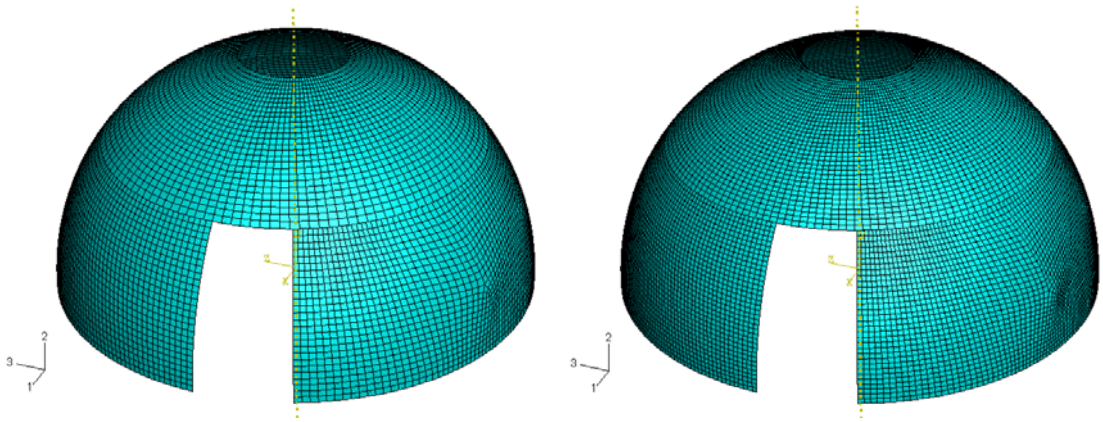

Figure 189. Messes sizes. (a) 0.1. (b) 0.08.

With the biggest 0.1 size, nine nodes were calculated in the upper frame of the door with ABAQUS, Figure 190, on the left the meridional stresses and on the right the hoop stresses; and the following results were obtained, Table 29.

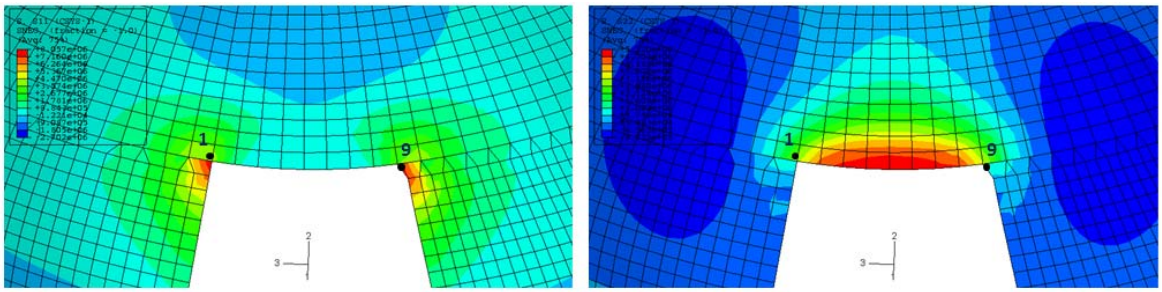

Figure 190. Upper frame of the door. Mess size: 0.1.

Table 29. Upper frame of the door stresses. Mess size: 0.1. Concrete Shell.

Upper Door Frame Points	σ_θ (KPa)	σ_φ (KPa)
1	4108	3024
2	1153	4476
3	160	4877
4	292	5150
5	119	5220
6	271	5202
7	165	4981
8	980	4758
9	3545	3281

With the smallest 0.08 size, eleven nodes were calculated in the upper frame of the door with ABAQUS, Figure 191, and the following results were obtained, Table 30.

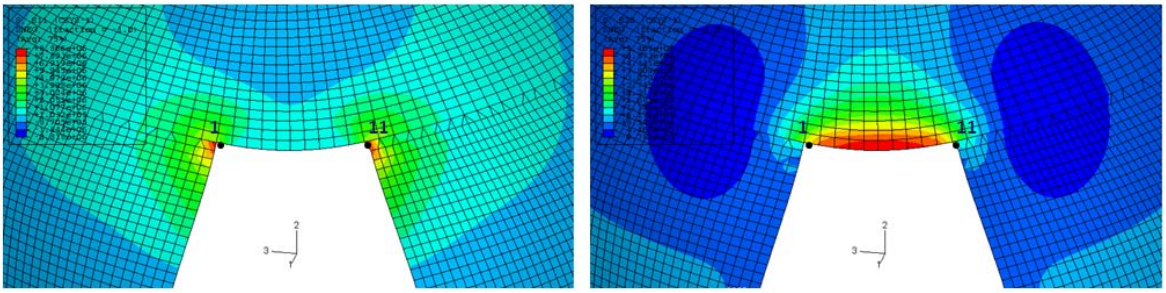

Figure 191. Upper frame of the door. Mess size: 0.08.

Table 30. Upper frame of the door stresses. Mess size: 0.08. Concrete Shell.

Upper Door Frame Points	σ_θ (KPa)	σ_φ (KPa)
1	4591	3284
2	1164	4598
3	120	4911
4	276	5205
5	92	5329
6	188	5405
7	97	5351
8	259	5255
9	140	4991
10	1048	4804
11	4118	3437

The results obtained were quite similar. As the size of the mesh decreases, the results become more accurate. The stresses results comparison between both messes sizes are present in the following figures. The relative differences are less than 8%, so for the ice shell the 0.1 mesh is used.

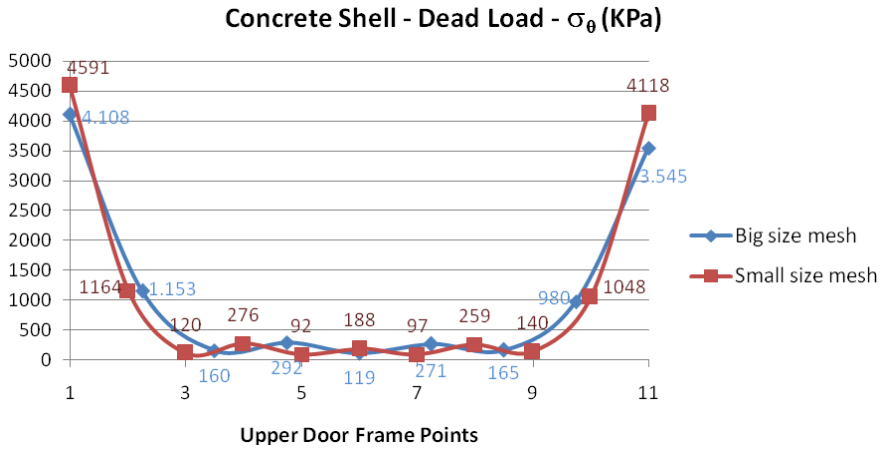

Figure 192. Meridional stresses (σ_θ, [KPa]) in the upper door frame.

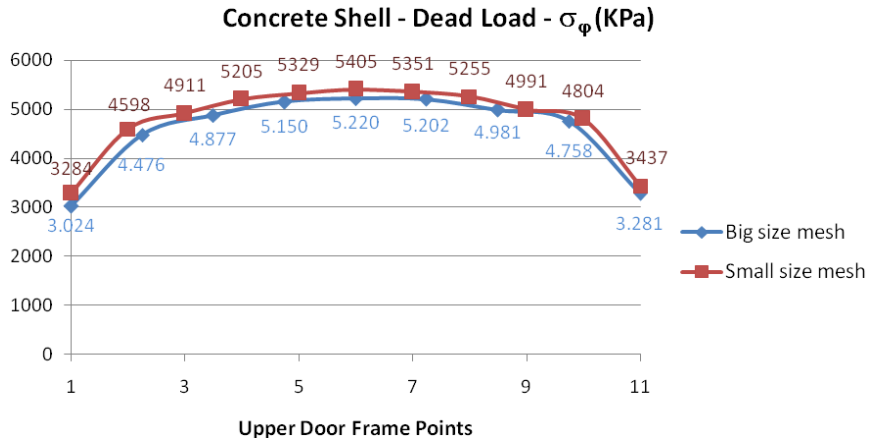

Figure 193. Hoop stresses (σ_φ, [KPa]) in the upper door frame.

In the upper corners of the upper door frame the maximum meridional stresses are suffered, with a value of 4.5MPa. This value is much lower than the tendons resistance (188MPa), so the meridional tendons are able to support the structure. In the middle point of the upper door frame the maximum hoop stress reaches a value of 5.4MPa, again the ring tendons can support the stresses.

4.6.2. Ice Shell

The ice shell analyzed has the same geometrical structure as the concrete one. Its main characteristics: radius, angle of each element, thickness, and density, were shown in Table 23.

The Von Misses stresses obtained are shown in the following figures, the meridional, the hoop, and the radial stresses, Figure 194. The radial stresses are neglected.

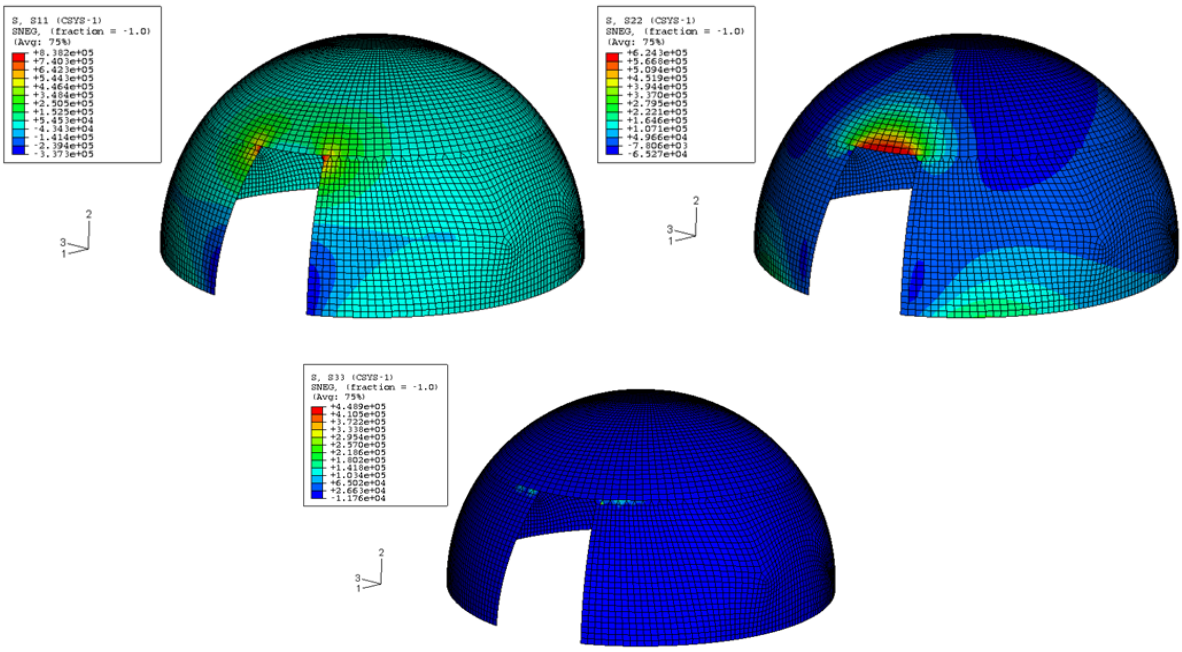

Figure 194. a. meridional stresses (σ_θ, [N/m^2]), b. hoop stresses (σ_φ, [N/m^2]), c. radial stresses (σ_r, [N/m^2]).

The values obtained in the edges of the elements, Figure 194, are shown in Table 31. As can be seen the highest stress point is as in the concrete shell the four, placed in the corner of the upper frame in the door.

Table 31. Stresses in the edges of the elements. Ice Shell.

Shell Point	σ_θ (KPa)	σ_φ (KPa)
1	-3	-7
2	-36	2
3	83	88
4	478	501
5	76	1
6	-231	-2
7	-337	5

The stresses concentration in the upper frame of the door is studied deeply with a mesh size of 0.1, Figure 195, on the left the meridional stresses and on the right the hoop stresses.

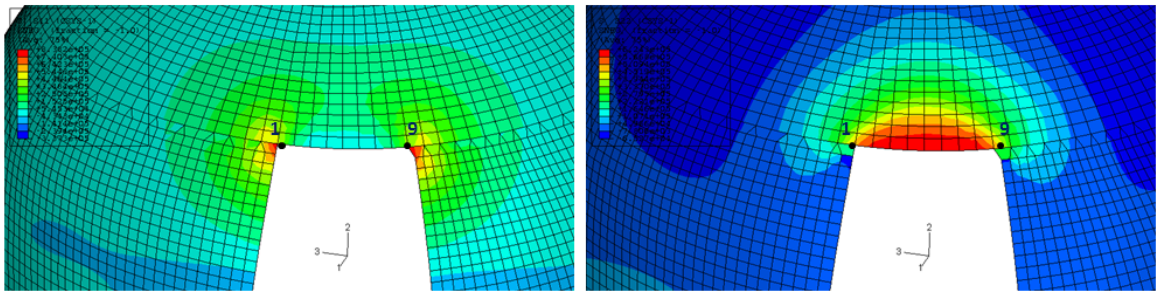

Figure 195. Upper frame of the door. Mess size: 0.1.

Table 32. Upper frame of the door stresses. Mess size: 0.1. Ice Shell.

Upper Door Frame Points	σ_θ (KPa)	σ_φ (KPa)
1	478	501
2	111	593
3	-2	581
4	25	612
5	4	616
6	22	617
7	3	596
8	96	624
9	407	523

In the upper corners of the upper door frame the maximum meridional stresses are suffered, with a value of 0.4MPa. In the middle point of the upper door frame the maximum hoop stress reaches a value of 0.6MPa. The values obtained in the ice shell are much lower than in the concrete shell due to the bigger thickness of the ice shell.

4.6.3. Comparison analysis

The stresses in the upper door frame follow the same behavior in both shells, see the following figures. In point four, are much higher than in the rest of the shell. In the concrete shell values in point four are much higher than in the ice shell, this can be due to the smaller thickness of the concrete shell.

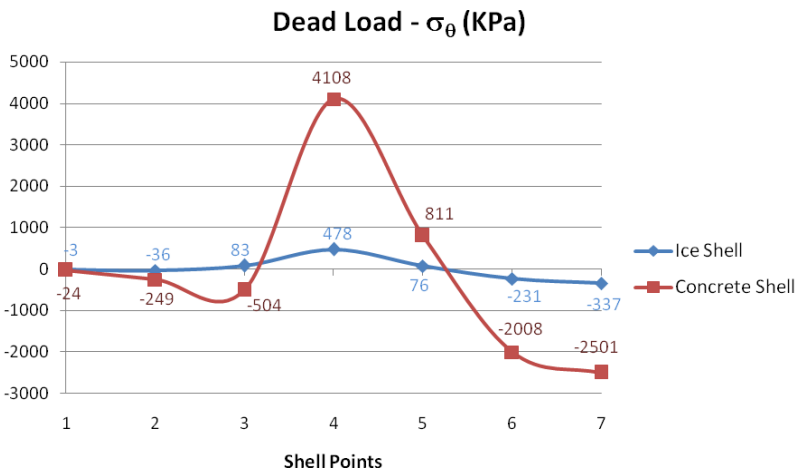

Figure 196. Meridional stresses in the edges of the elements.

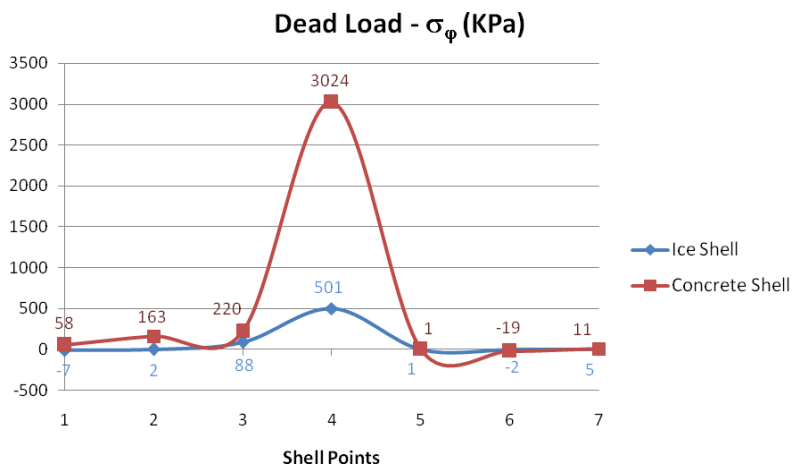

Figure 197. Hoop stresses in the edges of the elements.

The stresses in the upper door frame also follow the same behavior in both shells. But in the concrete shell peak values are much higher, see the following figures.

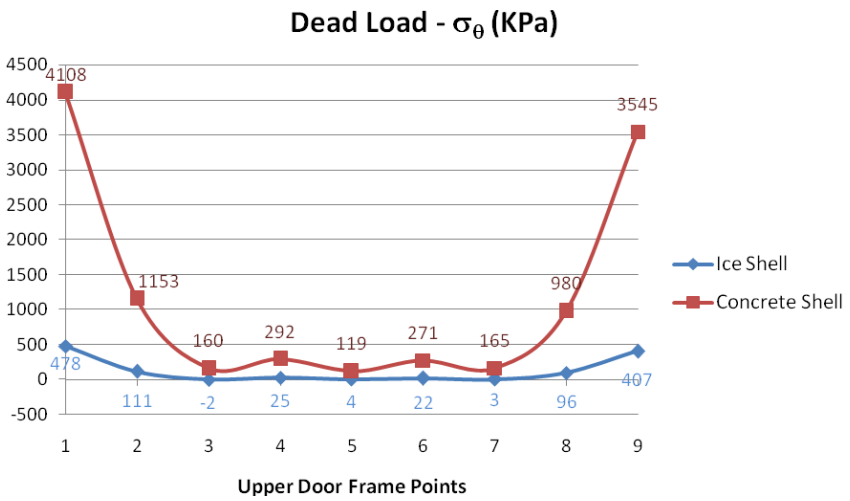

Figure 198. Figure. Meridional stresses in the upper door frame.

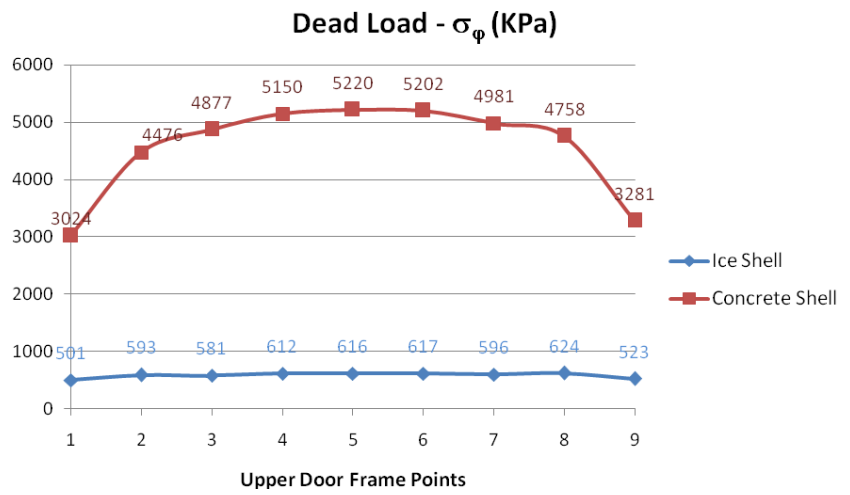

Figure 199. Hoop stresses in the upper door frame.

5. TENDONS AND PNEUMATIC FORMWORK ANALYSIS

5.1. Tendons analysis

In this section the elements that form the final shell are studied deeply. Each element weights, and this gravity load can be divided in two forces. The first component parallel to the element surface will be the force carried by the tendons; and the second one, normal to the element surface, will be carried by the pneumatic formwork.

For calculations see Annex III and Annex IV.

5.1.1. Shell planar elements

The weight of each trapezoidal element can be calculated knowing the density of the material and the volume. In a trapezium, a four sides polygon, *B* is the biggest base, *b* is the lowest base and *h* the height. The volume and weight of each element are calculated with the following expressions, and the results can be seen in Table 33 and Table 34 depending on the material.

$$Volume = \frac{(B+b)\cdot h}{2} \tag{43}$$

$$Weight(N) = \rho_{Concrete}(Kg/m^3)\cdot Volume(m^3)\cdot g \tag{44}$$

Concrete Shell

The precast elements are made of concrete with a thickness of 5cm and a density of 2400 Kg/m^3.

Table 33. Precast concrete elements volume and weight.

Precast Elements	*b* (m)	*B* (m)	*h* (m)	Area (m^2)	Volume (m^3)	Mass (Kg)	Weight (N)
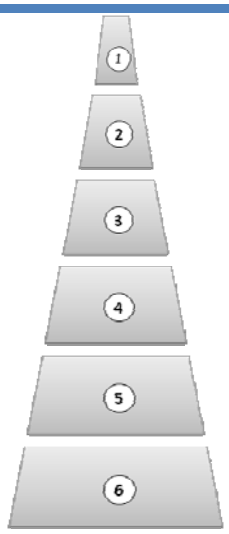	0,368	0,717	0,93	0,504	0,025	60,543	593,927
	0,717	1,03	0,93	0,812	0,041	97,483	956,304
	1,03	1,292	0,93	1,080	0,054	129,568	1271,058
	1,292	1,489	0,93	1,293	0,065	155,180	1522,314
	1,489	1,611	0,93	1,441	0,072	172,980	1696,934
	1,611	1,652	0,93	1,517	0,076	182,075	1786,160

Ice Shell

The elements in the ice shell have a thickness of 20cm and a density of 916.7 Kg/m^3.

Table 34. Ice shell elements volume and weight.

Precast Elements	*b* (m)	*B* (m)	*h* (m)	Area (m^2)	Volume (m^3)	Mass (Kg)	Weight (N)
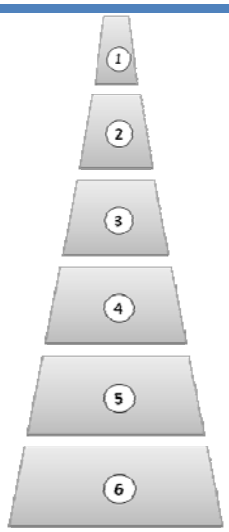	0,368	0,717	0,93	0,504	0,101	92,500	907,421
	0,717	1,03	0,93	0,812	0,162	148,937	1461,074
	1,03	1,292	0,93	1,080	0,216	197,958	1941,965
	1,292	1,489	0,93	1,293	0,259	237,089	2325,842
	1,489	1,611	0,93	1,441	0,288	264,285	2592,632
	1,611	1,652	0,93	1,517	0,303	278,181	2728,954

5.1.2. Geometrical calculations

Before calculating the forces some geometrical parameters must be calculated. The *angle of inclination* of each element, γ, can be obtained from the *meridional angle* θ, Figure 200.

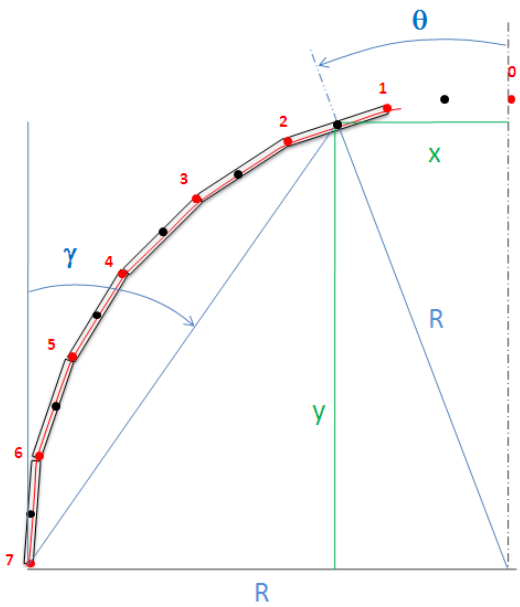

Figure 200. Remarkable points and angles in the shell.

The cartesian position of each point can be obtained easily:

$$x = R \cdot sen(\theta) \tag{45}$$

$$y = R \cdot \cos(\theta) \tag{46}$$

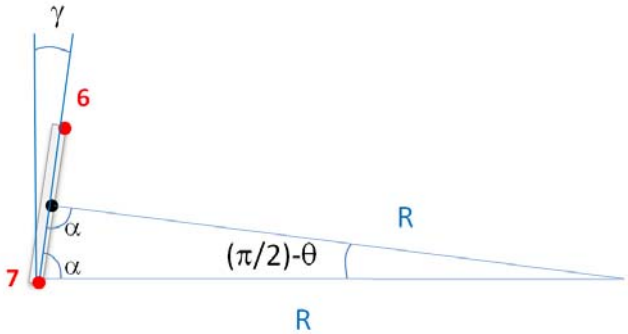

Figure 201. The inclination angle of each element.

The *angle of inclination* of each element, γ, is obtained with simple geometrical relations.

$$2 \cdot \alpha + (90^{o} - \theta) = 180^{o} \tag{47}$$

$$\alpha = \frac{180^{o} - (90^{o} - \theta)}{2} = \frac{90^{o} + \theta}{2} \tag{48}$$

Finally, $$\gamma = 90^{o} - \alpha = 90^{o} - \frac{90^{o} + \theta}{2} = \frac{90^{o} - \theta}{2} \tag{49}$$

The inclination angle of each element is calculated in the points marked in Figure 201, the red points correspond to the edges of the elements and the black ones to the middle point of each element. In these middle points is where the weight load is located corresponding to the centre of masses of each element.

Table 35. Position and angles of remarkable points in the shell.

Shell Point	θ[º]	θ[rad]	x[m]	y[m]	γ[º]	γ[rad]
0	0,000	0,000	0,000	4,153	45,000	0,785
	6,429	0,112	0,465	4,127	41,786	0,729
1	12,857	0,224	0,924	4,049	38,571	0,673
	19,286	0,337	1,372	3,920	35,357	0,617
2	25,714	0,449	1,802	3,742	32,143	0,561
	32,143	0,561	2,210	3,516	28,929	0,505
3	38,571	0,673	2,589	3,247	25,714	0,449
	45,000	0,785	2,937	2,937	22,500	0,393
4	51,429	0,898	3,247	2,589	19,286	0,337
	57,857	1,010	3,516	2,210	16,071	0,280
5	64,286	1,122	3,742	1,802	12,857	0,224
	70,714	1,234	3,920	1,372	9,643	0,168
6	77,143	1,346	4,049	0,924	6,429	0,112
	83,571	1,459	4,127	0,465	3,214	0,056
7	90,000	1,571	4,153	0,000	0,000	0,000

5.1.3. Forces calculation

For the force calculations some assumptions are made in order to simplify the calculation process:

- No friction between the pneumatic formwork and the elements.
- Tendons in circumference direction are tension-free.

With the angle of inclination of each element in the final structure now the two weight force components can be obtained. In Figure 202, the forces acting in one element and its inclination angle are shown.

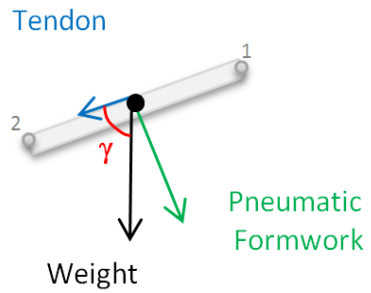

Figure 202. Forces in one element.

The forces supported by the tendons, F_T, and by the pneumatic formwork, F_{NF}, are calculated as follows:

$$F_T = W \cdot \cos\gamma \tag{50}$$

$$F_{PF} = W \cdot \sin\gamma \tag{51}$$

The shell raising process is differentiate in six steps. In the initial position all elements are place in the planar surface forming the initial plate. In step one the first ring formed by sixteen elements, type one, are raised. Then in step two the next ring formed by sixteen elements, type two, are raised. The process finishes in the step six when the last ring formed by type six elements are raised conforming the final shell shape.

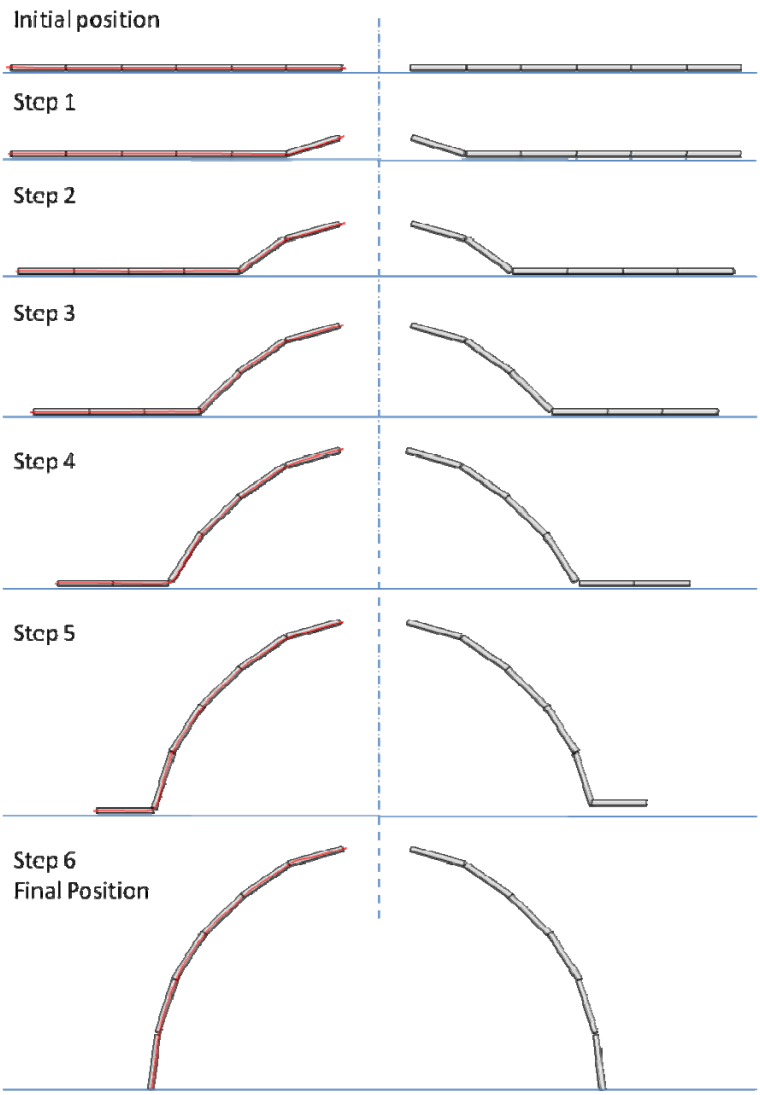

Figure 203. Elements position in the 6 Steps in raising process.

To calculate the forces in each step during the construction process, the forces to raise each element type are calculated separately due to the spherical symmetry of the shell in the concrete shell, Table 33, and in the ice shell, Table 34.

Table 36. Forces needed to raise each type element in Concrete Shell.

Precast Element	Weight (N)	γ (rad)	$F_{Tendons}$ (N)	F_{PF} (N)
1	593,927	0,6171	484,38	343,69
2	956,304	0,5049	836,98	462,58
3	1271,058	0,3927	1174,30	486,41
4	1522,314	0,2805	1462,82	421,43
5	1696,934	0,1683	1672,96	284,25
6	1786,160	0,0561	1783,35	100,15
		Total	7414,79	2098,51

Table 37. Forces needed to raise each type element in Ice Shell.

Precast Element	Weight (N)	γ (rad)	$F_{Tendons}$ (N)	F_{PF} (N)
1	907,421	0,617	740,057	525,099
2	1461,074	0,505	1278,766	706,749
3	1941,965	0,393	1794,142	743,158
4	2325,842	0,280	2234,942	643,876
5	2592,632	0,168	2556,001	434,282
6	2728,954	0,056	2724,661	153,014
		Total	11328,568	3206,177

For the step one only the first element is taken into account. For step two the forces of elements one and two are sum up. Following this calculation scheme the total forces in each step are calculated.

Table 38. Total forces in each step in the Concrete Shell.

Steps	$F_{Tendons}$ (KN)	F_{PF} (KN)
Step 1	0,484	0,344
Step 2	1,321	0,806
Step 3	2,496	1,293
Step 4	3,958	1,714
Step 5	5,631	1,998
Step 6	7,415	2,098

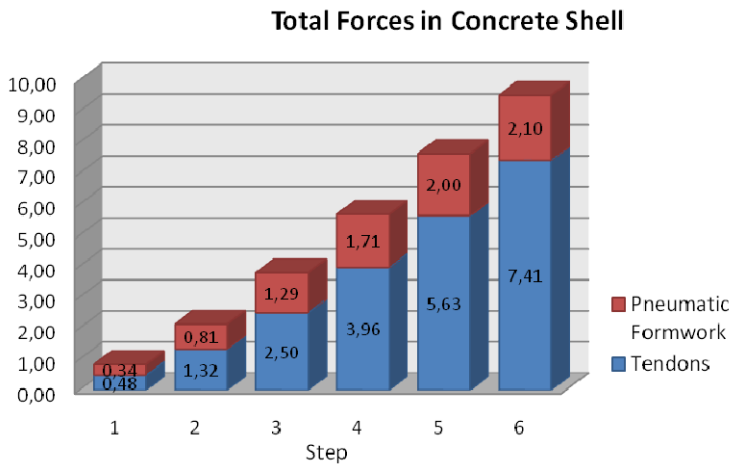

Figure 204. Total forces in each step in the Concrete Shell.

Table 39. Total forces in each step in the Ice Shell

Steps	$F_{Tendons}$ (N)	F_{PF} (N)
Step 1	0,740	0,525
Step 2	2,019	1,232
Step 3	3,813	1,975
Step 4	6,048	2,619
Step 5	8,604	3,053
Step 6	11,329	3,206

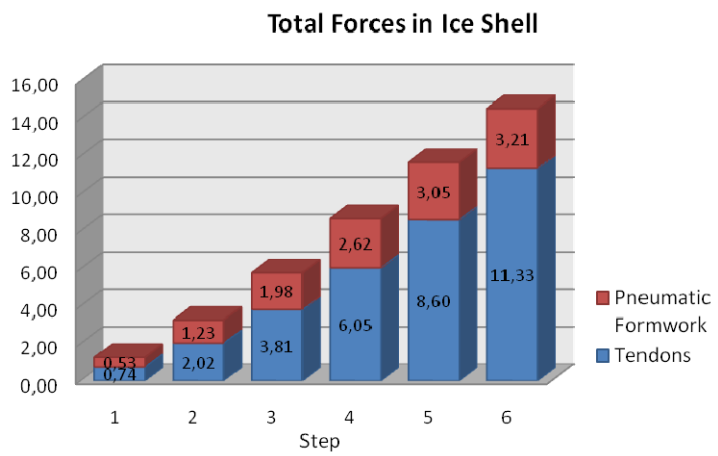

Figure 205. Total forces in each step in the Ice Shell.

Moreover the **central ring force**, Figure 206, can be calculated with the following procedure:

$$F_{Ring} = \frac{F_{Tendons}}{l} \cdot R \tag{52}$$

R central ring radius

l arc longitude $\quad l = \frac{\beta \cdot \pi \cdot R}{180}$ (53)

β arc angle $\quad \beta = \frac{360^{o}}{16}$ (54)

Substituting in equation 52, equations 53 and 54,

$$F_{Ring} = F_{Tendons} \cdot \frac{180}{\frac{360}{16} \cdot \pi \cdot R} \cdot R \tag{55}$$

Finally we obtain equation 56

$$F_{Ring} = \frac{8 \cdot F_{Tendons}}{\pi} \tag{56}$$

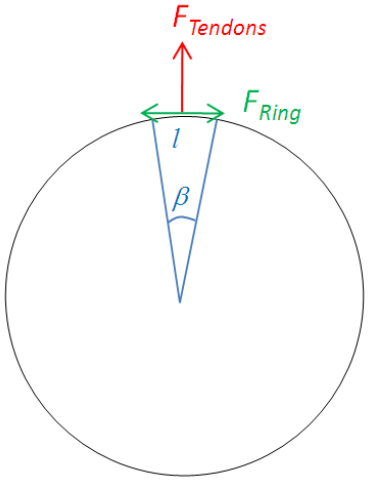

Figure 206. Force carried by tendons and ring force relationship.

In Figure 207 the ring force increasing in each step can be notice. The maximum value is reached in step six when the final shell is obtained. In the concrete shell the ring must support a force of at least 19KN, and in the ice shell of 29KN.

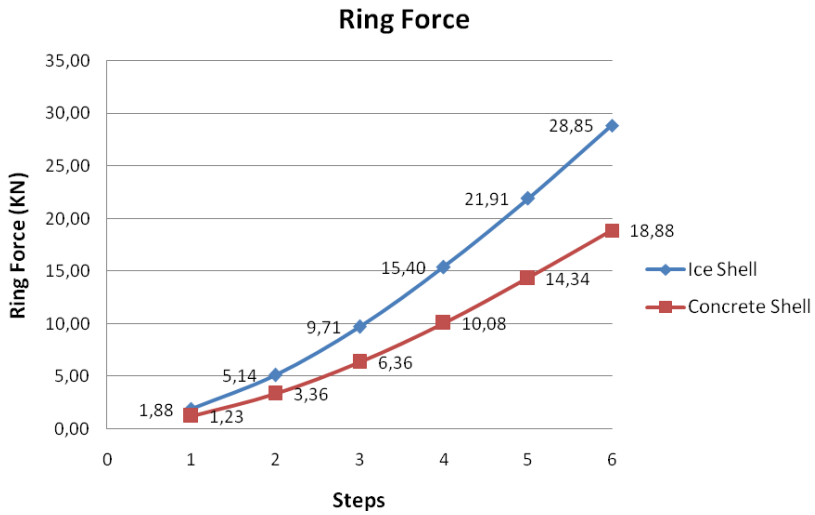

Figure 207. Ring force evolution in each step.

The force supported by the tendons previously calculated belongs to one element. Each element has two tendons in meridional direction, so the force that one tendon must support is known.

$$F_{1Tendon} = \frac{F_{Tendons}}{2} \tag{57}$$

The force supported by each tendon increases as long as the structure rises up step by step. The maximum force that should be able to support the cable in the concrete shell is of at least 4KN and in the ice shell 6KN, Figure 208.

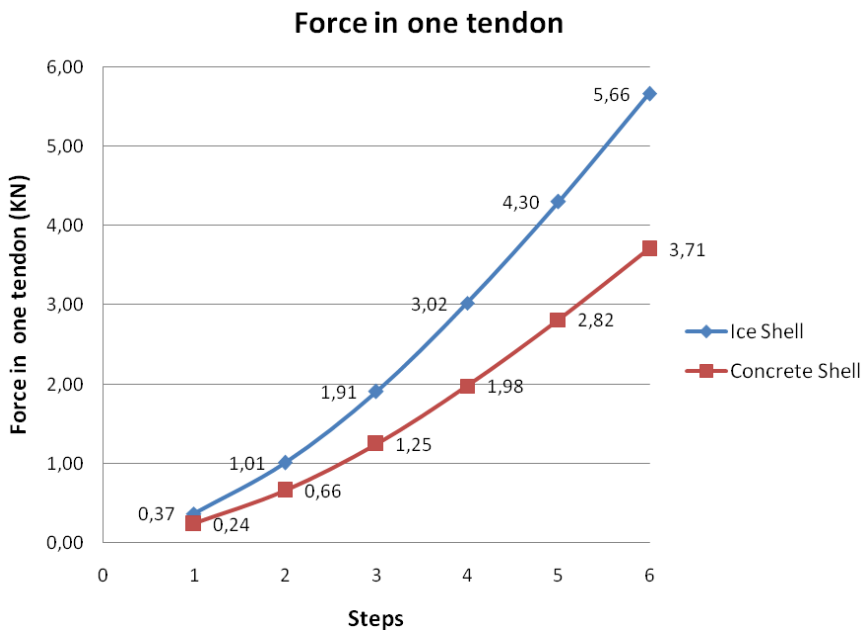

Figure 208. Force in one tendon evolution in each step.

As it was told in section 3.2.1, the maximum traction force that can support the cable is of 14,8KN, so the cable fulfills the load requirements in the process and in the final structure in both cases: concrete and ice shells.

5.2. Pneumatic Formwork

The total pressure needed in the pneumatic formwork, P, depends on the weight load that have to support, G, and the area of the base of the shell, A_{base}.

$$P(Pa) = \frac{G(N)}{A_{base}(m^2)} \tag{58}$$

The area of the circular base

$$A_{base} = \pi r^2 \tag{59}$$

The weight of the pneumatic formwork itself is neglected in comparison with the weight of the shell, formed by 96 elements.

$$G(N) = V_{shell}(m^3) \cdot \rho(Kg/m^3) \cdot g \tag{60}$$

The volume of the shell can be calculated in two different ways

$$V_{shell} = 2\pi r^2 \cdot t \tag{61}$$

$$V_{shell} = \sum_{m=1,n=1}^{m=6,n=16} V_{element(m,n)} \tag{62}$$

m type of element, there are 6 types of elements
n number of element in the same ring, there are 16 elements in every ring.

Using the simplest way to calculate the volume of the shell, formula 61, considering the shell a homogeneous hemisphere with thickness t, we can simplify expression 58.

$$P(Pa) = \frac{2\pi r^2 \cdot t \cdot \rho \cdot g}{\pi r^2} = 2 \cdot t(m) \cdot \rho(Kg/m^3) \cdot g \tag{63}$$

With this simplification the pressure needed in the pneumatic formwork, knowing that $1bar = 10^5 Pa$, is shown in Table 40.

Table 40. Pressure needed in the pneumatic formwork. Simplification method.

Shell material	t (m)	ρ (Kg/m^3)	P(KPa)	P(mbar)
Concrete	0,05	2400	2,354	23,54
Ice	0,2	916,7	3,597	35,97

Considering the weight of each element in the shell (see Table 33 andTable 34), and expression 62, the following values are obtained.

Table 41. Pressure needed in the pneumatic formwork.

Shell material	*G* (KN)	*P* (KPa)	*P* (mbar)
Concrete	125,23	2,311	23,11
Ice	191,33	3,531	35,31

Hydrostatic pressure can be analyzed by the height of a water column, which effectively yields the pressure at a given depth of the column.

6. CONCLUSIONS

This thesis has presented a study into the new technology to build double curved shells from plane elements, developed at the *Institute for Structural Engineering* of the *Vienna University of Technology.*

The thin concrete shells are considered by both designers and the public to be among the most striking of structural systems, not only because of their superior aesthetics but also because of the ability to fit perfectly in the natural environment. This functional technology can be used in buildings in many different applications as schools, gymnasiums, community centers, or industrial facilities.

The ice shells highlight due to its ephemeral and beauty nature. Shells can be used in temporary architecture, as roof structures for sport and music events, or presentations and promotions of sale products. Moreover the translucent nature of ice, allows several possibilities to make attractive this structure. For instance the internal illumination of the ice shell during the night creates a luminous atmosphere in the surroundings.

Like the arch, the curved shapes are naturally strong structures, allowing wide areas to be spanned without the use of internal supports, giving an open and clear interior. Thin concrete shells are also durable and demand minimal maintenance.

One of the main advantages is the economical aspect. The use of concrete as a building material reduces both materials cost and construction costs, as concrete is relatively inexpensive and easily cast into elements. Moreover the resulting structure may be immensely strong and safe.

This new construction method consists on transforming a plate formed by plane elements into a shell with the combined usage of precast elements, post tensioning and pneumatic formworks.

A concrete shell can be prefabricated in a factory in the form of a large number of precast elements and then transported to the site for assembly into a shell. In the case of the ice shell the elements are cut from an initial ice plate.

The tendons in radial and meridional direction in the structure support the forces and hold the structure. The pneumatic formwork allows the raising of the structure in a fast and economical way. The pneumatic formwork, manufactured in the laboratory, had problems to hold the elements in the raising process. A new pneumatic formwork was manufactured finding the best way to obtain a stronger element capable to hold the precast elements.

This technology eliminates the need for temporary formwork and the high labor costs associate to it.

The elements used to tighten the cables were tested in the laboratory in order to ensure their demanded properties were appropriate to support the forces created in the structure. It was observed that the enclosure elements worked much better holding two cables together than with one single cable as it was used in the experiments. This leads

us to conclude that in future designs enclosure elements joining two cables will work better, so modifications in the elements design would have to be made.

An analytical and finite element analysis was carried out on the structure based on a hemispherical shape. This approximation allows us to work with simpler calculation methods.

The program ABAQUS, based on finite element analysis, is a powerful tool that permitted us to study deeply the structure with different load configurations in an accurate and fast way.

The numerical modeling results were compared to the analytical ones ensuring the adequate behavior of the structure.

This technology under development has real possibilities nowadays in the market. New experiments will take place to ensure their structural capabilities and improve the construction method finding equilibrium between costs and benefits.

References

[1] *Theory of Shell Structures*. C. R. Calladine. Edition: reprint. Cambridge University Press, 1989

[2] *Design and Analysis of Shell Structures*. Mehdi Farshad. Edition: illustrated. Springer, 1992

[3] Mark Ketchum's. Concrete Shell Page. www.ketchum.org. January 2009.

[4] *Thin Shell Concrete Structures*. David P.Billington. Princeton University. McGraw-Hill, Inc. 1965.

[5] Lite Strabo Blog. Domes. January 2009. http://litestraboen.blogspot.com/2007/01/domes.html

[6] Building Big Bridges, Domes, Skyscrapers, Dams, and Tunnels. January 2009. http://www.pbs.org/wgbh/buildingbig/dome/index.html

[7] Building the roman Pantheon. January 2009. http://www.angelfire.com/super/tyvernon/

[8] Architectural Record. The grate Stupa of Sanchi. January 2009. http://rogershepherd.com/WIW/solution12/stupa.html

[9] Encyclopedia Encarta UK. January 2009. Article. Domes: Introduction; Origins; Renaissance, Baroque, and Neo-Classical Domes; 20th-Century Domes http://uk.encarta.msn.com/encyclopedia_761555109/Dome.html

[10] *Análisis de tipologías estructurales: bóveda, lámina, cúpula y paraboloide*. Ignacio Requena Ruiz.

[11] *Equilibrium analysis of masonry domes*. Wanda W. Lau. Thesis. B. S., Civil Engineering; Michigan State University; 2002.

[12] Monolitic dome institute. January 2009. http://static.monolithic.com/index.html

[13] *Behaviour and modelling of steel-concrete composite shell roofs*. Hon-Ting Wong. Department of Civil and Structural Engineering. The Hong Kong Polytechnic University. July, 2005

[14] Geo-Dome. Different dome construction techniques. Dome calculation tools. Steel-framework domes. January 2009. http://www.geo-dome.co.uk/

[15] Geodesic Dome Notes. Rene K. Mueller, January 15, 2009. Simply Differently. Temporary buildings: studying, planning, building and living in. Wooden Strut with Pipe Hub domes. January 2009. http://simplydifferently.org

[16] Goodkarmadomes. Dome basics. Wood panel domes. January 2009. http://www.goodkarmadomes.com

[17] Dome Technology. Concrete dome construction process. January 2009. http://www.dometech.com

[18] Architecture week. Building Monolithic Domes. January 2009. http://www.architectureweek.com/2001/0328/building_1-2.html

[19] University of Sharjah. Reinforced Concrete Thin Shell Structures. January 2009. https://www.sharjah.ac.ae/oldsite/bbmaterials/0401513_1/content/_55993_1/!4c6563747572652030313 2.pdf

[20] The Dome: A Simple Violation of Determinism in Newtonian Mechanics. January 2009. http://www.pitt.edu/~jdnorton/Goodies/Dome/index.html

[21] *Thin Post-Tensioned Concrete Shell Structures: Connection and Construction Technology.* Sonja Dallinger. 7th fib International PhD Symposium in Civil Engineering in Stuttgart, Germany. Institute for Structural Engineering, Vienna University of Technology, Vienna, Austria. September 2008.

[22] *Joining of spatially curved surfaces from thin-walled prefabricated elements.* Master´s Thesis Diplomarbeit. Patricia Fernández Alloza. Institute for Structural Engineering, Vienna University of Technology, Vienna, Austria. July 2008.

[23] *Concrete shell technical plans*. Sonja Dallinger. Institute for Structural Engineering, Vienna University of Technology, Vienna, Austria. October 2008.

[24] *Ice Shells for Temporary Event Architectur*e. Johann Kollegger, Prof., Clemens Preisinger, Eng., Michael Kaulfus, Eng., Vienna University of Technology, Vienna, Austria. April 2004.

[25] Oberndorfer. January 2009. www.oberndorfer.at.

[26] Teufelberger. *Catalogue Stahl- und Faserseile*. January 2009. www.teufelberger.com.

[27] Seilerei Wüstner. *Catalogue anchorage elements.* January 2009. www.seil.at.

[28] *Elementare Schalenstatik*. Alf Pflüger. Fünfte Auflage. Springer-Verlag. Berlin Heidelberg New York 1981.

[29] *Eurocode 1:* Actions on structures. *Part 1-3: General Actions Snow loads.* UNE-EN 1991-1-3.

[30] *Önorm B 1991-1-3*. Eurocode 1 – Einwirkungen auf Tragwerke. Teil 1-3: Allgemeine Einwirkungen – Schneelasten.

[31] *Eurocode 1*: Actions on structures. General actions. *Part 1-4: Wind actions*. UNE-EN 1991-1-4. 1998.

[32] *Önorm B 1991-1-4*. Eurocode 1 – Einwirkungen auf Tragwerke. Teil 1-4. National Annex (Table A.1).

[33] *ABAQUS Tutorial*. Mechanics of Solids. Division of Engineering Brown University. www.engin.brown.edu. January 2009.

[34] *Goto Kokawa Ice domes.* www.htokai.ac.jp/DA/kkw/indexe.html. February 2009.

[35] Medwadowski, S.J. (1998). *Concrete thin shell roofs at the turn of the millennium*, Current and Emerging Technologies of Shell and Spatial Structures, Proceedings of the IASS Symposium, April 1997, Edited by J. Abel, R. Astudillo and N. K. Srivastava, 9-22.

[36] Bini, D. (1991). *The cause of the collapse of the Pittwater Binishells*, Engineer Australia, 3rd March, 5-8.

[37] Levy, M. and Salvadori, M. (1991). *Why Building Fall Down*. W. W. Norton & Company Limited, New York and London.

[38] Grad, P. (1991). *Binishell collapse: cause of accident finally public*, Engineers Australia, 8th March, 27-28.

[39] Nervi, P.L. (1957). *The works of Pier Luigi Nervi*. Frederick A. Praeger, Inc., New York.

[40] Huxtable, A.L. (1960). *Pier Luigi Nervi*. George Braziller, Inc., London.

[41] Love, A. E. H.: *A Treatise on the Mathematical Theory of Elasticity*, 4th ed., Dover Publications, Inc., New York, 1944.

[42] Wang, Chi-tech: *Applied Elasticity*, McGraw-Hill Book Company. New York, 1953.

[43] Timoshenko, S. P., and S. Woinowsky-Krieger: *Theory of Plates and Shells*, 2d ed., McGraw-Hill Book Company. New York, 1959.

List of Figures

Figure 1. Surfaces with positive, negative and zero Gaussian curvature. (Source: [2]). 23
Figure 2. Developable and nondevelopable surfaces. (Source: [2]). 23
Figure 3. Surfaces of revolution examples. (Source: mathworld.wolfram.com) 24
Figure 4. Translational surfaces. 24
Figure 5. Ruled surfaces. (Source: mathworld.wolfram.com) 25
Figure 6. Barrel shells. (Source: [3]) 26
Figure 7. Folded plates. (Source: [3]) 26
Figure 8. Short shells. (Source: [3]) 27
Figure 9. Hyperbolic paraboloid. (Source: [3]) 27
Figure 10. Dome. (Source: [3]) 28
Figure 11. Translation shells. (Source: [3]) 28
Figure 12. Arch and dome structures. (Source: [4]) 29
Figure 13. Beam and barrel systems. (Source: [4]) 31
Figure 14. Equilibrium of a differential element cut from the shell. (Source: [4]) 33
Figure 15. Stress resultants and stress couples. (Source: [4]) 33
Figure 16. Treasury of Atreus, Mycenae. (Source: [9]) 37
Figure 17. Sectioned view of Treasury of Atreus at Mycenae, Greece. (Source: dkimages.com) 38
Figure 18. Stupa in Sanchi. (Source: fog.ccsf.org) 38
Figure 19. Pantheon of Hadrianus, Rome. (Source: [9]) 39
Figure 20. Distributing the Pantheon's Weight. (Source: [7]) 39
Figure 21. The mausoleums of Bokhara. (Source: losviajeros.com) 40
Figure 22. Church of Santa Costanza. (Source: intranet.arc.miami.edu and contracosta.edu) 40
Figure 23. Hagia Sophia, Constantinople (532). (Source: barber.org.uk and contracosta.edu) 41
Figure 24. Mosque of the Rock (691) in Jerusalem. (Source: [5]) 41
Figure 25. Santa Maria del Fiore, Florence. (Source: members.iinet.net.au) 42
Figure 26. The main dome of St Paul's Cathedral, London. (Source: alps-uk.com) 42
Figure 27. United States Capitol, Washington. (Source: [6]) 43
Figure 28. The Taj Majal dome. (Source: www.topnews.in) 43
Figure 29. Climatron, botanical garden completed in St Louis, Missouri. 45
Figure 30. Geodesic Dome, Montreal. (Source: [9]) 45
Figure 31. Epcot Center in Orlando, Florida. (Source: destination360.com) 46
Figure 32. Toronto SkyDome. (Source: dkimages.com and pbs.org) 46
Figure 33. Astrodome, Texas. (Source: johnnyroadtrip.com) 46
Figure 34. Millenium Dome, O2 Complex, Greenwich. (Source: [9]) 47
Figure 35. Fontana, graphical construction for domes. (Source: [10]) 49
Figure 36. Domes develop internal meridional and hoop forces. (Source: [10]) 49
Figure 37. Division into segments of the dome. (Source: [10]) 50
Figure 38. Segments deformation in the dome. (Source: [10]) 50
Figure 39. Effect of the hoop forces in the dome. (Source: [10]) 51
Figure 40. Boundary conditions effects. (Source: [10]) 51
Figure 41. The support structure reactions to applied and gravity loads. (Source: [11]) 52
Figure 42. Typical collapse mechanism for a dome. (Source: [11]) 52

Figure 43. Load transmission in domes (symmetrical load). (Source: [10]) 53
Figure 44. Use wing nuts for quick assembly/disassembly in flattened conduit. (Source: [14]) 54
Figure 45. Wooden Strut with Pipe Hub. (Source: [15]) 55
Figure 46. Tube and hub dome. (Source: [14]) 55
Figure 47. Geodesic dome. Fuller's dome, 1954. (Source: [14]) 56
Figure 48. Panel dome. (Source: [16]) 57
Figure 49. Stressed skin dome. (Source: geo-dome.co.uk) 57
Figure 50. Industrial enclosures. (Source: www.triodetic.com/Photos.htm) 58
Figure 51. Urstville boys' high school, 1973. 58
Figure 52. Monolitic dome layers. (Source: [14]) 59
Figure 53. Building a Monolitic Dome. Step 1: Concrete ring foundation. 60
Figure 54. Building a Monolitic Dome. Step 2: Airform. (Source: [14], [17]) 60
Figure 55. Building a Monolitic Dome. Step 3: Polyurethane insulation. (Source: [14], [17]) 60
Figure 56. Building a Monolitic Dome. Step 4: Steel reinforcing. 61
Figure 57. Building a Monolitic Dome. Step 5: Shotcrete layer. (Source: [14], [17]) ... 61
Figure 58. Preparations for the concrete cast of Kresge Auditorium, MIT. (*Source: [13]*) 63
Figure 59. The Kresge Auditorium during construction. (*Source [13]*) 63
Figure 60. The Kresge Auditorium, MIT. (Source: [13]) 64
Figure 61. Supporting formwork and falsework for Kresge Auditorium, MIT. 64
Figure 62. General construction process of a Binishell dome. (*Source: [13]*) 66
Figure 63. Process of manufacturing prefabricated units for a four-sided dome. 67
Figure 64. Palazzetto dello Sport, Roma. (Source: [13], After Huxtable 1960) 68
Figure 65. Forces developed in a dome. (Source: [10]) 70
Figure 66. Transforming a plate into a shell process. (Source: [21]) 71
Figure 67. Steel tendons in (a) singly and (b) doubly curved surface structures. 72
Figure 68. Hemispheric, non developable surface. 73
Figure 69. Flat plate and final shell diameter relationship. 73
Figure 70. Numbering of the pieces and location of the points. 74
Figure 71. Floor plan and cross section of the flat structure. (Source: [22]) 75
Figure 72. Cross section in the final position after the elevation. (Source: [22]) 75
Figure 73. Flat structure with tendons and weights. 76
Figure 74. Cross section in the initial position before the elevation 76
Figure 75. Cross section in the final position after the elevation 77
Figure 76. 1st Wooden model. Anchorage system in the central ring. (Source: [22]) 77
Figure 77. 1st Wooden model. Raising process of the shell. (Source: [22]) 78
Figure 78. 2nd Wooden model. Central ring pieces with anchorage system in meridional direction. (Source: [22]) 79
Figure 79. 2nd Wooden model. Hinges. (Source: [22]) 79
Figure 80. 2st Wooden model. Raising process of the shell. (Source: [22]) 80
Figure 81. Concrete shell elements plans. (Source: [23]) 82
Figure 82. Concrete shell elements plans (II). (Source: [23]) 83
Figure 83. Concrete shell special elements plans. (Source: [23]) 84
Figure 84. Concrete shell special elements plans (II). (Source: [23]) 85
Figure 85. Precast concrete elements. 86
Figure 86. Pneumatic formwork: cutting the elements. 87
Figure 87. Pneumatic formwork: wooden model. 87

Figure 88. Pneumatic formwork: joining segments to the base. 87
Figure 89. Pneumatic formwork: inflating the formwork. 88
Figure 90. Pneumatic formwork: joining the elements and reinforcement. 88
Figure 91. Pneumatic formwork: final inflated shape. 89
Figure 92. Cable elements. 89
Figure 93. Anchorage element: cable closure. *Seilerei Wüstner*. (Source: [27]) 90
Figure 94. Cable closure. Test 1: one element. 91
Figure 95. Cable closure, test 1 results: one element. 92
Figure 96. Cable closure. Test 2: two elements in series. 92
Figure 97. Cable closure, test 2 results: two elements. 93
Figure 98. Rope clips..... 93
Figure 99. Small rope clips Test. One element each side..... 94
Figure 100. Small rope clips, test1: one element..... 95
Figure 101. Big rope clips Test. One element each side. 95
Figure 102. Big rope clips, test1: one element. 96
Figure 103. Big rope clips Test. Two element each side..... 96
Figure 104. Big rope clips, test 2: two elements in single cable. 96
Figure 105. Big rope clips Test. One element in double cable..... 97
Figure 106. Big rope clips, test 3: one element in double cable..... 97
Figure 107. Big rope clips Test. Three elements in double cable. 98
Figure 108. Failure of the steel cable. 98
Figure 109. Big rope clips, test 4: three elements in double cable..... 99
Figure 110. Pneumatic formwork, plastic layer and precast elements. 99
Figure 111. Allocation of the elements in the plane..... 100
Figure 112. Cables allocated in the conducts element by element..... 100
Figure 113. Anchorage system in the central ring with a spring in all meridional tendons..... 100
Figure 114. Anchorage systems in elements 6 type in all meridional tendons. 101
Figure 115. Cable winches anchored..... 101
Figure 116. Raising process. Concrete Shell..... 101
Figure 117. Kokawa's ice dome. (Source: [34]) 103
Figure 118. (a) Plan view of ice plate, (b) Section of ice plate, (c) Section of ice shell, (d) Detail D. (Source: [24]) 103
Figure 119. Raising process of the ice shell. (Source: [24])..... 104
Figure 120. Completed ice shell in laboratory. (Source: [24])..... 104
Figure 121. Austria map, Obergurgl location. (Source: azerb.com) 104
Figure 122. Circular plate of ice formation, cutting the elements..... 105
Figure 123. Raising process in the small ice shell..... 105
Figure 124. Door built in the small ice shell 106
Figure 125. Circular plate formation in the big ice shell..... 106
Figure 126. Raising process in the big ice shell. 106
Figure 127. Position of the analyzed points 109
Figure 128. Dimensional parameters. (Source: [28]) 111
Figure 129. Deformations. (Source: [28]) 112
Figure 130. Load components and resultant forces. (Source: [28]) 112
Figure 131. Shell element with local axis. 113
Figure 132. Forces caused by a distributed load over the shell. (Source: [28]) 114
Figure 133. Forces caused by a distributed load. (Source: [28])..... 115
Figure 134. Roof shape coefficient for snow loads in cylindrical roofs..... 116

Figure 135. Roof shape coefficient for snow loads in cylindrical roofs, as function of *h/l* relationship. 116
Figure 136. Snow load. (Source: [29]) 117
Figure 137. Ilustrations of the exposure factor $c_e(z)$ for c_0=1.0, k_i=1.0. 122
Figure 138. External pressure coefficient for buildings with a loaded area 123
Figure 139. Recommended values of external pressure coefficients $cp_{e,10}$ 124
Figure 140. Sphere near a plain surface. (Source: [31], Figure 7.31) 126
Figure 141. Alongwind force coefficient of a sphere. (Source: [31], Table 7.30) 126
Figure 142. Pressure distribution due to wind load. 127
Figure 143. Shell geometry drawing in Abaqus. 131
Figure 144. Loads and boundary conditions. 131
Figure 145. Shell meshed. 131
Figure 146. Shell meridional forces (N_θ, [N/m]). (Concrete Shell, Case 1). 132
Figure 147. Shell hoop forces (N_φ, [N/m]). (Concrete Shell, Case 1). 132
Figure 148. Shell radial forces (N_φ, [N/m^2]). (Concrete Shell, Case 1). 132
Figure 149. Shell meridional stresses (σ_θ, [N/m^2]). (Concrete Shell, Case 1). 133
Figure 150. Shell hoop stresses (σ_φ, [N/m^2]). (Concrete Shell, Case 1). 133
Figure 151. Shell radial stresses (σ_r, [N/m^2]). (Concrete Shell, Case 1). 133
Figure 152. Concrete Shell – Case 1: Dead Load. Meridional forces comparative. 134
Figure 153. Concrete Shell – Case 1: Dead Load. Hoop forces comparative. 134
Figure 154. Concrete Shell – Case 1: Dead Load. Meridional stresses comparative... 135
Figure 155. Concrete Shell – Case 1: Dead Load. Hoop stresses comparative. 135
Figure 156. Snow load distribution. 136
Figure 157. Case 2. Meridional stresses. Concrete shell. 137
Figure 158. Case 2. Hoop stresses. Concrete shell. 137
Figure 159. Pressure distribution due to wind load. 138
Figure 160. Wind pressure loads in ABAQUS. 139
Figure 161. Shell meridional stresses (σ_θ, [N/m]). (Concrete Shell, Case 3). 140
Figure 162. Shell hoop stresses (σ_φ, [N/m]). (Concrete Shell, Case 3). 140
Figure 163. Shell radial stresses (σ_φ, [N/m^2]). (Concrete Shell, Case 3). 141
Figure 164. Wind load. General Von Misses Stresses 141
Figure 165. Shell displacements (u_1, u_2, u_3, [m]). (Concrete Shell, Case 3). 142
Figure 166. General shell displacements [m]. (Concrete Shell, Case 3). 142
Figure 167. Shell meridional forces (N_θ, [N/m]). (Ice Shell, Case 1). 144
Figure 168. Shell hoop forces (N_φ, [N/m]). (Ice Shell, Case 1). 144
Figure 169. Shell radial forces (N_φ, [N/m^2]). (Ice Shell, Case 1). 144
Figure 170. Shell meridional stresses (σ_θ, [N/m^2]). (Ice Shell, Case 1). 145
Figure 171. Shell hoop stresses (σ_φ, [N/m^2]). (Ice Shell, Case 1). 145
Figure 172. Shell radial stresses (σ_φ, [N/m^2]). (Ice Shell, Case 1). 145
Figure 173. Ice Shell – Case 1: Dead Load. Meridional forces comparative. 146
Figure 174. Ice Shell – Case 1: Dead Load. Hoop forces comparative. 146
Figure 175. Ice Shell – Case 1: Dead Load. Meridional stresses comparative. 147
Figure 176. Ice Shell – Case 1: Dead Load. Hoop stresses comparative. 147
Figure 177. Case 2. Meridional stresses. Ice shell. 149
Figure 178. Case 2. Hoop stresses. Ice shell. 149
Figure 179. Shell meridional stresses (σ_θ, [N/m]). (Ice Shell, Case 3). 150
Figure 180. Shell hoop stresses (σ_φ, [N/m]). (Ice Shell, Case 3). 151
Figure 181. Shell radial stresses (σ_φ, [N/m^2]). (Ice Shell, Case 3). 151

Figure 182. Wind load. General Von Misses Stresses 151
Figure 183. Shell displacements (u_1, u_2, u_3, [m]). (Ice Shell, Case 3). 152
Figure 184. General shell displacements [m]. (Ice Shell, Case 3)..... 152
Figure 185. Views of the shell with a door. 153
Figure 186. Shell with a door model: dead load, boundary conditions, and meshing.. 153
Figure 187. a. meridional stresses (σ_θ, [N/m^2]), b. hoop stresses (σ_φ, [N/m^2]),..... 154
Figure 188. Points in the edges of the elements. 154
Figure 189. Messes sizes. (a) 0.1. (b) 0.08. 155
Figure 190. Upper frame of the door. Mess size: 0.1. 155
Figure 191. Upper frame of the door. Mess size: 0.08. 156
Figure 192. Meridional stresses (σ_θ, [KPa]) in the upper door frame. 157
Figure 193. Hoop stresses (σ_φ, [KPa]) in the upper door frame..... 157
Figure 194. a. meridional stresses (σ_θ, [N/m^2]), b. hoop stresses (σ_φ, [N/m^2]),..... 158
Figure 195. Upper frame of the door. Mess size: 0.1. 159
Figure 196. Meridional stresses in the edges of the elements. 160
Figure 197. Hoop stresses in the edges of the elements. 160
Figure 198. Figure. Meridional stresses in the upper door frame..... 161
Figure 199. Hoop stresses in the upper door frame. 161
Figure 200. Remarkable points and angles in the shell. 164
Figure 201. The inclination angle of each element. 165
Figure 202. Forces in one element. 166
Figure 203. Elements position in the 6 Steps in raising process. 167
Figure 204. Total forces in each step in the Concrete Shell. 168
Figure 205. Total forces in each step in the Ice Shell..... 169
Figure 206. Force carried by tendons and ring force relationship. 170
Figure 207. Ring force evolution in each step. 170
Figure 208. Force in one tendon evolution in each step. 171

List of Tables

Table 1. Cable selection. *Teufelberger, Catalogue Stahl- und Faserseile.* (Source: [26]) 90
Table 2. Cable closure geometrical parameters. (Source: [27]) 91
Table 3. Rope clips geometrical parameters. (Source: [26]) 94
Table 4. Position of the analyzed points. 110
Table 5. Material properties of the shell 110
Table 6. Snow load values. (Source:[30]) 117
Table 7. Wind velocity and velocity pressure. 119
Table 8. Terrain categories and terrain parameters. (Source: [31], Table 4.1) 120
Table 9. Peak velocity values. 122
Table 10. Equivalent surface roughness *k*. (Source: [31], Table 7.13) 125
Table 11. Reynolds values. 126
Table 12. Force coefficients. 126
Table 13. Coefficients c_{pe} in a spherical shape structure. 127
Table 14. Pressure values in surfaces of the shell. 127
Table 15. Units used in ABAQUS. 129
Table 16. Concrete shell analysis parameters. 130
Table 17. Concrete shell. Dead load analytical results. 130
Table 18. Concrete shell. Dead load ABAQUS results. 134
Table 19. Concrete shell. Snow load analytical results. 136
Table 20. Coefficients c_{pe} in a spherical shape structure. 138
Table 21. Pressure values in surfaces of the shell in Wien. 138
Table 22. Shell division in three surfaces. 139
Table 23. Ice shell analysis parameters. 143
Table 24. Ice shell. Dead load analytical results. 143
Table 25. Ice shell. Dead load ABAQUS results. 146
Table 26. Ice shell. Snow load analytical results. 148
Table 27. Pressure values in surfaces of the shell in Obergurgl. 150
Table 28. Stresses in the edges of the elements. Concrete Shell. 155
Table 29. Upper frame of the door stresses. Mess size: 0.1. Concrete Shell. 156
Table 30. Upper frame of the door stresses. Mess size: 0.08. Concrete Shell 156
Table 31. Stresses in the edges of the elements. Ice Shell 158
Table 32. Upper frame of the door stresses. Mess size: 0.1. Ice Shell. 159
Table 33. Precast concrete elements volume and weight. 163
Table 34. Ice shell elements volume and weight. 164
Table 35. Position and angles of remarkable points in the shell. 165
Table 36. Forces needed to raise each type element in Concrete Shell. 167
Table 37. Forces needed to raise each type element in Ice Shell. 168
Table 38. Total forces in each step in the Concrete Shell. 168
Table 39. Total forces in each step in the Ice Shell 169
Table 40. Pressure needed in the pneumatic formwork. Simplification method. 172
Table 41. Pressure needed in the pneumatic formwork 173

ANNEXES

ANNEX I. DEAD LOAD IN THE SHELL

DEAD LOAD IN THE SHELL

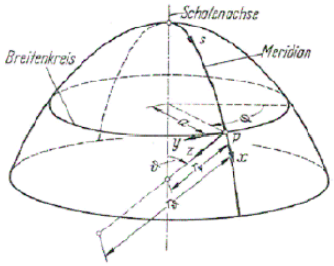

SHELL PARAMETERS

r (m)		4,1530
θo (º)		12,8571
θo (rad)		0,2244

MATERIAL PROPERTIES

		CONCRETE	ICE
Density (Kg/m3)		2400	916,7
Poisson's Ratio	μ	0,2000	0,3300
Shell Thickness	t (m)	0,0500	0,2000
Shell Parameter	x	11,8726	0,0000

θ: Meridian angle

s: Meridian lenght

$$x = \sqrt[4]{3(1-\mu^2)\frac{r^2}{t^2}}$$

Dead Load

	CONCRETE	ICE
self-weight (N/m3) (dens*grav)	23520	8983,66
pe - weight (N/m2) (dens*g*t)	1176	1796,732

$$p_E = \rho(\frac{Kg}{m^3})\cdot g(\frac{N}{Kg})\cdot t(m)$$

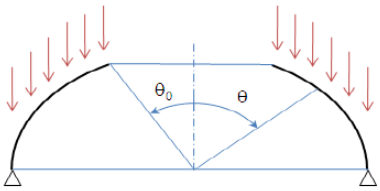

$$N_\theta = -p_E r \frac{\cos\theta_0 - \cos\theta}{\sin^2\theta} \qquad \sigma_\theta = \frac{N_\theta}{t}$$

$$N_\varphi = p_E r\left(\frac{\cos\theta_0 - \cos\theta}{\sin^2\theta} - \cos\theta\right) \qquad \sigma_\varphi = \frac{N_\varphi}{t}$$

CONCRETE SHELL RESULTS

Shell Point	θ [°]	θ [rad]	s [rad]	Nθ [N/m]	Nφ [N/m]	σθ [N/m2]	σφ [N/m2]
1	12,8571	0,2244	0,0000	0,00	-4761,47	-0,08	-95229,47
2	25,7143	0,4488	0,9319	-1918,73	-2481,54	-38374,62	-49630,73
3	38,5714	0,6732	1,8639	-2425,97	-1392,44	-48519,34	-27848,83
4	51,4286	0,8976	2,7958	-2807,97	-237,11	-56159,32	-4742,27
5	64,2857	1,1220	3,7277	-3255,24	1136,18	-65104,71	22723,58
6	77,1429	1,3464	4,6597	-3866,14	2779,36	-77322,71	55587,19
7	90,0000	1,5708	5,5916	-4761,48	4761,48	-95229,56	95229,56

ICE SHELL RESULTS

Shell Point	θ [°]	θ [rad]	s [rad]	Nθ [N/m]	Nφ [N/m]	σθ [N/m2]	σφ [N/m2]
1	12,8571	0,2244	0,0000	-0,01	-7274,74	-0,03	-36373,69
2	25,7143	0,4488	0,9319	-2931,50	-3791,37	-14657,50	-18956,87
3	38,5714	0,6732	1,8639	-3706,47	-2127,42	-18532,37	-10637,09
4	51,4286	0,8976	2,7958	-4290,10	-362,27	-21450,52	-1811,35
5	64,2857	1,1220	3,7277	-4973,46	1735,89	-24867,29	8679,46
6	77,1429	1,3464	4,6597	-5906,81	4246,40	-29534,05	21231,99
7	90,0000	1,5708	5,5916	-7274,74	7274,74	-36373,72	36373,72

ANNEX II. WIND LOAD IN THE SHELL

WIND LOAD IN THE SHELL

SHELL PARAMETERS

	r (m)	4,1530
	θo (º)	12,8571
	θo (rad)	0,2244

MATERIAL PROPERTIES

		CONCRETE	ICE
Density (Kg/m3)		2400	916,7
Poisson's Ratio	μ	0,2000	0,3300
Shell Thickness	t (m)	0,0500	0,2000
Shell Parameter	x	11,8726	5,8268

Dead Load	CONCRETE	ICE
self-weight (N/m3) (dens*grav)	23520	8983,66
pe - weight (N/m2) (dens*g*t)	1176	1796,732

Snow Load	CONCRETE	ICE
snow pressure	1360,0000	7000,0000
coef(0,8)*psnow (N/m2)	1088,0000	5600,0000

Dead Load

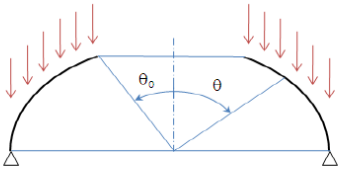

Snow Load

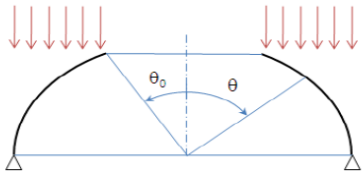

CONCRETE SHELL RESULTS

Shell Point	θ [°]	θ [rad]	s m	DEAD LOAD Nθ (N/m)	DEAD LOAD Nφ (N/m)	DEAD LOAD σθ N/m2	DEAD LOAD σφ N/m2
1	12,8571	0,2244	0,0000	0,00	-4761,47	-0,08	-95229,47
2	25,7143	0,4488	0,9319	-1918,73	-2481,54	-38374,62	-49630,73
3	38,5714	0,6732	1,8639	-2425,97	-1392,44	-48519,34	-27848,83
4	51,4286	0,8976	2,7958	-2807,97	-237,11	-56159,32	-4742,27
5	64,2857	1,1220	3,7277	-3255,24	1136,18	-65104,71	22723,58
6	77,1429	1,3464	4,6597	-3866,14	2779,36	-77322,71	55587,19
7	90,0000	1,5708	5,5916	-4761,48	4761,48	-95229,56	95229,56

Shell Point	SNOW LOAD Nθ (N/m)	SNOW LOAD Nφ (N/m)	SNOW LOAD σθ N/m2	SNOW LOAD σφ N/m2	TOTAL Nθ (N/m)	TOTAL Nφ (N/m)	TOTAL σθ N/m2	TOTAL σφ N/m2
1	0,00	-4294,73	-0,08	-85894,52	-0,01	-9056,20	-0,16	-181123,99
2	-1665,00	-2002,84	-33300,03	-40056,78	-3583,73	-4484,38	-71674,64	-89687,50
3	-1971,46	-790,49	-39429,27	-15809,90	-4397,43	-2182,94	-87948,61	-43658,73
4	-2076,22	319,72	-41524,43	6394,32	-4884,19	82,60	-97683,75	1652,06
5	-2121,42	1270,80	-42428,43	25415,95	-5376,66	2406,98	-107533,14	48139,53
6	-2141,54	1917,80	-42830,75	38356,06	-6007,67	4697,16	-120153,46	93943,25
7	-2147,37	2147,37	-42947,30	42947,30	-6908,84	6908,84	-138176,86	138176,86

WIND LOAD IN THE SHELL

ICE SHELL RESULTS

Shell Point	θ [°]	θ [rad]	s m	DEAD LOAD Nθ (N/m)	DEAD LOAD Nφ (N/m)	DEAD LOAD σθ N/m2	DEAD LOAD σφ N/m2
1	12,8571	0,2244	0,0000	-0,01	-7274,74	-0,03	-36373,69
2	25,7143	0,4488	0,9319	-2931,50	-3791,37	-14657,50	-18956,87
3	38,5714	0,6732	1,8639	-3706,47	-2127,42	-18532,37	-10637,09
4	51,4286	0,8976	2,7958	-4290,10	-362,27	-21450,52	-1811,35
5	64,2857	1,1220	3,7277	-4973,46	1735,89	-24867,29	8679,46
6	77,1429	1,3464	4,6597	-5906,81	4246,40	-29534,05	21231,99
7	90,0000	1,5708	5,5916	-7274,74	7274,74	-36373,72	36373,72

Shell Point	SNOW LOAD Nθ (N/m)	SNOW LOAD Nφ (N/m)	SNOW LOAD σθ N/m2	SNOW LOAD σφ N/m2	TOTAL Nθ (N/m)	TOTAL Nφ (N/m)	TOTAL σθ N/m2	TOTAL σφ N/m2
1	-0,02	-22105,21	-0,10	-110526,04	-0,03	-29379,95	-0,13	-146899,73
2	-8569,86	-10308,73	-42849,30	-51543,65	-11501,36	-14100,10	-57506,80	-70500,52
3	-10147,24	-4068,72	-50736,19	-20343,62	-13853,71	-6196,14	-69268,56	-30980,71
4	-10686,44	1645,60	-53432,18	8227,99	-14976,54	1283,33	-74882,70	6416,64
5	-10919,08	6540,87	-54595,41	32704,35	-15892,54	8276,76	-79462,69	41383,81
6	-11022,62	9871,04	-55113,09	49355,22	-16929,43	14117,44	-84647,15	70587,21
7	-11052,61	11052,61	-55263,07	55263,07	-18327,36	18327,36	-91636,79	91636,79

CONCRETE SHELL RESULTS

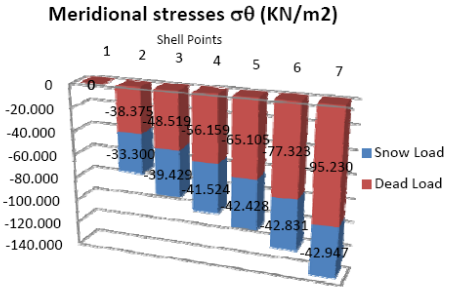

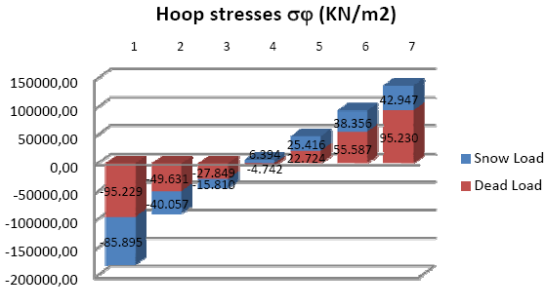

ICE SHELL RESULTS

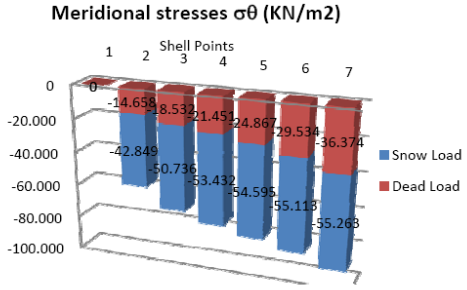

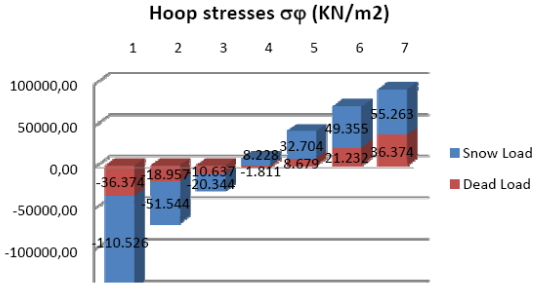

ANNEX III. TENDONS ANALYSIS - CONCRETE SHELL

TENDONS ANALYSIS - CONCRETE SHELL

MATERIAL PROPERTIES

	CONCRETE
Radious (m)	4,1530
Thickness (m)	0,05
Density (Kg/m3)	2400

SHELL PARAMETERS

Shell Point	θ [°]	θ [rad]	x	y	phi rad	phi º
0	0,0000	0,0000	0,0000	4,1530	0,785398163	45
	6,4286	0,1122	0,4650	4,1269	0,729298295	41,78571429
1	12,8571	0,2244	0,9241	4,0489	0,673198426	38,57142857
	19,2857	0,3366	1,3716	3,9199	0,617098557	35,35714286
2	25,7143	0,4488	1,8019	3,7417	0,560998688	32,14285714
	32,1429	0,5610	2,2095	3,5164	0,504898819	28,92857143
3	38,5714	0,6732	2,5894	3,2469	0,448798951	25,71428571
	45,0000	0,7854	2,9366	2,9366	0,392699082	22,5
4	51,4286	0,8976	3,2469	2,5894	0,336599213	19,28571429
	57,8571	1,0098	3,5164	2,2095	0,280499344	16,07142857
5	64,2857	1,1220	3,7417	1,8019	0,224399475	12,85714286
	70,7143	1,2342	3,9199	1,3716	0,168299606	9,642857143
6	77,1429	1,3464	4,0489	0,9241	0,112199738	6,428571429
	83,5714	1,4586	4,1269	0,4650	0,056099869	3,214285714
7	90,0000	1,5708	4,1530	0,0000	0	0

ELEMENTS CALCULATIONS

Element	b (m)	B (m)	h (m)	Area (m2)	Volume (m3)	mass (Kg)	Weight (N)
1	0,368	0,717	0,93	0,504525	0,02522625	60,543	593,92683
2	0,717	1,03	0,93	0,812355	0,04061775	97,4826	956,304306
3	1,03	1,292	0,93	1,07973	0,0539865	129,5676	1271,058156
4	1,292	1,489	0,93	1,293165	0,06465825	155,1798	1522,313838
5	1,489	1,611	0,93	1,4415	0,072075	172,98	1696,9338
6	1,611	1,652	0,93	1,517295	0,07586475	182,0754	1786,159674

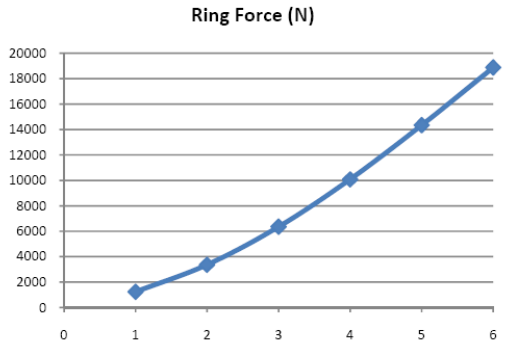

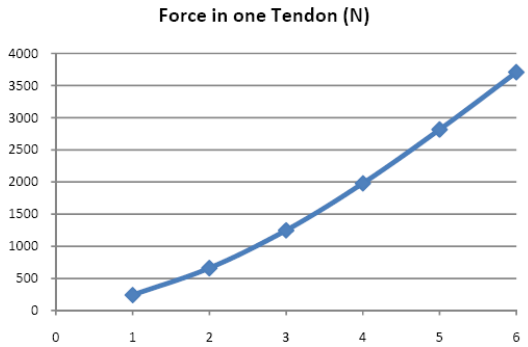

TENDONS ANALYSIS - CONCRETE SHELL

			1 element			
Element	Weight	phi (rad)	Tendonds	Pneumatic Formwork	Force in 1 tendon	Ring Force
Step 1						
1	593,92683	0,6171	484,38	343,69		
			484,38	343,69	242,19	1233,47
Step 2						
1	593,92683	0,6171	484,38	343,69		1233,47
2	956,304306	0,5049	836,98	462,58		2131,35
			1321,36	806,27	660,68	3364,82
Step 3						
1	593,92683	0,6171	484,38	343,69		1233,47
2	956,304306	0,5049	836,98	462,58		2131,35
3	1271,058156	0,3927	1174,30	486,41		2990,34
			2495,67	1292,68	1247,83	6355,17
Step 4						
1	593,92683	0,6171	484,38	343,69		1233,47
2	956,304306	0,5049	836,98	462,58		2131,35
3	1271,058156	0,3927	1174,30	486,41		2990,34
4	1522,313838	0,2805	1462,82	421,43		3725,03
			3958,49	1714,11	1979,24	10080,20
Step 5						
1	593,92683	0,6171	484,38	343,69		1233,47
2	956,304306	0,5049	836,98	462,58		2131,35
3	1271,058156	0,3927	1174,30	486,41		2990,34
4	1522,313838	0,2805	1462,82	421,43		3725,03
5	1696,9338	0,1683	1672,96	284,25		4260,15
			5631,44	1998,36	2815,72	14340,35
Step 6						
1	593,92683	0,6171	484,38	343,69		1233,47
2	956,304306	0,5049	836,98	462,58		2131,35
3	1271,058156	0,3927	1174,30	486,41		2990,34
4	1522,313838	0,2805	1462,82	421,43		3725,03
5	1696,9338	0,1683	1672,96	284,25		4260,15
6	1786,159674	0,0561	1783,35	100,15		4541,26
		Total	7414,79	2098,51	3707,40	18881,62

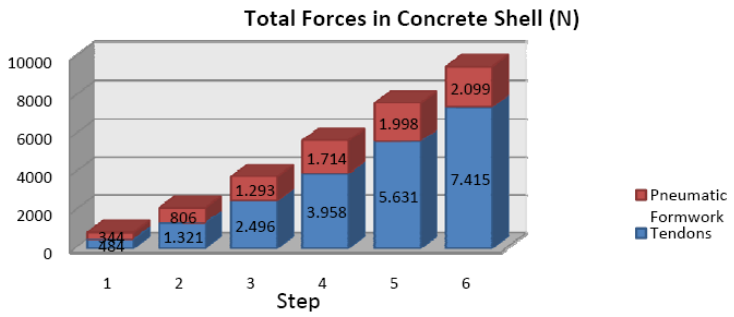

ANNEX IV. TENDONS ANALYSIS - ICE SHELL

TENDONS ANALYSIS - ICE SHELL

MATERIAL PROPERTIES

	CONCRETE
Radious (m)	4,1530
Thickness (m)	0,2
Density (Kg/m3)	916,7

SHELL PARAMETERS

Shell Point	θ [°]	θ [rad]	x	y	phi rad	phi º
0	0,0000	0,0000	0,0000	4,1530	0,785398163	45
	6,4286	0,1122	0,4650	4,1269	0,729298295	41,78571429
1	12,8571	0,2244	0,9241	4,0489	0,673198426	38,57142857
	19,2857	0,3366	1,3716	3,9199	0,617098557	35,35714286
2	25,7143	0,4488	1,8019	3,7417	0,560998688	32,14285714
	32,1429	0,5610	2,2095	3,5164	0,504898819	28,92857143
3	38,5714	0,6732	2,5894	3,2469	0,448798951	25,71428571
	45,0000	0,7854	2,9366	2,9366	0,392699082	22,5
4	51,4286	0,8976	3,2469	2,5894	0,336599213	19,28571429
	57,8571	1,0098	3,5164	2,2095	0,280499344	16,07142857
5	64,2857	1,1220	3,7417	1,8019	0,224399475	12,85714286
	70,7143	1,2342	3,9199	1,3716	0,168299606	9,642857143
6	77,1429	1,3464	4,0489	0,9241	0,112199738	6,428571429
	83,5714	1,4586	4,1269	0,4650	0,056099869	3,214285714
7	90,0000	1,5708	4,1530	0,0000	0	0

ELEMENTS CALCULATIONS

Element	b (m)	B (m)	h (m)	Area (m2)	Volume (m3)	mass (Kg)	Weight (N)
1	0,368	0,717	0,93	0,504525	0,100905	92,4996135	907,4212084
2	0,717	1,03	0,93	0,812355	0,162471	148,9371657	1461,073596
3	1,03	1,292	0,93	1,07973	0,215946	197,9576982	1941,965019
4	1,292	1,489	0,93	1,293165	0,258633	237,0888711	2325,841825
5	1,489	1,611	0,93	1,4415	0,2883	264,28461	2592,632024
6	1,611	1,652	0,93	1,517295	0,303459	278,1808653	2728,954289

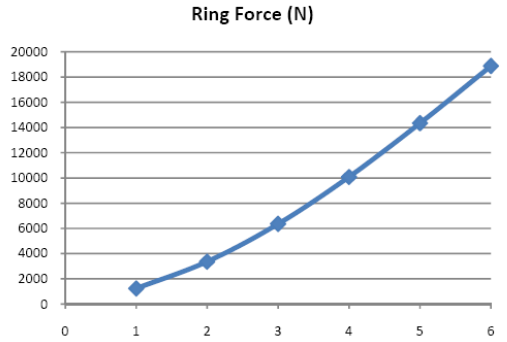

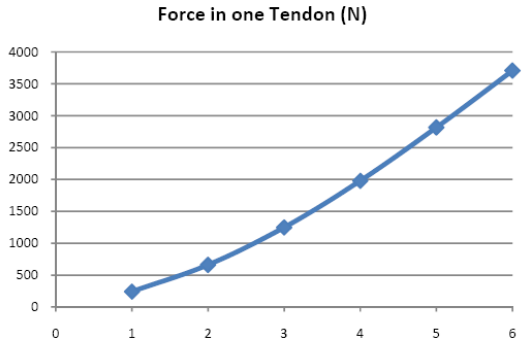

TENDONS ANALYSIS - CONCRETE SHELL
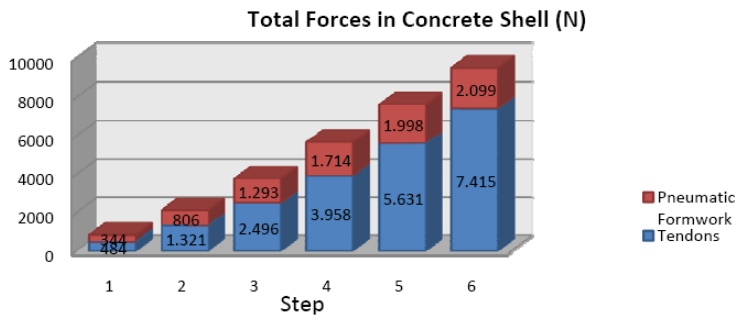
			1 element			
Element	Weight	phi (rad)	Tendonds	Pneumatic Formwork	Force in 1 tendon	Ring Force
Step 1						
1	907,4212084	0,6171	740,06	525,10		
			740,06	525,10	370,03	1884,54
Step 2						
1	907,4212084	0,6171	740,06	525,10		1884,54
2	1461,073596	0,5049	1278,77	706,75		3256,35
			2018,82	1231,85	1009,41	5140,89
Step 3						
1	907,4212084	0,6171	740,06	525,10		1884,54
2	1461,073596	0,5049	1278,77	706,75		3256,35
3	1941,965019	0,3927	1794,14	743,16		4568,74
			3812,96	1975,01	1906,48	9709,64
Step 4						
1	907,4212084	0,6171	740,06	525,10		1884,54
2	1461,073596	0,5049	1278,77	706,75		3256,35
3	1941,965019	0,3927	1794,14	743,16		4568,74
4	2325,841825	0,2805	2234,94	643,88		5691,23
			6047,91	2618,88	3023,95	15400,87
Step 5						
1	907,4212084	0,6171	740,06	525,10		1884,54
2	1461,073596	0,5049	1278,77	706,75		3256,35
3	1941,965019	0,3927	1794,14	743,16		4568,74
4	2325,841825	0,2805	2234,94	643,88		5691,23
5	2592,632024	0,1683	2556,00	434,28		6508,80
			8603,91	3053,16	4301,95	21909,67
Step 6						
1	907,4212084	0,6171	740,06	525,10		1884,54
2	1461,073596	0,5049	1278,77	706,75		3256,35
3	1941,965019	0,3927	1794,14	743,16		4568,74
4	2325,841825	0,2805	2234,94	643,88		5691,23
5	2592,632024	0,1683	2556,00	434,28		6508,80
6	2728,954289	0,0561	2724,66	153,01		6938,29
		Total	11328,57	3206,18	5664,28	28847,96